887-

STRUCTURAL RELATIONSHIPS BETWEEN THE EXSHAW THRUST AND HEART MOUNTAIN SYNCLINE EXSHAW, ALBERTA

STRUCTURAL RELATIONSHIPS BETWEEN THE EXSHAW THRUST AND HEART MOUNTAIN SYNCLINE EXSHAW, ALBERTA

By

ERIC MICHAEL LEGRESLEY

A Thesis

Submitted to the Department of Geology

in Partial Fulfillment of the Requirements for the

Degree Honours Bachelor of Science

McMASTER UNIVERSITY

April, 1982

HONOURS BACHELOR OF SCIENCE (1982)
(Geology)

McMASTER UNIVERSITY
Hamilton, Ontario

TITLE: Structural Relationships between the Exshaw Thrust and Heart Mountain syncline, Exshaw, Alberta

AUTHOR: Eric Michael LeGresley

SUPERVISOR: Dr. P. M. Clifford

NUMBER OF PAGES: xiv, 127

ABSTRACT

Displacement transfer between faults and folds has been extensively documented in the Rocky Mountains as an explanation for structural variability along strike producing seemingly similar overall shortenings. A series of subparallel imbricate thrusts and an associated syncline in the Southern Canadian Front Ranges at Heart Mountain has been mapped at a scale of 1:16,667. Megascopic, mesoscopic and microscopic evidence supports the contention that the folding observed at Heart Mountain occurred synchronously with thrusting as the result of displacement transfer from the adjacent thrust.

Numerical dynamic analyses (NDA) suggest that twinning of calcite grains occurred very early in the deformational history in response to a regional stress field orientation of 246/03, 340/02, and 159/84 for σ_1, σ_2, and σ_3 respectively in the Exshaw plate. Megascopic and mesoscopic fabrics indicate similar results. Ambiguous NDA results for the Heart Mountain Syncline are explained using neutral surface folding theories rather than flexural slip theories generally proposed for folding within the Front Ranges. Neutral surface folds are consistent with the deformational model (displacement transfer) proposed.

An orthogonal fracture system is pervasive throughout

the thesis area. Observations indicate that fractures are oriented parallel and perpendicular to the strike of the Rocky Mountains. Their development is inferred to have taken place in the same regional stress field thought to be responsible for twinning, with fracture opening occurring after the relaxation of tectonic stresses and the removal of substantial amounts of overburden.

ACKNOWLEDGEMENTS

So many people graciously gave of their time and experience during the course of this study that I feel somewhat guilty putting only my name on it.

Firstly, I would like to thank my supervisor, Dr. Paul Clifford for his thoughtful comments and criticisms throughout the course of this study. During the anxious early days of scrambling to find a suitable topic, Steve Brown of Mobil Oil was very kind in taking me on a tour of the Front Ranges and explaining a great deal of the basic structure to me. For his generosity and suggestion of this thesis area I am deeply indebted. Thanks are also extended to Ian Moffat at Gulf Canada for his aid in evaluating the potential of twin investigation in this study.

I wish to express my gratitude to Gulf Canada for allowing me ample oppurtunity to research my topic during my summer with them, and for providing me with some of my thin sections, a Brunton compass, and extensive use of their photocopying facilities. The University of Calgary Geology Department is also thanked for the loan of an altimeter for the summer.

My sincere thanks go out to Rick Groshong at Cities Service for providing me with a tape of his computer program TWIN, and to the numerous user assistants who lead me through the modification of the program for our computer system. Dr. John

Starkey from the University of Western Ontario is gratefully acknowledged for the loan of some critical microscope objectives.

To John Cekr, who I ran ragged all first term; Jack Whorwood, whose photographic expertise made reasonable illustrations out of my patchwork drafting; and Len Zwicker, who prepared the thin sections, your technical abilities are greatly appreciated and admired.

Most of all, I would like to thank Stephanie for her patience, support, and love. This paper is as much the result of her stamina as it is mine. She was also capable of making sense out of the scrawl I called the manuscript.

TABLE OF CONTENTS

LIST OF TABLES

LIST OF FIGURES

LIST OF PLATES

INTRODUCTION

1.1 Introduction and Purpose

Regional mapping of the southern Canadian Rocky Mountains at a large scale has indicated numerous variations in deformational style, but the mechanisms for these deformations are not usually definable in such gross studies. Dahlstrom (1970) emphasizes the importance of displacement transfer along strike between faults and folds as a mechanism for the development of new deformational features. Observation and determination of the geometry, kinematics and dynamics of this process through both mesoscopic and microscopic fabrics should permit determination of a sequence of deformational events consistent with deformational theories.

With this in mind, a fault bounded syncline on Heart Mountain was investigated to determine:

(1) the geometry and geometric variations along the Exshaw Thrust and Heart Mountain syncline

(2) the paleostrain and inferred paleostress distributions through analysis of macroscopic and microscopic (twin) fabrics

(3) the relationships between macro- and mesoscopic fabrics and the local and/or regional stress field distributions

(4) the differential stress responsible for such structures

(5) a deformational model and history consistent with observed structural elements and theoretical concepts of displacement transfer

1.2 Previous Work

Due in part to the accessibility provided by the Bow River Valley, the Exshaw area has been the subject of over 100 years of geologic exploration. The earliest accounts are those of Hector (1858), Dawson (1886) and McConnell (1887) for whom the McConnell Thrust was named (Gallup 1953, 1956). McConnell's stratigraphic and structural section through the Bow River Valley provided the framework for generations of future geologists.

During this century Dowley (1907), Allen (1912-1915), Shimer (1926), Kindle (1924) and Warren (1926) undertook stratigraphic studies of the Eastern Canadian Cordillera. The first comprehensive structural mapping of the Bow River Valley was by Clark (1949) "out of geological curiosity and for week-end physical recreation". Data collected in previous studies was published by the GSC in 1970 at a scale of 1:50,000 as a portion of Operation Bow-Athabasca. The present thesis area is a small portion of Map 1265A, Canmore East by Price (1970).

More recently, numeric dynamic analyses of the Front

Ranges have been completed by graduate students from the University of Calgary, notably Jamison (1974), Brown (1976) and Moffat (1980). Jamison's thesis included samples from this present thesis area.

1.3 Local Geographical Setting

The study area is located just south of the Trans-Canada Highway adjacent to the town of Exshaw. The study area is reached by travelling westward along Hwy 1 from Calgary to Exshaw, and then by foot up the northwest ridge of Heart Mountain. A pathway leads directly from the highway and begins at Heart Creek. Heart Mountain rises over 7050 feet above sea level; the synclinal peak observed from the highway is a false summit and the region of most intensive study.

Figure 1.31 illustrates the position of the thesis area in a regional context.

1.4 Regional Geological Setting

The area of study is located near the eastern margin of the Front Range Structural Subprovince, one of four such subprovinces which constitute the Rocky Mountains. These subprovinces from east to west are:

Figure 1.31 Location map of the thesis area illustrating position relative to the major structural subdomains of the Rocky Mountains.

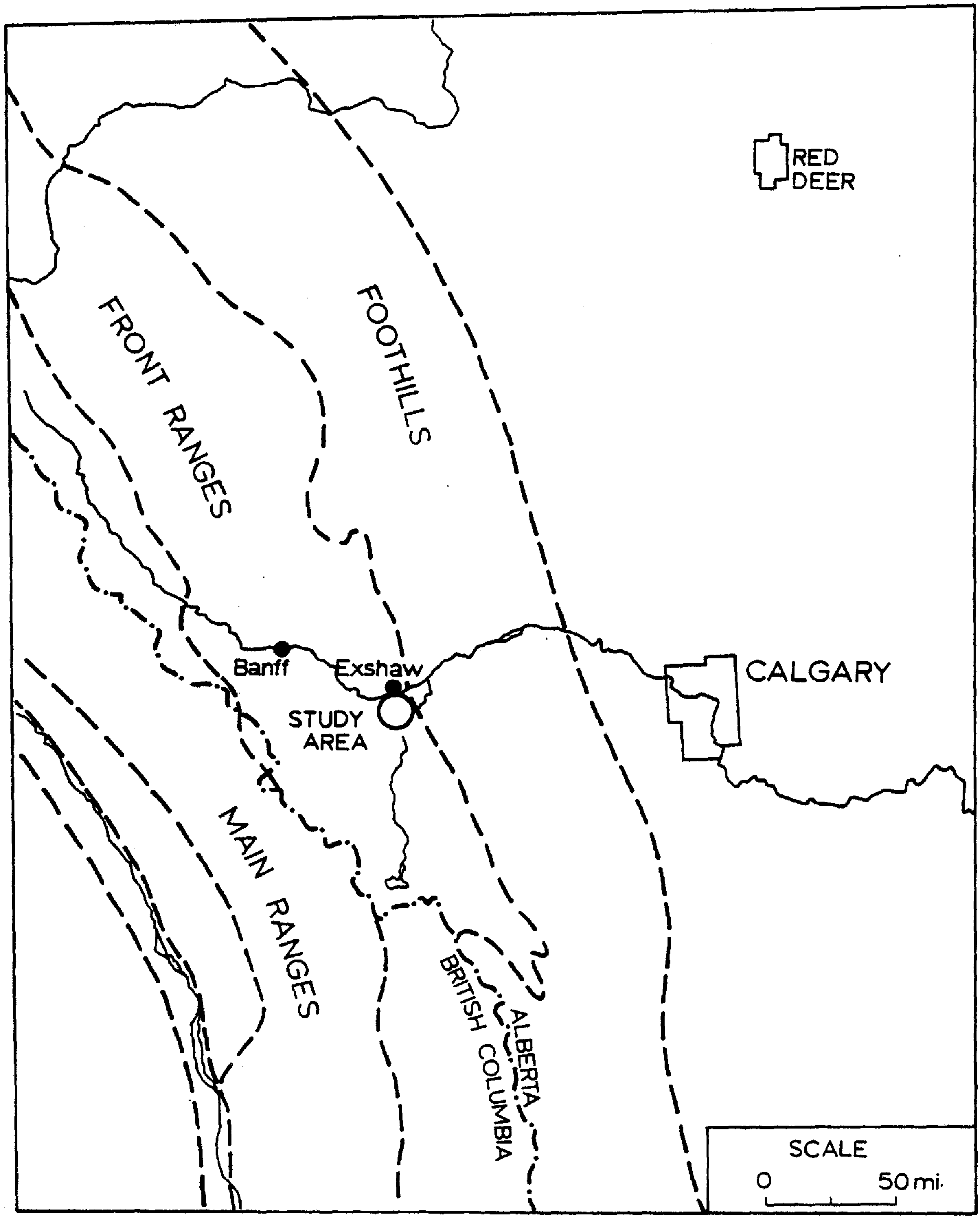
RED DEER
FRONT RANGES
FOOTHILLS
Banff
Exshaw
CALGARY
STUDY AREA
MAIN RANGES
BRITISH COLUMBIA
ALBERTA
SCALE
0
50 mi.

(1) Foothills

(2) Front Ranges

(3) Main Ranges

(4) Western Ranges

The Rocky Mountains, also known as the Foreland Fold and Thrust Belt (Wheeler and Gabrielse, 1972), are contained within the eastern margin of the Columbian Orogen (Brown, 1976).

Norris (1956) and Dahlstrom (1970) emphasize the importance of stratigraphic control of the suite of deformational structures produced within each of the subprovinces. The variations in deformational expression between the Foothills and Front Ranges illustrate this point. Surface exposures in the Canadian Foothills are primarily of incompetent Mesozoic clastics. These are highly folded and intensively thrust imbricated, with low topographic relief (Moffat, 1980). The extensive imbrication of thrusts at high structural levels results from the large number of incompetent shaley horizons (Douglas, 1956; Price and Mountjoy, 1970; Dahlstrom, 1970) within the Mesozoic clastic sequence.

Deformation mechanisms within the Front Ranges are essentially the same as those within the Foothills, but thrusting occurs at a deeper stratigraphic level. The more resistant nature of the Paleozoic carbonates produces the topographical variation from the Foothills. Thrusts within the Front Ranges and Foothills strike NW-SE and are commonly concave upwards. Figure 1.41 illustrates the nature of thrusting in

Figure 1.41 Structural section of eastern margin of the Front Ranges approximately 6.75 km north of the thesis area. Note the listric, concave upward appearance of thrust faults, steepening and becoming more imbricated at higher stratigraphic levels. Faults coring into concentric folds are also common.

modified after Price (1970)

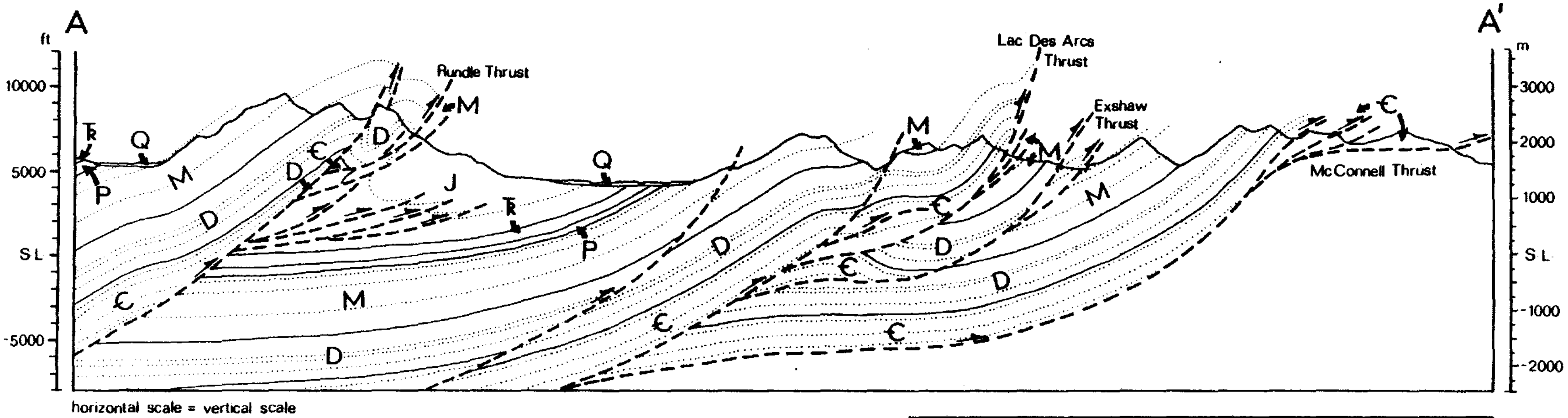

Q - QUATERNARY
J - JURASSIC
Ꞧ - TRIASSIC
P - PERMIAN
M - MISSISSIPPIAN
D - DEVONIAN
Ꞓ - CAMBRIAN

Cenozoic alluvium: Q
Mesozoic clastics: J, Ꞧ
Paleozoic carbonates: P, M, D, Ꞓ

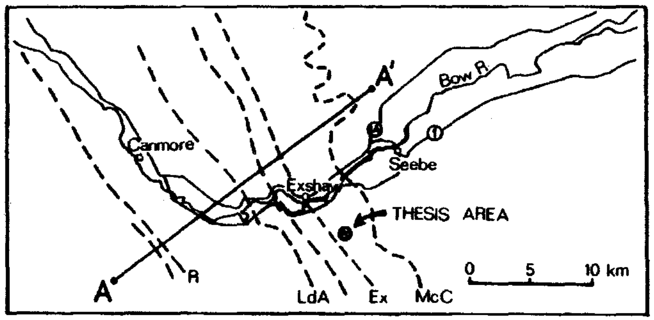

the Front Ranges. The thesis area is located 6.75 km SE of this cross section. Thrusting commonly is bedding plane parallel and "steps" steeply through competent units as it cuts up-section to the NE. As the thrust steepens, imbrications develop, with the greatest displacement occurring along the lowermost fault (Dahlstrom, 1970; Brown, 1976, 1978). At depth, a series of thrusts merge. Seismic evidence suggests that there is no involvement of the Hudsonian basement in the Main and Front Ranges (Bally et al, 1966). Dahlstrom (1970) defines a family of structures occurring within the Phanerozoic strata of both the Foothills and Front Range subprovinces. The family includes:

(1) thrust faults (imbricate, listric, often folded)

(2) concentric folds

(3) transverse tear faults

(4) normal faults (late stage)

Deformation is believed to have migrated from west to east from the Upper Cretaceous through to the Eocene (Bally et al, 1966). Rapid loading triggers imbricate thrusting from the toe of the advancing wedge (Gretener, 1972; Elliot, 1976a). The advancing warped thrust is preceded geographically by a foreland bulge (Price, 1970, 1980), producing a set of orthogonal joints seen throughout all of Alberta (Babcock, 1973; Riek and Currie, 1974; Moffat, 1980). As deformation proceeds, the developing thrusts rotate from the toe. This yields a monoclinically folded hanging wall and a folded thrust (Dahlstrom, 1970). Late stage deformations consist of back-limb thrust-

Figure 1.42 Orogenic evolution of the Western Cordillera.

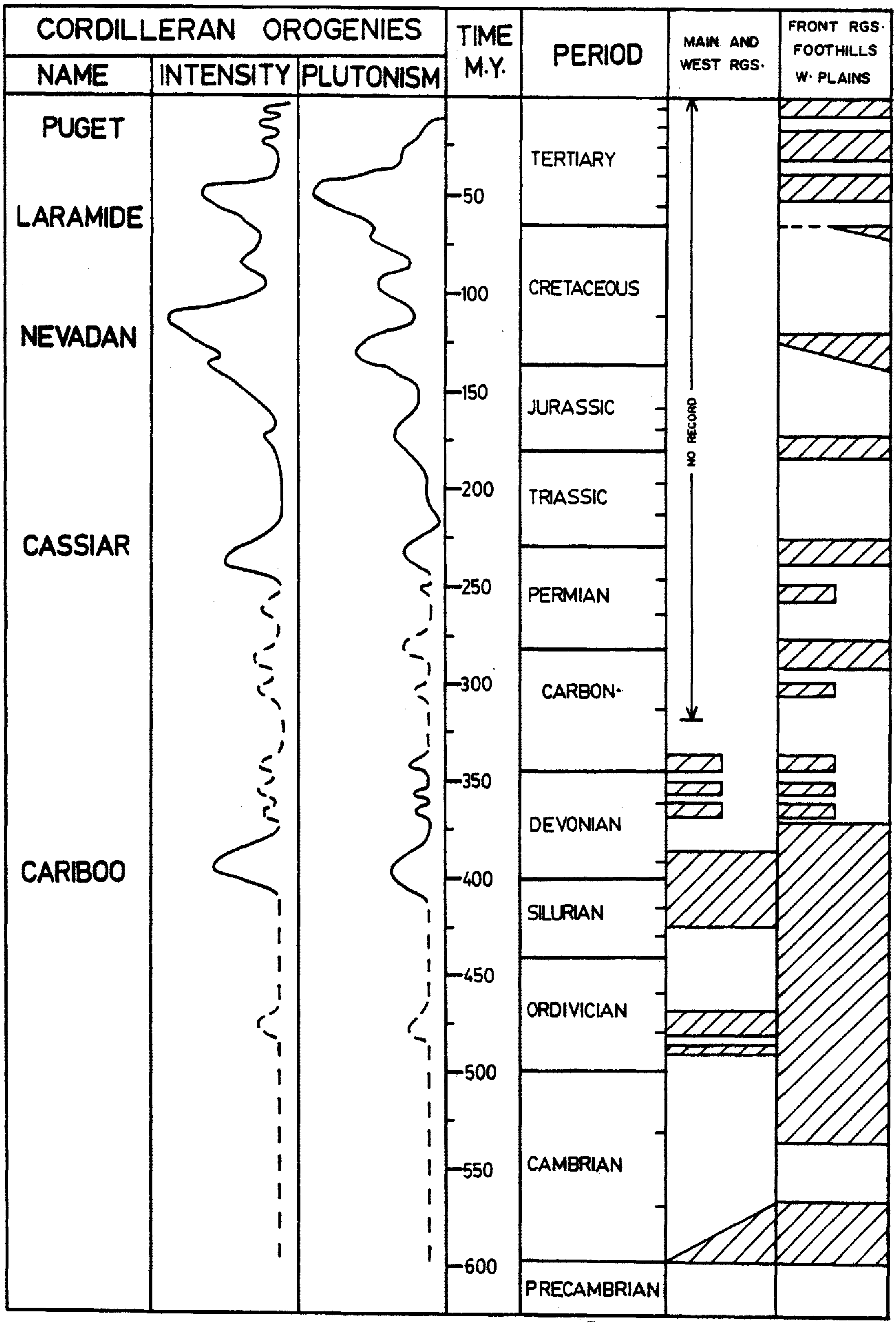

CORDILLERAN OROGENIES
NAME
INTENSITY
PLUTONISM
TIME M.Y.
PERIOD
MAIN AND WEST RGS.
FRONT RGS. FOOTHILLS W. PLAINS
PUGET
LARAMIDE
NEVADAN
CASSIAR
CARIBOO
50
100
150
200
250
300
350
400
450
500
550
600
TERTIARY
CRETACEOUS
JURASSIC
TRIASSIC
PERMIAN
CARBON.
DEVONIAN
SILURIAN
ORDIVICIAN
CAMBRIAN
PRECAMBRIAN
NO RECORD

Plate 1.4I Eastern margin of the Front Ranges as viewed from Heart Mountain looking north. The Lac des Arcs (LdA), Exshaw (Ex) and McConnell (McC) thrusts are shown; each lends its name to the plate which lies above it. The McConnell Thrust divides the Foothills (to the right) composed of Mesozoic clastics, from the Front Ranges (to the left) composed of Paleozoic carbonates. Prominent geomorphic features are Mount Yamnuska (eastern most mountain), Loder Peak, and the Bow River Valley.

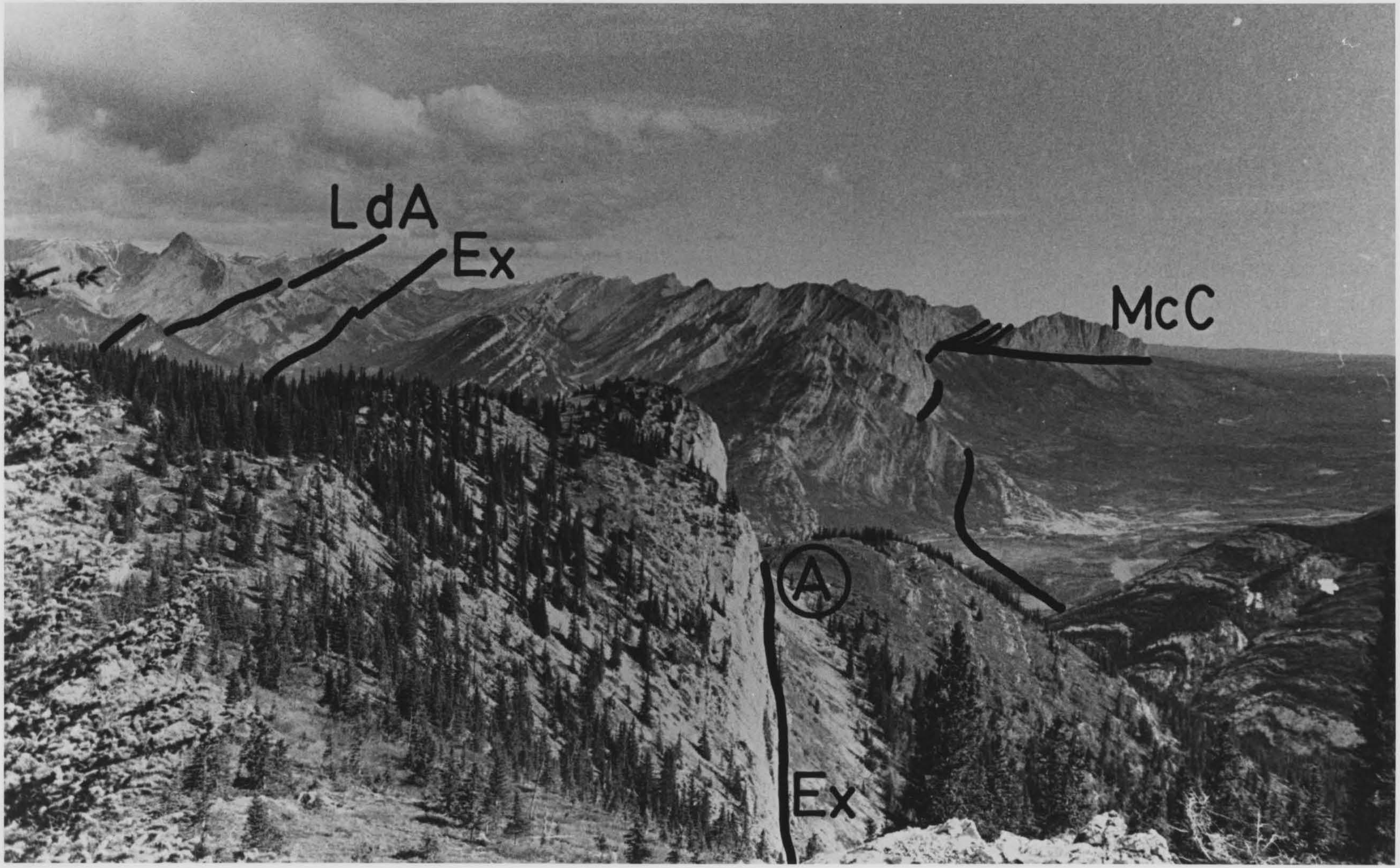
LdA
Ex
McC
A
Ex

ing (Bally et al, 1966) and normal faulting (Dahlstrom, 1970; Moffat, 1980).

Shortening of the Paleozoic strata in the Main and Front Ranges is about 160 km and believed to be relatively constant along the length of the Foreland Fold and Thrust belt. The dominant deformation mechanism in the Northern Rockies is concentric folding, and thrusting in the Southern Rockies (Dahlstrom, 1970; Brown, 1976). Transfer of displacement from thrusts to adjacent thrusts or folds occurs along a deformed belt as the thrust terminates (Moffat, 1980).

1.5 Stratigraphy of the Thesis Area

The stratigraphic units comprising the thesis area are almost exclusively Paleozoic carbonates, ranging in age from Upper Devonian to Pennsylvanian. A stratigraphic summary with thicknesses determined from structural sections is given in Figure 1.51. Lithologic descriptions given below are based on field observations and literature descriptions. References listed provide a more complete description of stratigraphic details for the type section.

DEVONIAN

Palliser Formation

Type section: southern end of the Palliser Range at the north

Figure 1.51 Stratigraphic summary of the thesis area. Thickness are based on field measurements, calculations or literature.

	PERIOD	FORMATION	THICKNESS (meters)
PALEOZOIC	PERMO-PENN.	ROCKY MTN. GP.	120
	MISS.	ETHERINGTON FMN.	90
		MOUNT HEAD FMN.	170
		LIVINGSTONE FMN.	320
		U. BANFF FMN.	105
		M. BANFF FMN.	140
		L. BANFF FMN.	140
	UPPER DEVONIAN	PALLISER FMN.	335

end of Lake Minnewanka, near Banff, Alberta.

References: Beach (1943); deWit and McLaren (1950); Shriner (1926)

Description: The Palliser consists primarily of very resistant, massive, fine-grained dolomitic limestones. Fresh surfaces are medium grey. Surficial exposures are usually prominent cliffs with a blue/grey mottled appearance. Bedding is virtually absent. Both upper and lower boundaries within the thesis area are fault contacts, but complete exposures in adjacent areas put the stratigraphic thickness at about 335 m.

MISSISSIPPIAN

Banff Formation

Type section: Lake Minnewanka area, near Banff, Alberta

References: Beales (1950); Moore (1958); Penner (1958); Shriner (1926)

Description: Commonly divided into 3 formations: the Lower Banff being calcareous, brownish-grey recessive shales; the Middle Banff is a medium grey, argillaceous wackestone of a slightly more resistant nature; the Upper Banff is a recessive calcareous mudstone, often containing numerous chert nodules. Substantial stratigraphic variability over short lateral distances has often resulted in the three Banff formations being mapped together as a single stratigraphic unit. The incompetent Lower Banff often acts as a decollement zone in the thick, competent Paleozoic carbonate sequence of the Front Ranges (Stockmal, 1979). The Banff Formation lies unconformably on top of the Palliser. Locally their total thickness is about 285 m.

Livingstone Formation

Type section: north bank of the head waters of Flat Creek Alberta in the southern Kananaskis area.

References: Beales (1950); Douglas (1950, 1953); Douglas and Harker (1958); Moore (1958).

Description: Exposures of the Livingstone within the thesis area are primarily from the upper portion. The Livingstone is a grey, medium-grained, massive limestone, and the unit becomes coarser and more fossiliferous down section. At lower stratigraphic levels the term grainstone is appropriate. Outcropping generally consists of prominent blue/grey cliffs adjacent to thrusts. Distinctive karst features (rill and cairn structures) are typical. The unit as a whole is very resistant and very competent. A complete section of Livingstone is not seen within the thesis area. Total thickness is believed to be approximately 340 km.

Mount Head Formation

Type section: Mount Head map area, Alberta

References: Beales (1950); Douglas (1950, 1953); Douglas and Harker (1958); Moore (1958).

Description: The observed sections were primarily from the Lower Mount Head. The lithology is recessive, medium-bedded, fine grained dolomites and limestones. Interbeds of clastic limestones and calcarenites as well as nodular chert are common.

Lithologically the lowermost units are similar to those of the conformably-underlying Livingstone Formation, but the recessive nature of the Mount Head Formation allows one to define the boundary. A complete section of Mount Head Formation is found along the eastern side of Heart Mountain; the calculated stratigraphic thickness is 170 m.

Etherington Formation

Type section: no type section, but the formation outcrops along Etherington Creek in the Mount Head map area and the name may have been coined for this locality.

References: Douglas (1953); Douglas and Harker (1958).

Description: A section of Etherington outcrops along the eastern slope of Heart Mountain and consists dominantly of slightly resistant, fine grained grey wackestones and packstones. Argillaceous horizons exist. Locally chert nodules are abundant. The Etherington Formation is believed to behave incompetently in conjunction with the Mount Head Formation (Stockmal, 1979). The lower contact with the Mount Head Formation is conformable. The Etherington Formation is unconformably overlain by the Rocky Mountain Group. Stratigraphic thickness within the thesis area is 90 m.

PERMIAN - PENNSYLVANIAN

Rocky Mountain Group

Type section: no type section

References: Douglas and Harker (1958); Dowling (1907); McGugan and Rapson (1960); Moore (1958); Raasch (1958);

Warren (1947).

Description: The Rocky Mountain Group is dominantly interbedded dolomite and dolomitic siltstone and sandstone, fine grained and well bedded, the upper portion being noticeably more argillaceous. Exposures are of resistant, blocky, tan-coloured rocks, often well cross bedded. The lower unconformable contact with the Etherington Formation is sharp and the upper contact is not seen at this locality. Warren (1947) describes an uppermost chert bed, but this was not observed. Price (1970) maps a very thin sliver of Spray River Group adjacent to the A splay in the footwall. This lithology was not observed. This fact, combined with the absence of a chert horizon and an anomalously thin stratigraphic thickness (120 m) suggests that the Spray River Group does not exist at this locality. The Rocky Mountain Group is apparently fault bounded. Some degree of uncertainty exists in this interpretation since there was extensive talus cover shed from the cliff formed by the Livingstone Formation in the hanging wall of the A splay.

Plate 1.5I Exposure patterns of the lower Mount Head, upper Livingstone Formations, and the Rocky Mountain Group as seen looking northwestward along strike from outcrop 2-2 at the A thrust. Price (1970) maps a very thin sliver of Spray River Group in the footwall of the A thrust, but ground traverses do not support this. The trace of the Exshaw thrust is continued to the horizon.

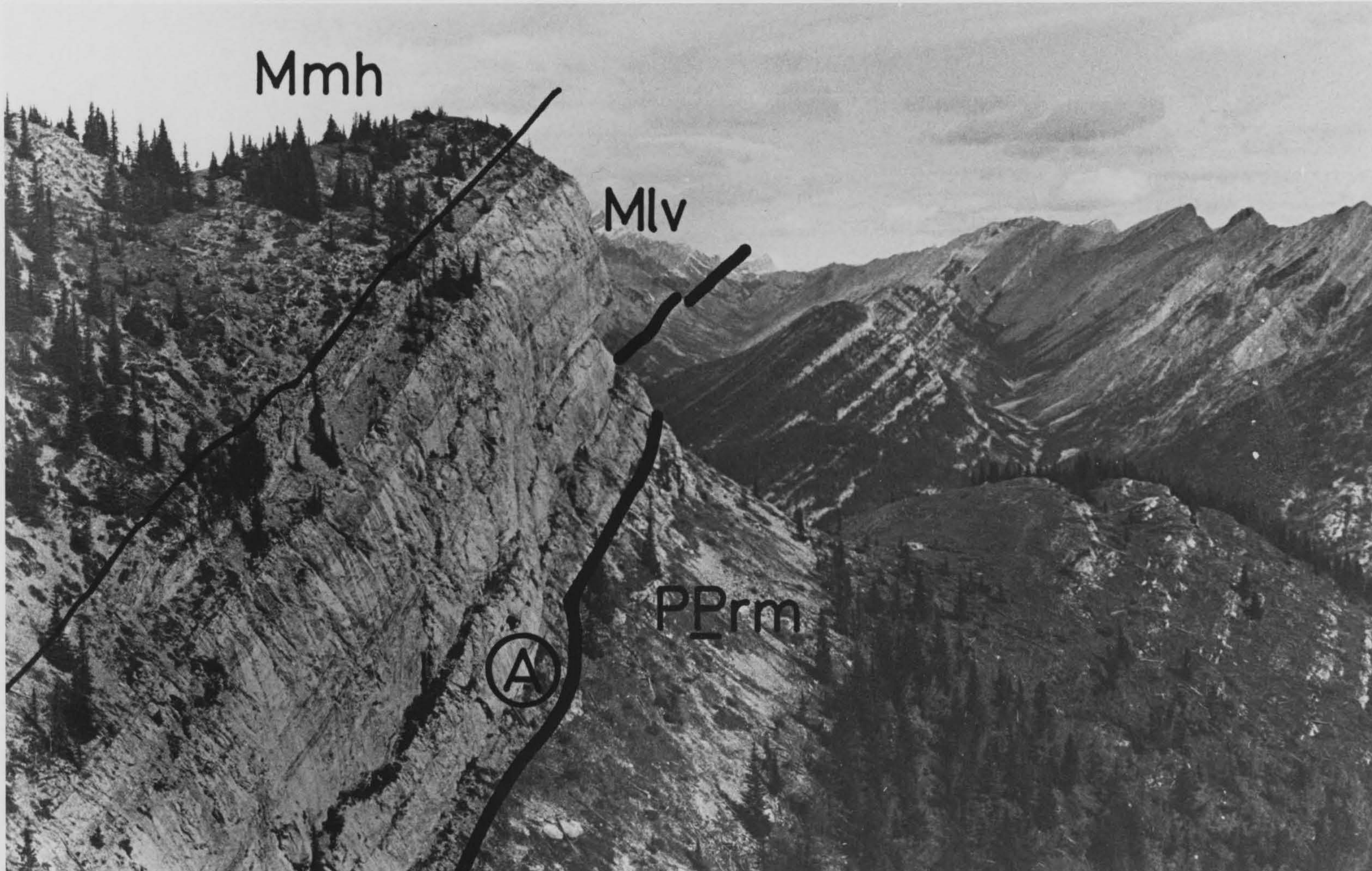
Mmh
Mlv
PPrm
A

MACROSCOPIC STRUCTURAL GEOLOGY

2.1 Field Procedures

Stratigraphic and structural field mapping of the thesis area was undertaken over many weekends during the summer of 1981. Detailed mapping at a scale of 1:16,667 was aided by the careful use of air photos, Thommen altimeter and a Brunton pocket transit. The Geological Survey of Canada map 1265A at a scale of 1:50,000 (Price, 1970) was extremely valuable, especially for tentative stratigraphic identification and initial familiarization. Outcrop observations generally consisted of a statistically suitable number of bedding plane, fracture and fold axis measurements. Oriented samples were collected when appropriate.

2.2 Regional Deformational Setting

The regional structural trend of the Front Ranges and Foothills west of Calgary is 157°. Regional transport direction of the thrusted sequences is considered to be normal to this and horizontal. If in the thin-skinned decollement hypothesis we assume that the basement gradient is negligible, then the kinematic axes are 067°, horizontal; 157°, horizontal; and

Figure 2.11 Outcrop locations visited during the course of the study.

OUTCROP LOCATIONS

LEGEND

CONTOUR 5000

STREAM

OUTCROP LOCATION 6-7

SCALE

0 0.5km

CONTOUR INTERVAL 250 FEET

Figure 2.12 Geology of the Exshaw Thrust at Heart Mountain, Alberta, based in part on the GSC map #1265A.

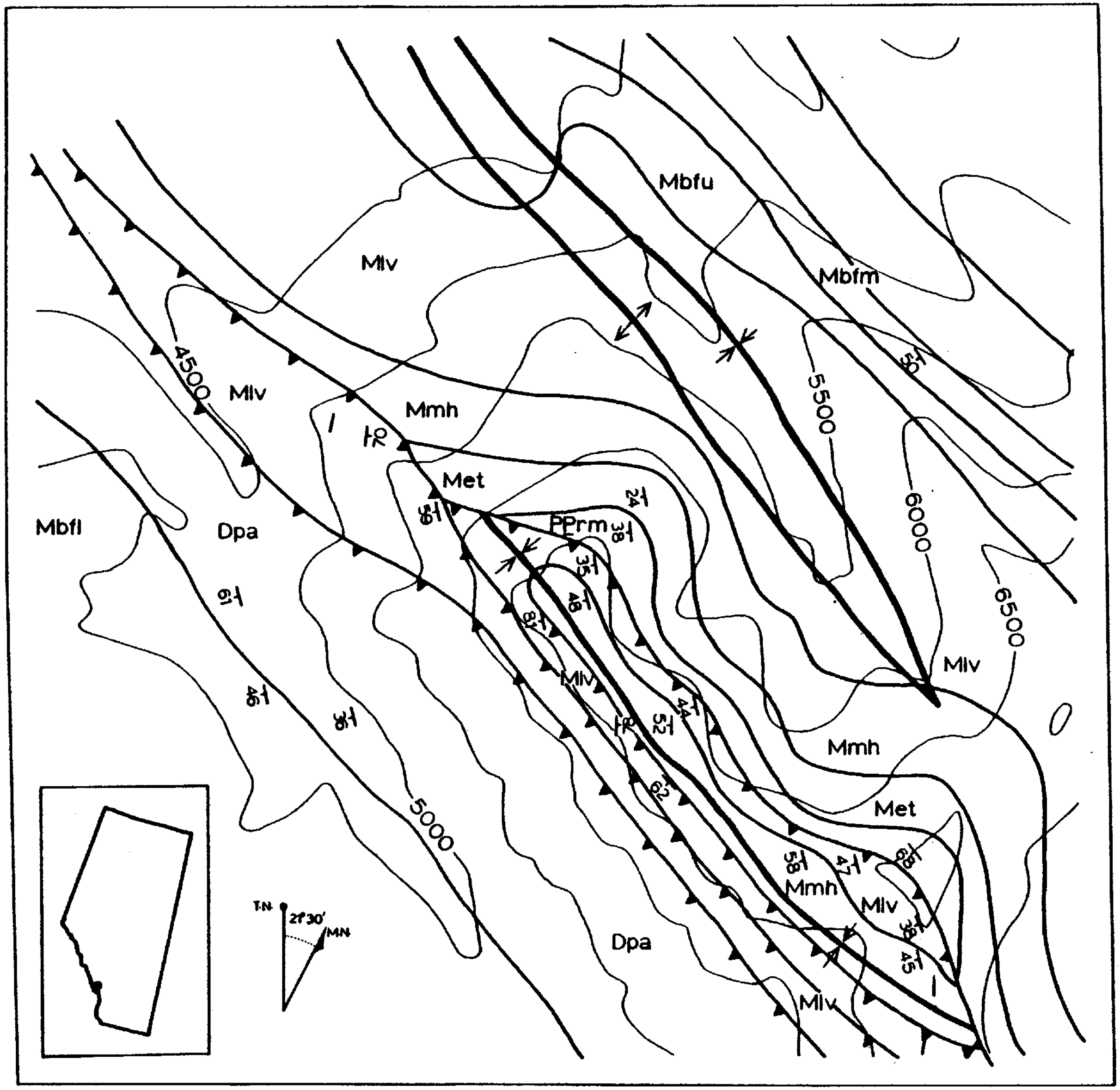

GEOLOGY
HEART MOUNTAIN, ALTA.

LEGEND

CONTOUR 5000

CONTACT

BEDDING 62

THRUST FAULT

ANTICLINE

SYNCLINE

Pennsylvanian

PPrm - ROCKY MOUNTAIN GROUP
light grey dolomitic sandstone; silty dolomite

Mississippian

Met - ETHERINGTON FORMATION
light grey limestone, dolomite; cherty and calcarenitic limestone

Mmh - MOUNT HEAD FORMATION
fine, light grey limestone; dense, black limestone; argillaceous limestone and dolomite

Mlv - LIVINGSTONE FORMATION
light grey, massive, calcarenitic limestone; dolomite

Mbf - BANFF FORMATION
fine, grey-brown limestone; calcareous shale

Devonian

Dpa - PALLISER FORMATION
grey, massive, dolomitic limestone

SCALE

0 0.5km

CONTOUR INTERVAL 500 FEET

vertical for a, b, and c respectively. Thin sections in this study are in the ac plane. On a regional scale, deformation within the Foreland Thrust belt is irrotational plane strain with respect to the regional stress field. Therefore these axes correspond to the maximum, intermediate and minimum principal stresses (σ_1, σ_2, σ_3) and strains (A, B, C) also.

Hafner's theoretical model for stress distribution (Hafner, 1951, p. 386) is an approximation of the regional stress regime (see Figure 2.21). This model produces concave upward shear fractures analogous to the concave upwards thrust faults observed in the Front Ranges and Foothills. In regional context the theory places σ_1 trending normal to the regional structural trend at 067° but increasing slightly in plunge towards the northeast. The plunging σ_1 produces an upward fanning distribution of σ_3 (so as to remain orthogonal). σ_2 remains horizontal (into the page in Figure 2.21) and trends parallel to the regional structure at 157°. Jamison (1974) points out the following inadequacies in the Hafner model:

(1) Hafner assumes the stressed body is isotropic, homogeneous and elastic, whereas the rocks within this region do not exhibit these characteristics;

(2) It is impossible to correlate a single point within the rock body to a single point in the model;

(3) The predicted stress fields are only valid before the initiation of non-elastic strain (such as fracturing).

Figure 2.21 Standard state stress model and superimposed horizontal pressures with constant lateral and vertical gradient.

after Hafner (1951)

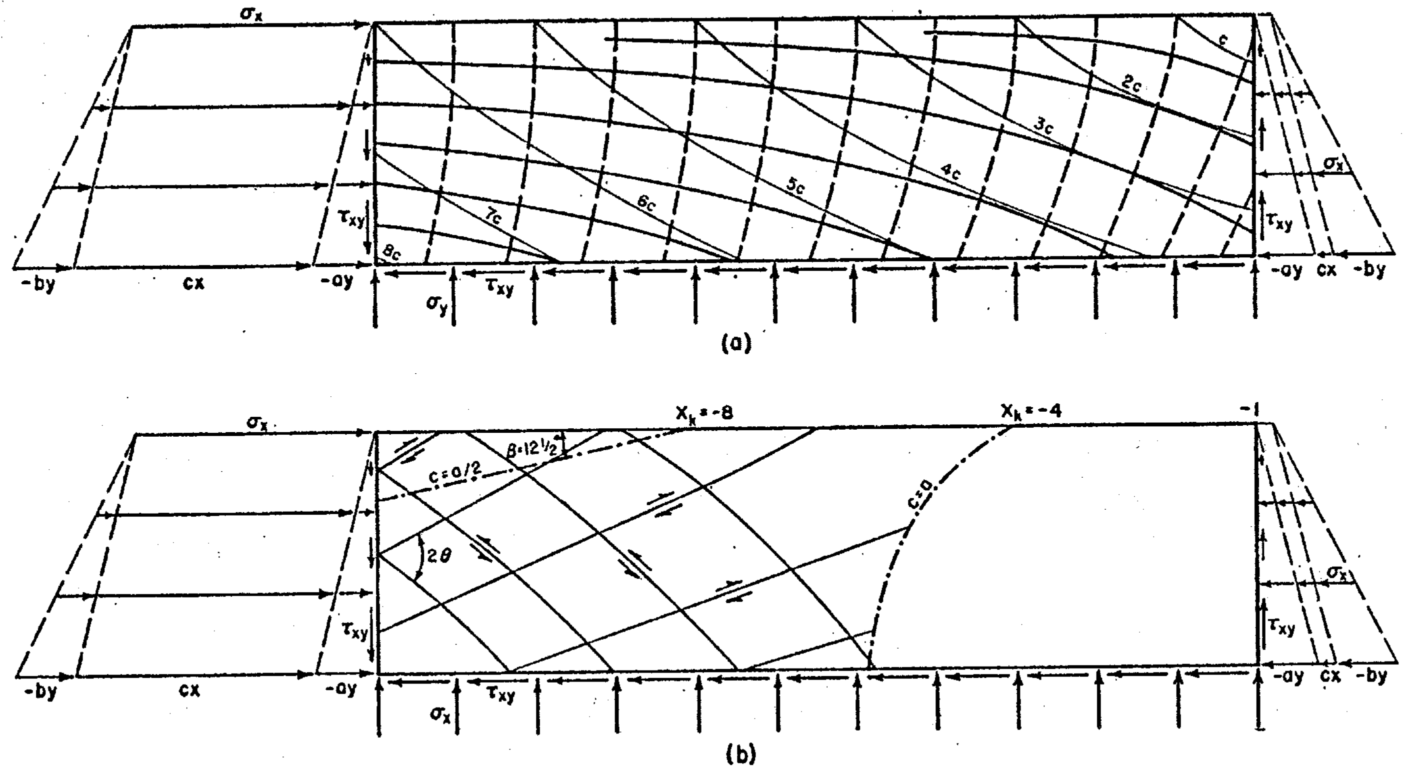

INTERNAL AND BOUNDARY STRESSES:

$\sigma_x = cx - (b+a)\,y$

$\sigma_x = -ay$

$\tau_{xy} = -cy$

a, b, and c are constants

$a = \rho g; \quad -b = c$

LEGEND

(a)
- = *Trajectories of maximum principal pressure* = σ_{min}
- = " " *minimum* " " = σ_{max}
- 4c = *Lines of equal maximum shearing stress* = τ_{max}

(b)
- = *Position of possible thrust-fault surfaces;* $\theta = 32°$
- = *Boundaries of areas of stability for various ratios of* a/c

Thus, Hafner's model is of limited use in describing the kinematics of deformation. Deviations between the orientation of Hafner's predicted strain orientations and dynamic methods should be expected. Local rotational components in the overall irrotational stress field may produce anomalous results.

Deformational structures observed during the course of this study have been subdivided into megascopic structures (mappable at a scale of 1:16,666; generally thrust faults and folds), mesoscopic structures (readily observable at the outcrop), and microscopic structures (visible only in thin section). Local structural trend is approximately 145°, whereas regional trend for the Front Ranges is approximately 157°.

2.3 Megascopic Deformational Features

The distinctive megascopic deformational features within the thesis area consist of the Exshaw Thrust and the Heart Mountain syncline. An excellent strike view of these can be obtained from the Trans-Canada Highway, and is shown in Plate 2.3I.

The Exshaw Thrust is a typical listric concave-up thrust fault within the Front Ranges. Along its length it thrusts Devonian Palliser Formation on top of Mississippian Etherington Formation implying a stratigraphic throw of about 1300 m in

Plate 2.3I Strike view looking south of Heart Mountain and the Exshaw Thrust as viewed from the Trans Canada Highway. Letters designate splays of the Exshaw Thrust; formation abbreviations are described in Figure 2.12. The Ⓑ thrust terminates just beyond the horizon, but is parallel to the Livingstone/Mount Head contact just to the left of the Ⓒ thrust. Access to the mountain top is along a pathway approximately on the trace of the Ⓒ thrust. The false summit in the picture is 6750 feet above sea level; the highway is at 4250 feet.

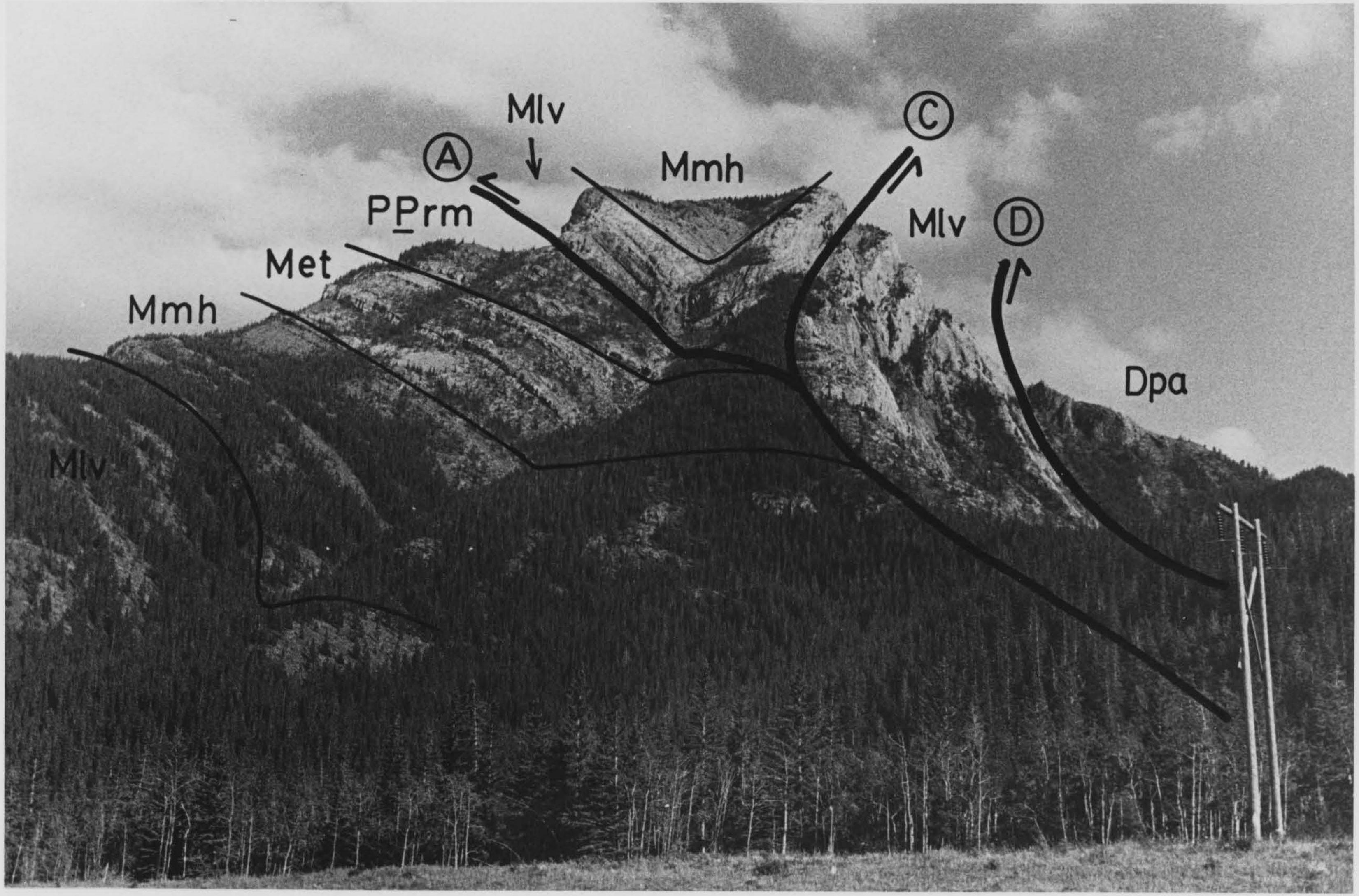

Mlv
Ⓐ
PPrm
Mmh
Ⓒ
Mlv
Ⓓ
Met
Mmh
Dpa
Mlv

the vicinity of the thesis area. The Exshaw Thrust is believed to join the Lac des Arcs Thrust at depth, and both join the McConnell Thrust above the Precambrian basement (Price, 1970).

Within the thesis area the single thrust surface divides to yield four individual thrusts. For simplification, these will be denoted Ⓐ, Ⓑ, Ⓒ, Ⓓ from east to west in both the text and on photographs. The Ⓐ and Ⓑ thrusts are bedding plane parallel. The Ⓐ thrust actually consists of three closely spaced planes of displacement which occur within more argillaceous units of the Livingstone Formation. The Ⓑ thrust dies out along strike within the thesis area, and is not visible from the highway. The geologic survey map (1265A) proposes that the Ⓑ thrust dies out laterally to the southeast as well as to the northwest. Although at the outcrops corresponding to cross section 4 in Figure 2.36 the fault plane was not readily observable, it easily could have existed, as it should be bedding plane parallel, and the rocks are intensely jointed. A doubly terminating fault would not be consistent with the presence of the adjacent "associated" fold in the proposed model (see section 5.1). Plates 2.3II and 2.3III are taken approximately 100 m apart. Plate 2.3II shows the characteristically different exposure of the Ⓑ thrust as compared to the more typical Ⓒ thrust. Direct exposure of the fault plane is usually shrouded by a large amount of surface rubble. Plate 2.3III shows the conformable contact between the Mount Head and Livingstone

Plate 2.3II Southward strike view of the western margin of Heart Mountain taken from outcrop 3-10. Note the characteristically different exposure of the B thrust as compared to the C and D thrusts. Displacement along the B thrust is decreasing toward the foreground. The Livingstone Formation (to the right of the B thrust) is massive and resistant, while the Lower Mount Head Formation (left of the B thrust) is recessive.


B
C
D

Plate 2.3III Conformable Mount Head (Mmh)/ Livingstone (Mlv) Formation contact at outcrop 3-11. The B thrust is observed approximately 150 m southeast of this location to trend parallel to the contact with appreciable displacement.

Plate 2.3IV Calcite filling of tension gashes (?). Very localized and on strike with the B thrust just north of the thrust's termination (see Table 5.1A) within the Livingstone Formation near outcrop 3-11. Gashes form parallel to bedding.


Mmh
Mlv

Plate 2.3V Strike view northward at northwestern ridge of Heart Mountain showing the characteristic outcropping of the B and C thrusts. Both thrusts parallel the vertical bedding. The competent, massive Livingstone Formation is internally undeformed and forms cliffs approximately 50 m high. Note how rubble obscures the trace of the C thrust. Termination of the B thrust occurs approximately 20 m past the horizon.

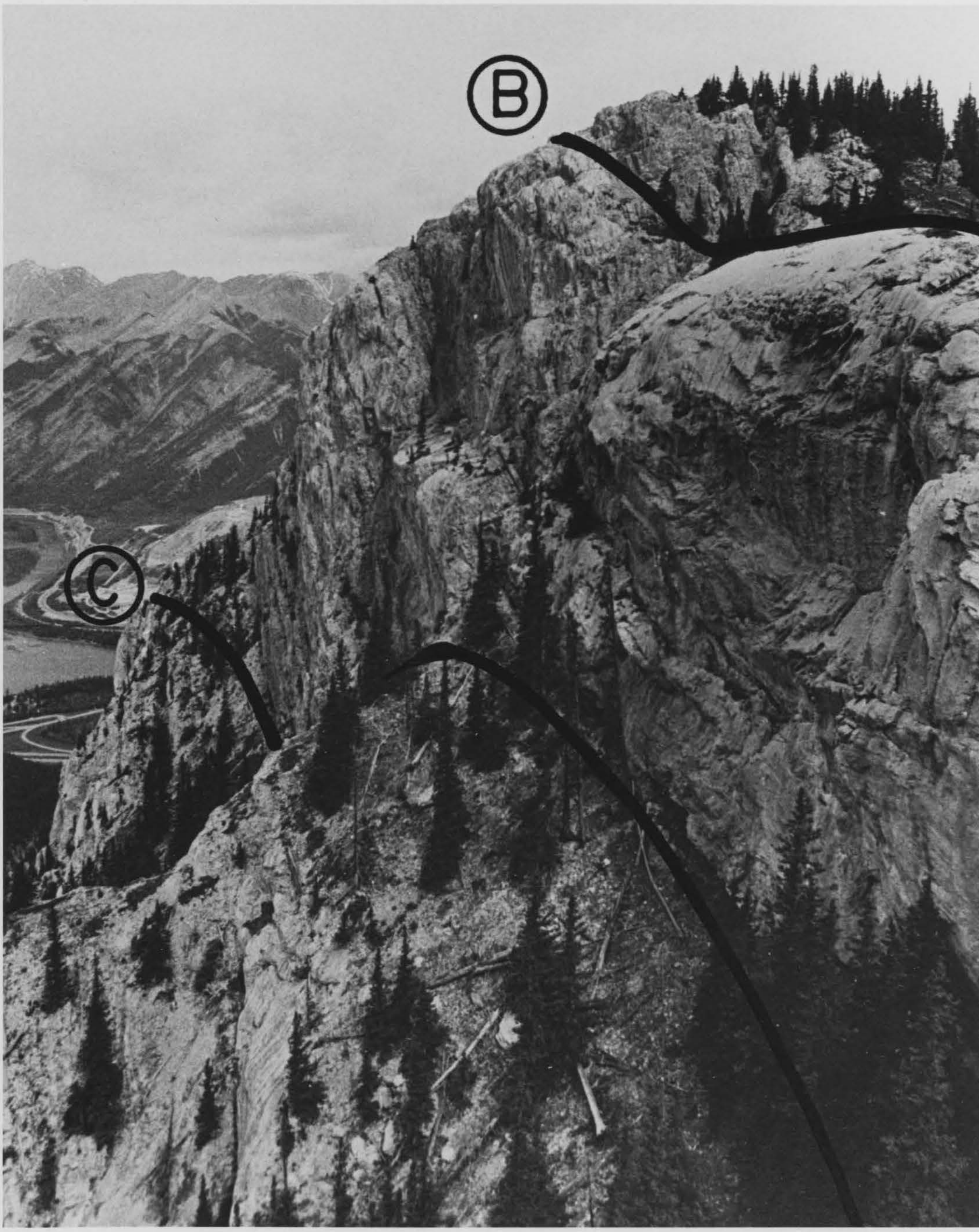
B
C

Formations approximately 20 m past the horizon in plate 2.3V The (A) thrust is believed to be the major thrust from deformation observations, and this is consistent with Dahlstrom (1970) (see Section 1.4). All thrusts within the thesis area strike approximately parallel to the regional structural trend of 157°; dips increase from 35°W to essentially vertical from east to west.

The Heart Mountain syncline is a wedge of Upper Livingstone and Lower Mount Head Formations totally separated from neighbouring rocks by the bedding plane parallel (A) and (C) thrusts. Limbs of the fold are quite straight with a dihedral angle of about 105°. The syncline is faulted out on both ends in the thesis area by the (A) thrust, and is not picked up on strike in adjacent areas.

Careful field observations indicate that the fold is conical through the thesis area. Plate 2.3I shows the northwest face of Heart Mountain in strike view. The summit is produced by the broad, straight limbed Heart Mountain syncline. Plate 2.3VI shows this same syncline at outcrop 1-4 (view is looking north) 550 m to the southeast of Plate 2.3I. Note here that the (B) thrust now has appreciable displacement and the dihedral angle of the fold is approximately 73°. In both cases, substantial structural thickening in the nose of the fold has taken place in the Mount Head Formation. Between these two locations, the axial line strikes 145° and dips gently (approximately 5°) to the northwest. A strike view

Plate 2.3VI The Heart Mountain syncline at outcrop 1-4. The trace of the B thrust is inferred from bedding variations and fracture patterns. Letters designate locations of samples. Note that the Livingstone Formation left of the fault, appears relatively undeformed, while the folded Lower Mount Head Formation is structurally thickened in the nose of the syncline. View is looking north approximately 500 m south of that in Plate 2.3I.

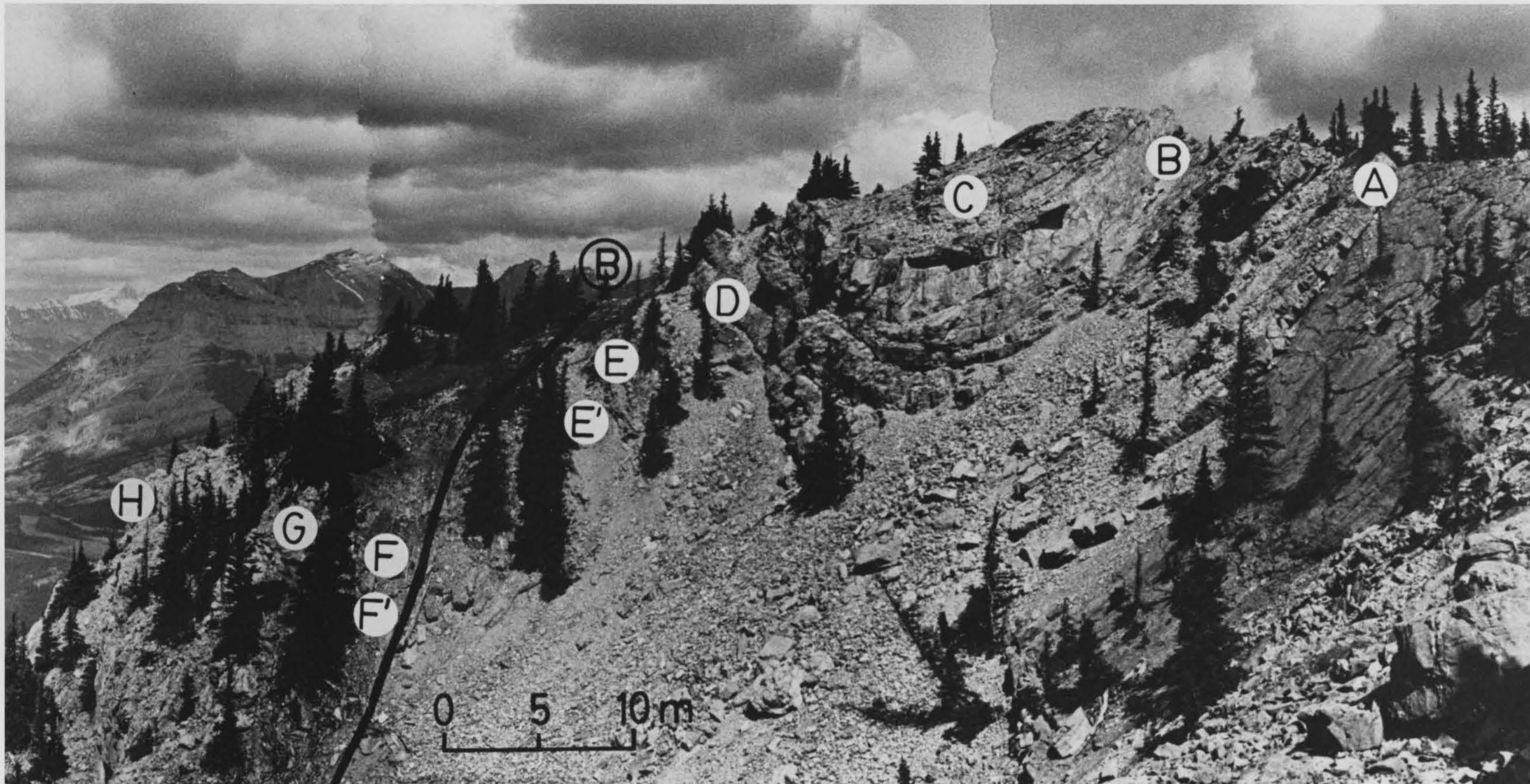

A
B
C
B
D
E
E'
H
G
F
F'
0 5 10 m

from outcrop 6-8 following distinctive lithologies to the next ridge indicates that through this 500 m section, the Heart Mountain syncline changes from a slightly irregular straight limbed acute fold on the ridge just below outcrop 6-13, to an isoclinal fold that is slightly overturned towards the west at outcrop 6-8. The ridge containing outcrop 6-8 was the last observable exposure of the syncline. At this location, the strike of the fold axis is approximately 152° and plunges gently toward the north. The geometric relationships between the folding and thrust surfaces through the thesis area are shown simplified in Figure 2.31.

2.4 Mesoscopic Deformational Features

Mesoscopic deformational features observed during the course of the field work consisted primarily of fractures and minor bedding displacement. Of these, fracturing is by far the greatest mesoscopic deformational feature. Small scale folding and displacement of beds along minor faults was not observed. At most localities, the actual fault contact was obscured by surface rubble, but outcrops less than 5 m from the fault trace exhibited no apparent deformation. Evidence of sulphur within the rocks increased dramatically over a very small distance normal to the thrust surface as did fracture intensity.

Figure 2.31 Schematic view of structural variations throughout the thesis area. Note the termination of the B thrust along strike and the broadening of the Heart Mountain syncline toward the northwest. Compare to characteristics outlined in Table 5.1A.

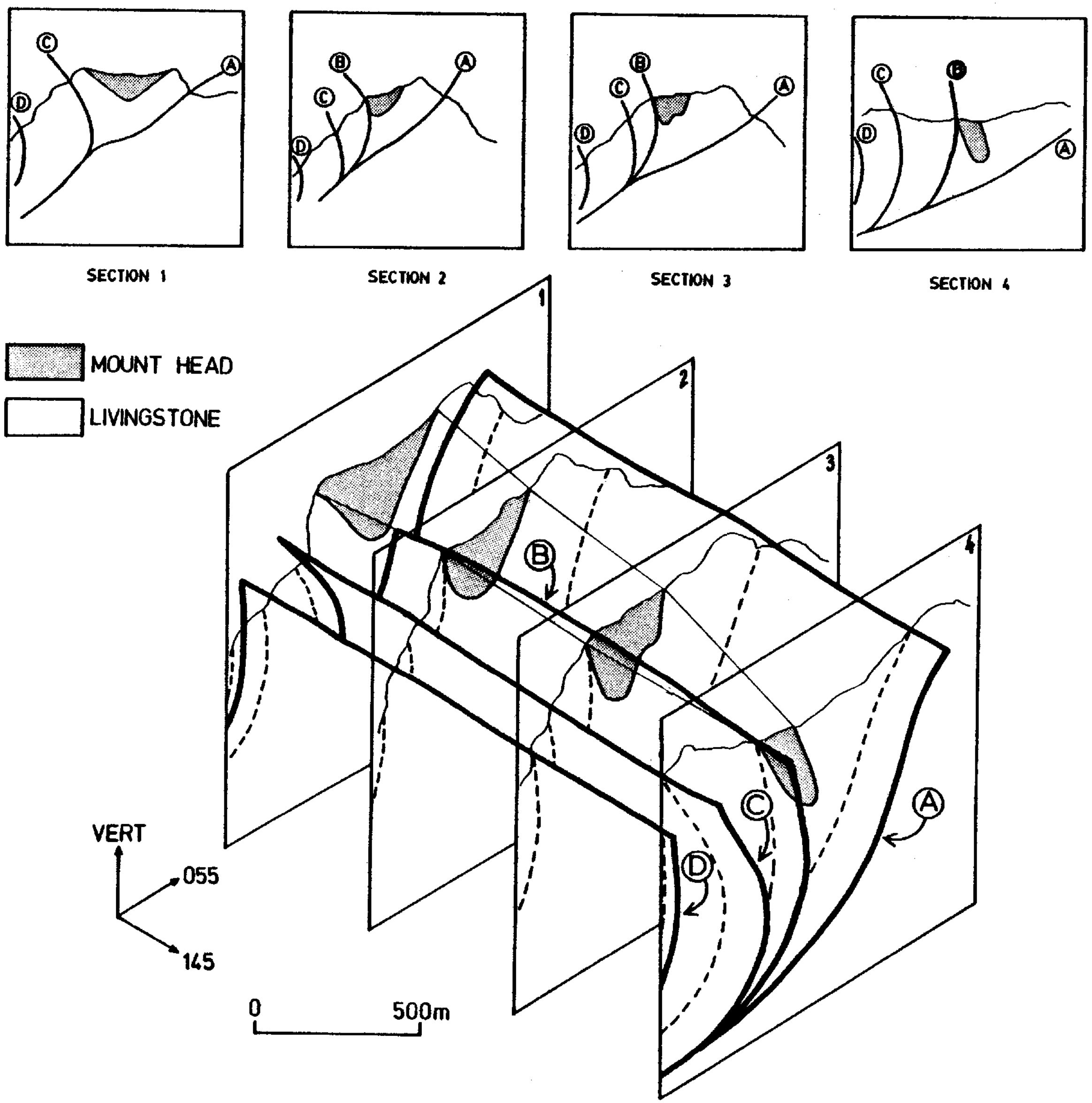

SECTION 1
SECTION 2
SECTION 3
SECTION 4
MOUNT HEAD
LIVINGSTONE
A
B
C
D
1
2
3
4
VERT
055
145
0
500m

Fractures are generally pervasive, but vary somewhat with lithological contrasts, being generally well developed in the Mount Head Formation and poorly developed in the Upper Livingstone Formation. During the course of field work, fracture patterns at outcrop locations were categorized into three groups: random, "strong" and "weak". At all locations, a suitable number of orientations of the fracture sets were taken. The poles to the fracture sets are plotted in Figure 2.41. Impressions from field work indicate that the two major fracture sets and bedding are all mutually orthogonal, the strong set being normal to regional strike and a much weaker set parallel to regional strike. Results indicated in Figure 2.41 substantiate this. In many instances these two fracture sets were difficult to determine because of intense development of random fracture sets.

Figure 2.41 illustrates a distinct human bias. Field impressions suggest that three mutually orthogonal planes exist, but Figure 2.41 suggests that the strong set is perpendicular to the bedding and the "weak set" is rather randomly distributed, but approximately parallel to bedding. Since bedding at most outcrops was nearly vertical, the theoretical weak set proposed would originally have had a horizontal orientation. Thus there was a tendency <u>not</u> to measure them. Field notes substantiate this and many "weak sets" were described as "almost horizontal"; such qualitative descriptions were not plotted. The "weak sets" plotted are

Figure 2.41 Lower hemisphere equal area plot of poles to fracture planes. Strong/weak designation is based on qualitative assessment in the field. For all data, bedding has been rotated to horizontal.

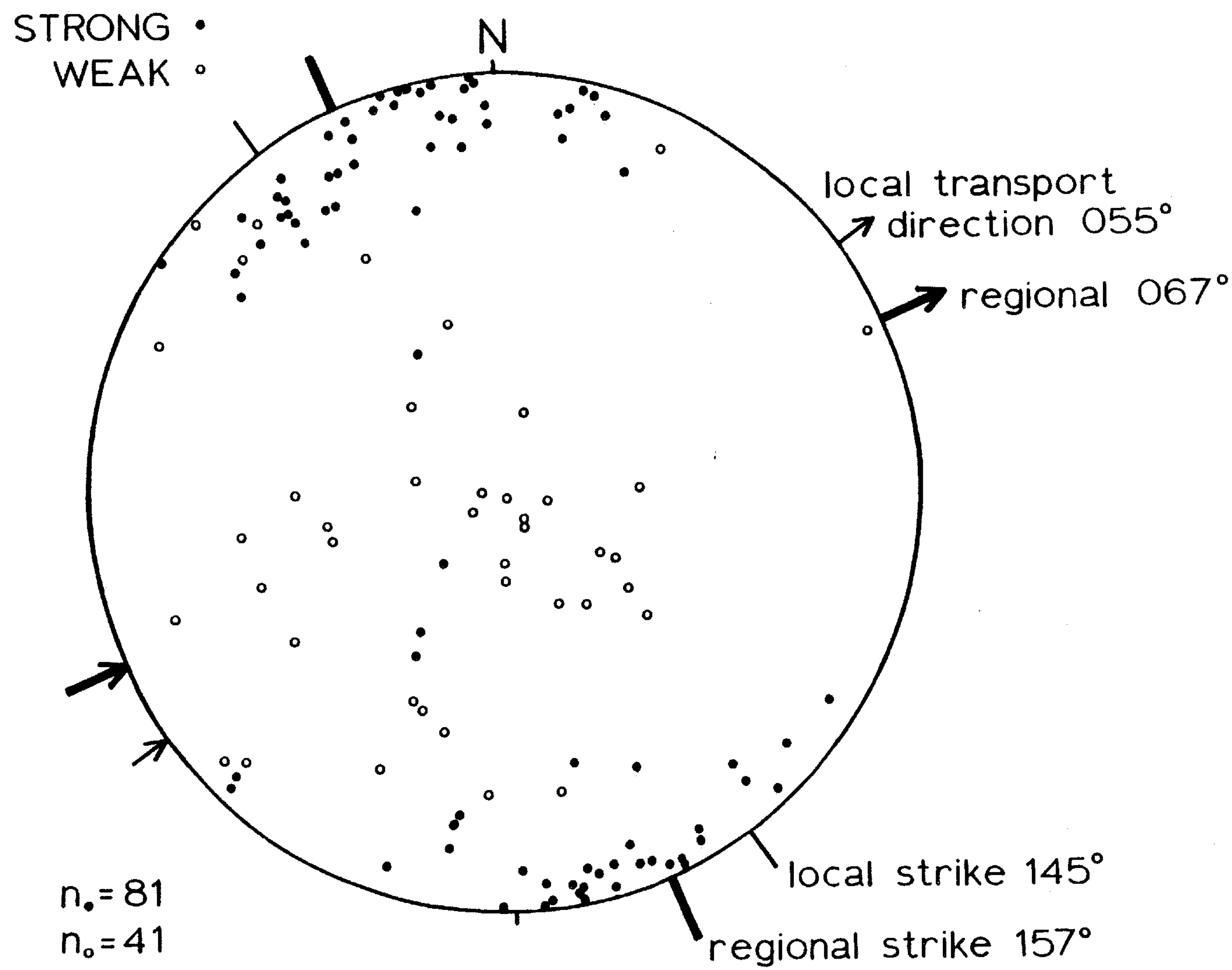
STRONG •
WEAK ∘
N
local transport direction 055°
regional 067°
local strike 145°
regional strike 157°
$n_{\bullet} = 81$
$n_{\circ} = 41$

more likely a random set of bedding plane partings mistaken for joint surfaces.

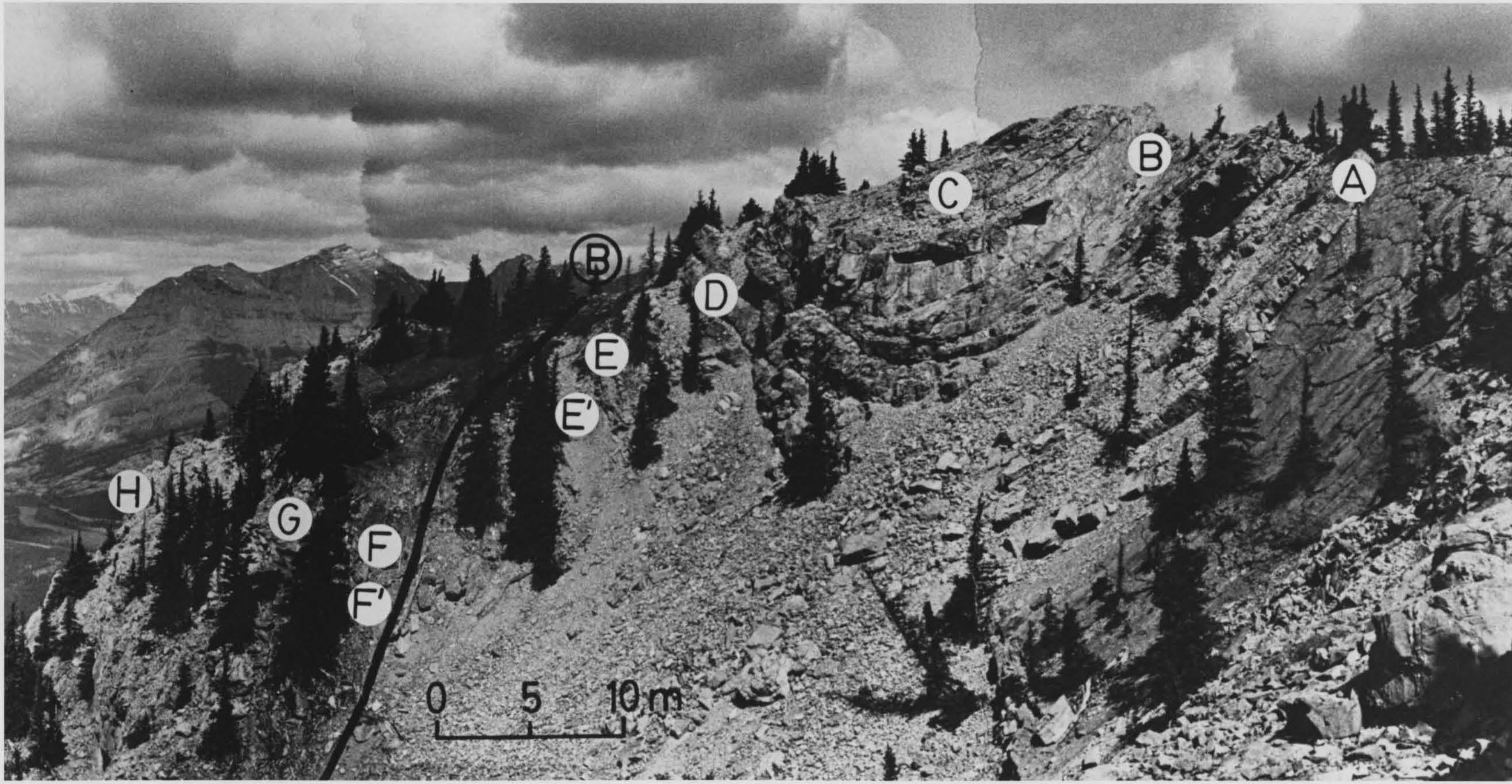
A
B
C
B
D
E
E'
H
G
F
F'
0 5 10 m

Plate 2.4I Well developed orthogonal jointing in the Livingstone Formation near outcrop 3-6. Bedding dips into the page at approximately 45°. Note that the jointing is more strongly developed in the argillaceous horizon. "Strong set" corresponds to the set in shadows. A thrust is about 200 m below.

Plate 2.4II Intense, somewhat random jointing as viewed on a bedding plane within the Livingstone Formation at outcrop 3-10. B thrust is approximately 30 m away and has only a minor amount of displacement. Tape measure is 20 centimeters long.

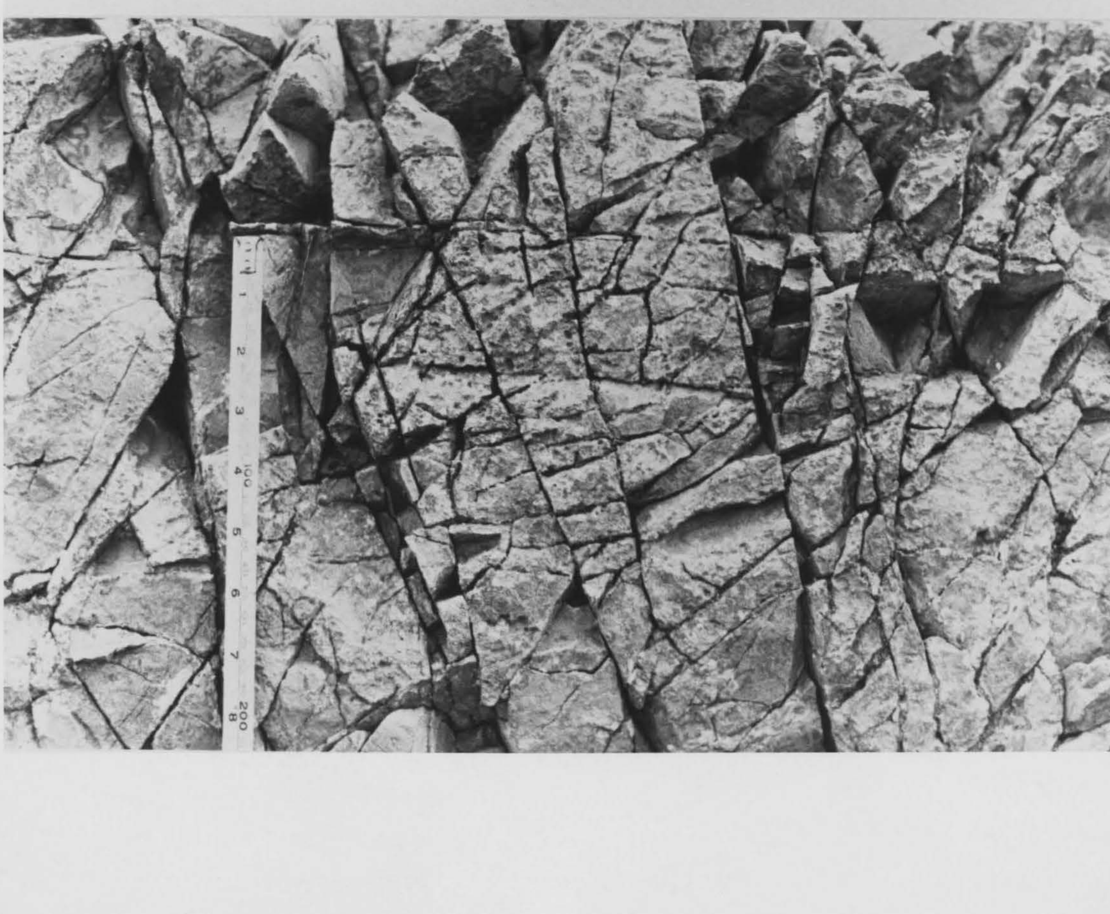
1 2 3 4 100 5 6 7 200 8

Plate 2.4III Plan view of bedding plane of Livingstone Formation within the Heart Mountain syncline at outcrop 4-1. Bedding is essentially vertical. Three major joint sets are seen:

W = weak set subparallel to the fold axis (arrow)

S = strong set parallel to transport direction

L = late, widely spaced set; apparently not related to the stress field which determines W and S

W and S are normal to bedding; L is oblique to bedding. Mount McGillvary is seen in the background.


W
S
L

Plate 2.4IV Well developed "strong joints" perpendicular to bedding and parallel to regional transport direction in Upper Rocky Mountain Group at outcrop 3-4 approximately 200 m from the A thrust. Note that jointing is pervasive throughout the varying lithologies. Plane of view corresponds to the "weak set".

Plate 2.4V Fracture patterns in Mount Head Formation at outcrop 1-4D. Jointing is regular, but not orthogonal.

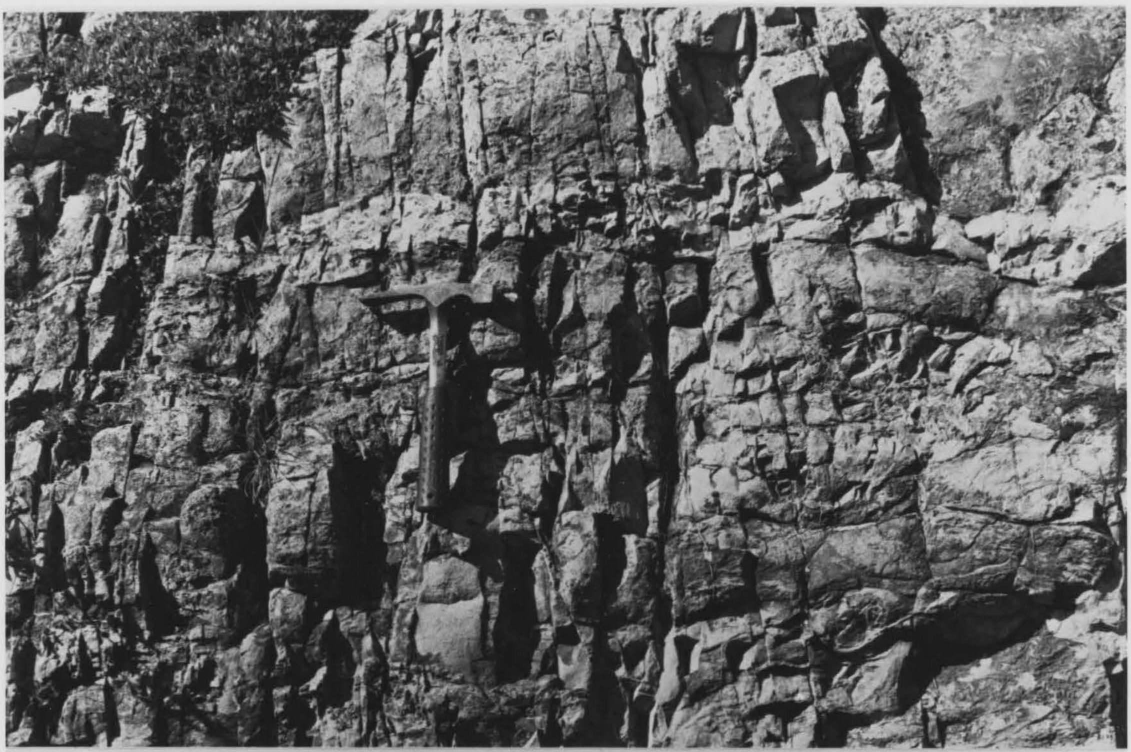

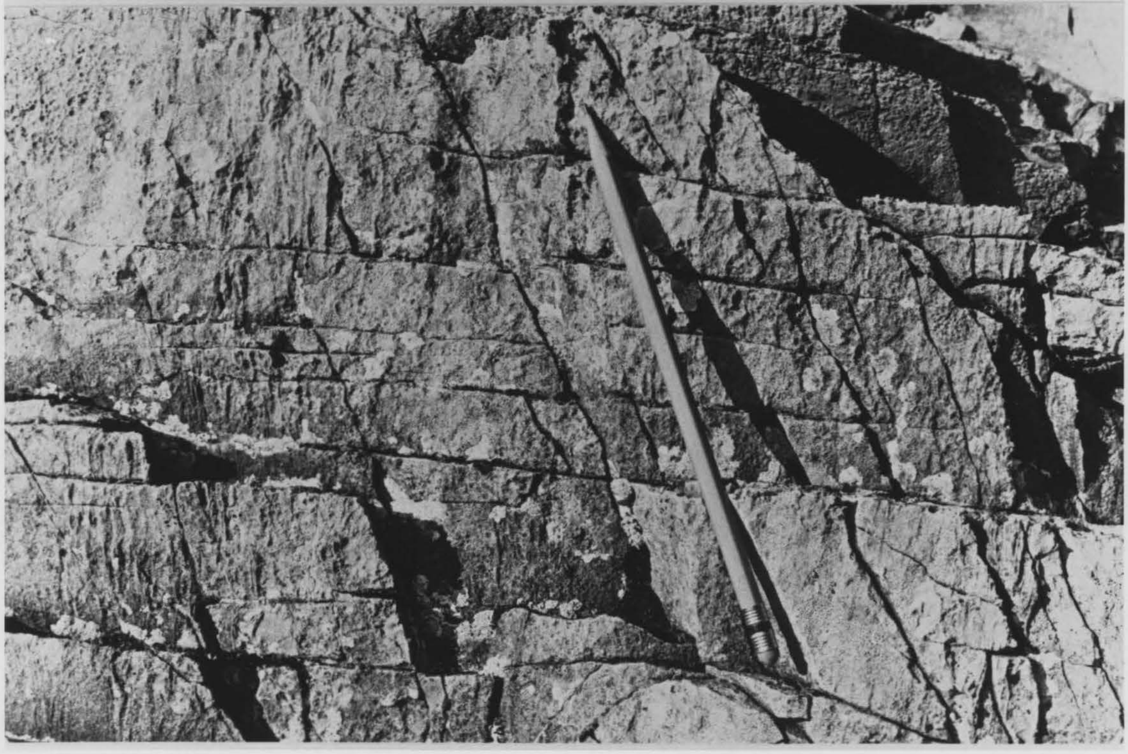

MICROSCOPIC STRUCTURAL GEOLOGY

3.1 Laboratory Procedures

Seven oriented samples of a total 26 collected in the field were considered coarse enough for optical dynamic analysis. These were re-oriented in the laboratory in a large container of small lead pellets for maximum accuracy and stability during this process. Thin sections were then cut perpendicular to the local structural trend at an orientation of 055° and vertical. These sections were then examined using a Leitz 4-axis universal stage to determine the orientation of c-axis and twin lamellae (after the technique of Groshong, 1976; and Turner and Weiss, 1963, p. 197 - 203) for use in the dynamic analysis. Glass hemispheres and mineral oil of refractive index approximately equal to that of calcite were chosen so as to minimize any optically induced tilts. Equant grains (i.e. crinoid ossicles) with two well-developed "thick twin" sets were preferentially measured. The tedious reduction of data was greatly simplified by the computer program TWIN of Groshong (1972, 1974). This computer program calculates strain magnitudes and orientations as well as the numeric dynamic analysis axes of Spang (1971, 1972) from oriented twin data. All slides were point counted (300 counts) to determine the percentage of grains untwinned, "thin twinned", and with one, two, or three twin sets.

3.2 Pressure Solution and Microfracturing

Evidence of pressure solution in the form of stylolitization is pervasive, but is of minor importance throughout the thesis area. Stylolites seen can be grouped into two broad families:

(1) parallel to bedding

(2) normal to bedding

those parallel to bedding being the most abundant. No change in the amount of stylolitization was seen with distance from the fault. Stylolites persist through varying grain sizes, although they are best developed in the micritic zones, perhaps as an alternate method of intragranular deformation due to the increased surface area per unit volume. As plate 3.2I suggests, stylolites commonly cut twinned calcite grains.

Microfracturing within the thesis area varies drastically with distance from the fault, and increases rapidly over a very short distance normal to the fault. The few samples obtained from the fault zone indicate that microfracturing is the dominant microscopic deformational feature. At all locations the orientations of microfractures appeared random, varying primarily with lithological contrasts. Boundaries between calcite grains and micrite were preferentially exploited.

Plate 3.2I (A) Stylolite cutting through twinned carbonate grains suggesting formation after twinning. Outcrop 2-3, magnification 160x, crossed polars.

(B) As above, stylolite is sharp through the grain, but "beads" in the micrite. Outcrop 1-4E-2, magnification 25x, crossed polars.

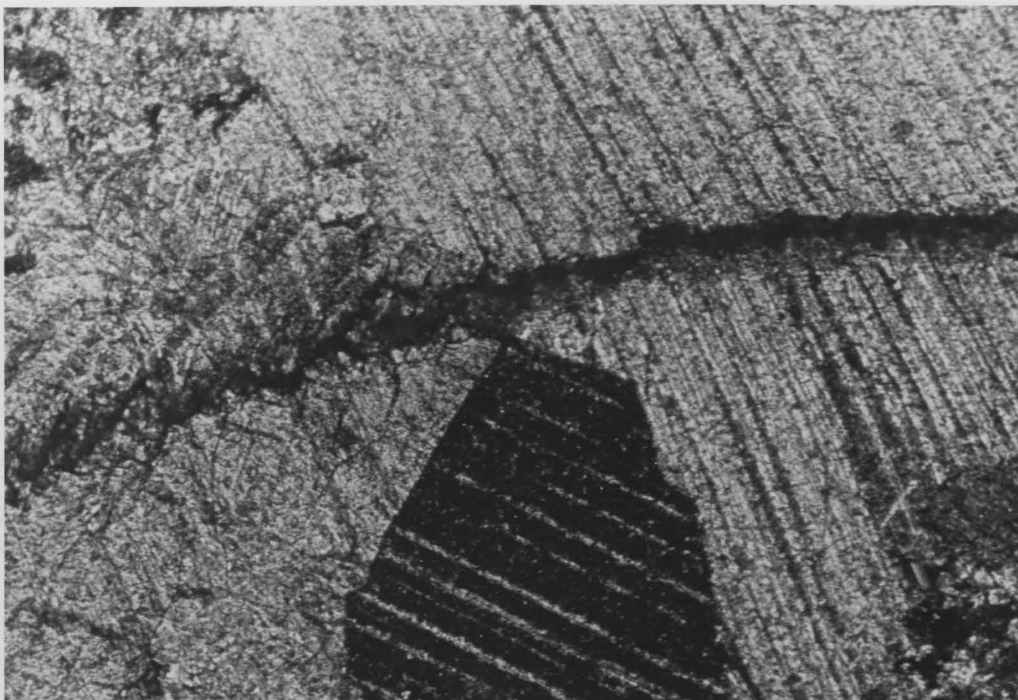

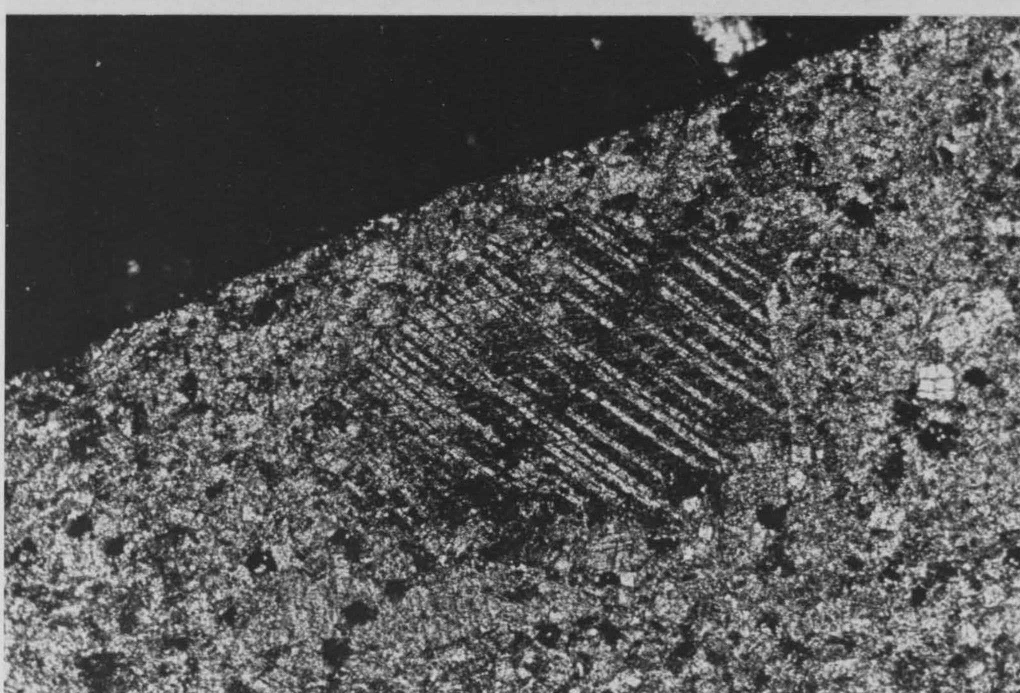

3.3 Carbonate Twinning

Twinning along the e{0112} plane is pervasive in the thesis area, but only those sections containing a suitable (>25) number of twinned grains with diameters greater than about 50 microns were observed intensely. The mechanics of carbonate twinning is discussed in Appendix A1. All samples for which Numeric Dynamic Analysis (NDA) was performed were point counted (300 points per section) to determine the percentages of twinned carbonate material. The results are presented in Table 3.3A. Twinning in calcite was primarily of the "thick" variety; that is, a measurable thickness of twinned material was observable between adjacent portions of host. Twinned material is identified under crossed polars as a band of dark material within a light host. Optical continuity between the twin and host is lost due to gliding. The host and the twin alternate in extinction.

The majority of the Upper Livingstone Formation (from which most samples were taken) is composed of micritic calcite and dolomite. Grains coarse enough for NDA were primarily from fossils, fractures, or the occasional coarse grain dispersed in a fine matrix. Observations indicate that there is no consistent trend in the degree of twinning. Plots of percentage grains twinned versus both longitudinal distance along the fault and distance perpendicular to the fault showed negligible correlation. Throughout the entire thesis

TABLE 3.3A

POINT COUNT RESULTS
(CARBONATE MATERIAL ONLY)

Section	Micrite	Untwin	Number of Twin Sets: One	Two	Three	Thin Twin
5-4 (Mlv)	132 44.0%	93 31.0%	43 14.3%	17 5.7%	0 0	15 5.0%
4-5 (Mlv)	124 41.3%	90 30.0%	41 13.7%	26 8.7%	2 0.7%	17 5.7%
4-4 (Mlv)	38 12.7%	68 22.7%	122 40.7%	41 13.7%	0 0	31 10.3%
4-2 (Mlv)	74 24.7%	124 41.3%	49 16.3%	26 8.7%	0 0	27 9.0%
3-5 (PPrm)	65 21.7%	132 44.0%	44 14.7%	35 11.7%	0 0	24 8.0%
3-7 (Mlv)	174 58.0%	62 20.7%	36 12.0%	14 4.7%	0 0	14 4.7%
6-10 (Mmh)	155 51.7%	80 26.7%	37 12.3%	12 4.0%	0 0	16 5.3%

area, it is therefore concluded that the shear stress associated with the Laramide Orogeny exceeds the critical value required for the initiation of crystal gliding (see Appendix A1). Untwinned grains therefore result from late (post orogenic) recrystallization of calcite in cavities and/or highly unfavourable angular relationships between the c-axis and σ_1 (see Appendix A1). Variations in the amount of twinned material observed can be accounted for by lithological variations. Finer grained samples characteristically contain fewer twinned grains.

Numerous grains contained more than one twin set. Often the chronological order of the twin sets can be determined through observation of kinking and distortion. Plates 3.3IC and 3.3IIA show examples of this. The later twin set kinks the earlier one due to the glide mechanism. Plate 3.3IIA also shows good evidence of grain boundary effects on e-twinning. Groshong (1972) makes the assumption that each grain may be treated as having been independently twinned (see Appendix I, Absolute Strain Calculation). Evidence from this study indicates that this is not strictly true in all cases, but in general it is. Moffat (1980) found similar grain boundary effects.

Plate 3.3I

(A) Typical microscopic appearance of the Upper Livingstone Formation. Note abundant very fine micrite, dolomite with "thin twins" and 3 well developed thick twin sets in a crinoid ossicle. Outcrop 4-2, magnification 63x, crossed polars.

(B) Heavily twinned and slightly kinked thick twins in calcite. Numerous truncations of one twin set by another are evident. Outcrop 4-2, magnification 63x, crossed polars.

(C) Kinked twins in one calcite grain in sutured contact with another untwinned grain. Second grain is not twinned due to unfavourable crystallographic orientation, suggesting that the differential stress was not greatly past the critical shear stress required for e-twinning in calcite. Outcrop 4-5, magnification 63x, crossed polars.

(D) Enlargement of plate C; note the small amount of twinning occurring in the "untwinned grain" adjacent to the contact. This suggests that grain boundary effects exist (see also Plate 3.3II). Outcrop 4-5, magnification 250x, crossed polars.

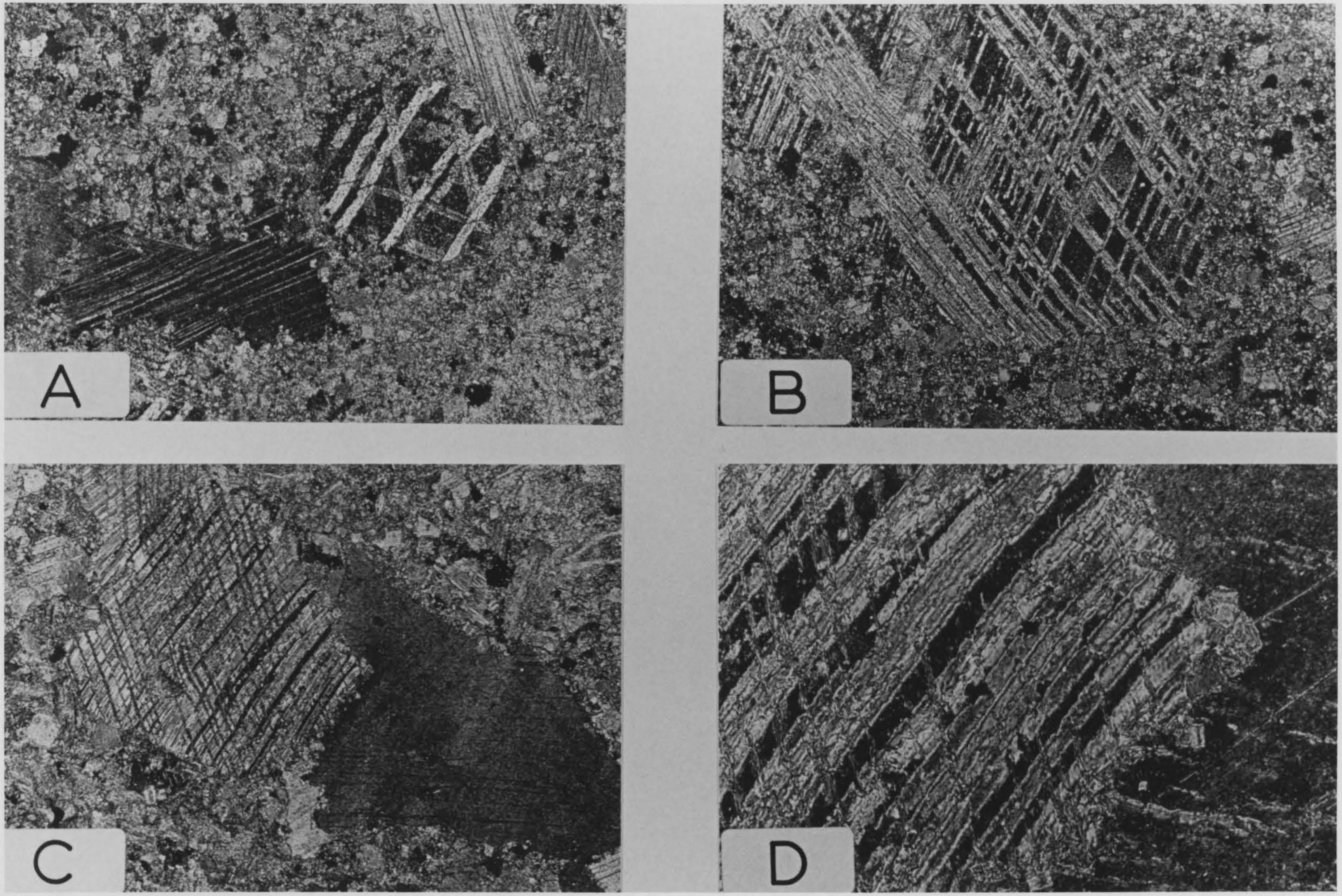
A
B
C
D

Plate 3.3II

(A) Grain boundary effects inducing e-twins in calcite. Twins from grain A induce twinning in grain B (see arrows) which distort a weaker and thinner earlier set. Note also the microfracturing (bottom left) preferentially exploiting the boundary between grains and micrite. Outcrop 4-2, magnification 63x, crossed polars.

(B) Close up of thick twins in a crinoid ossicle. Note how the twins are relatively constant in thickness; this is a practical assumption of the NDA theory. Orientation and measurement of twins is based on how sharp the boundary is. The twin set marked by the arrow is being viewed somewhat obliquely; the universal stage would be rotated to achieve a sharp boundary before measurement. Outcrop 4-4, magnification 63x, crossed polars.

(C) Dolomite thin twins adjacent to calcite twins. Outcrop 4-4, magnification 63x, crossed polars.

(D) Sparry twinned calcite filling void within a brachiopod surrounded by micrite. Outcrop 4-4, magnification 63x, crossed polars.

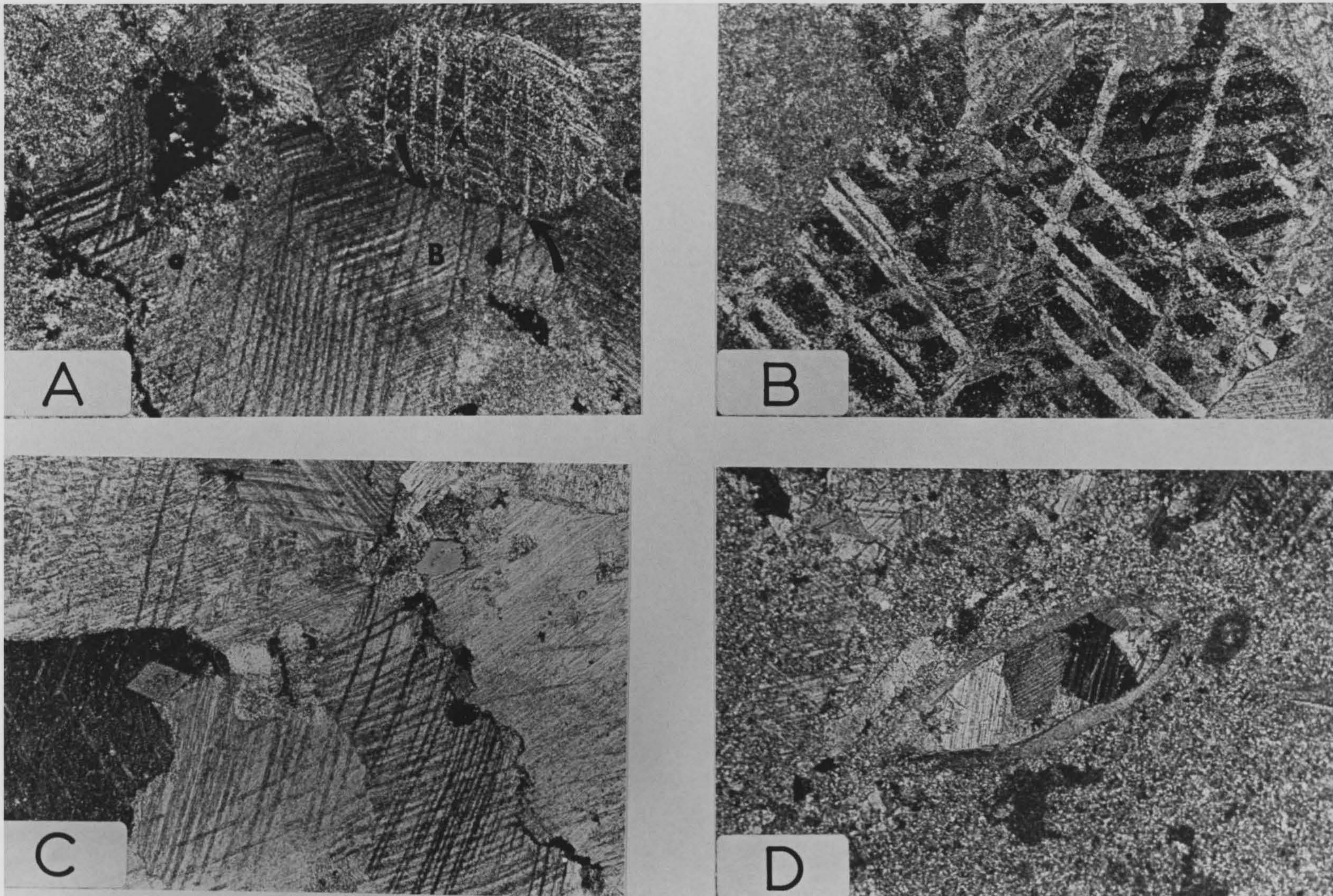
A
B
C
D

Figure 3.31 Calcite lattice with twinning along the e{01$\bar{1}$2} crystallographic plane. Section viewed is normal to zone axis a_2. Calcium ions are represented by solid large circles; CO_3 groups are shown as grouped circles (much reduced in size). Note the change in orientation of c-axis between twinned and untwinned calcite.

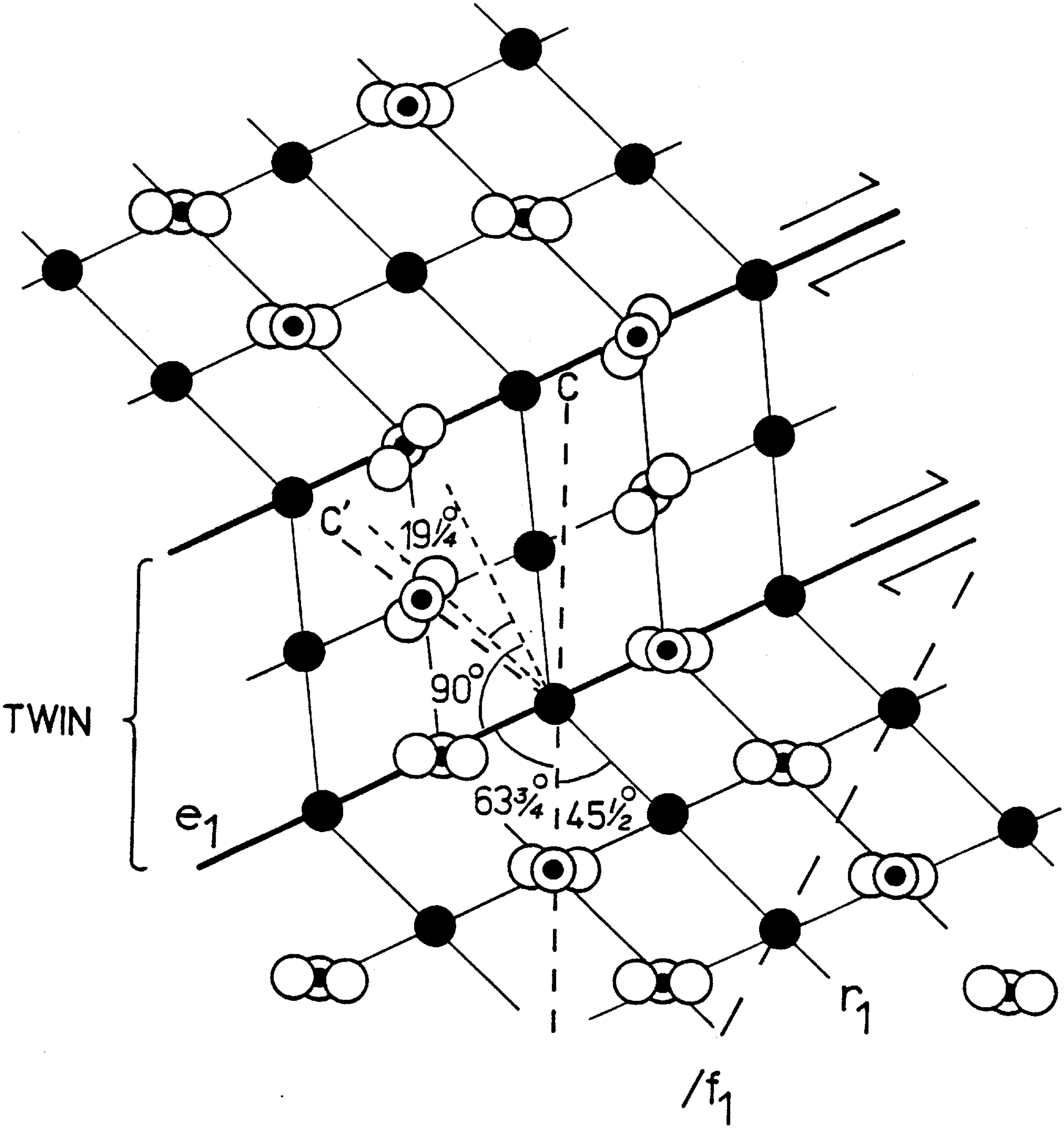

TWIN
c
c'
$19\frac{1}{4}^\circ$
90°
$63\frac{3}{4}^\circ$
$45\frac{1}{2}^\circ$
e_1
r_1
f_1

NUMERIC DYNAMIC ANALYSIS

4.1 Introduction

Under the (P,T) regime that is thought to have existed throughout the thesis area at the time of deformation (approximately 1.5 kb and 200°C) intragranular deformation of calcite occurs as a glide (twinning) along the e crystallographic plane. Since the orientation of gliding with respect to crystallography is fixed, and the critical shear stress required for glide initiation is know, a randomly oriented sample of twinned grains should be able to give a statistically reliable indication of orientations of strain axes. Groshong (1974) gives the upper limit of accurate strain determination as 8.5 per cent.

Spang (1974) interprets the results of the NDA as stress, assuming that the aggregate strain is irrotational and that the magnitude of differential stress is not so great that other (less favourable) crystallographic glide planes are exploited. The assumption of irrotational strain has a profound influence on the theoretical interpretation of twinning events and their dynamic meaning. Brown (1976) concisely summarizes the possible interpretations of both rotational and irrotational strain models in terms of twinning. This is given in Table 4.1A.

The values of the NDA axes determined are minimal if the stress field responsible for the twinning is continually

Table 4.1A

SUMMARY OF STRAIN MODELS

Irrotational Strain	Rotational Strain
Twinning occurs in response to one or more stress systems which maintain an orthogonal relationship to the strain axes. Both stress and strain ellipsoids may be stationary, or rotating with respect to an external coordinate system. Twinning may be continuous or discontinuous. A unique solution exists.	Twinning occurs at several discrete moments in a continuously rotating stress field relative to the strain ellipsoid. No unique solution exists.
Twinning occurs at one discrete moment in a continuously rotating stress field relative to the strain ellipsoid. A unique solution exists.	Twinning occurs continuously in a rotational environment with respect to the stress field. No unique solution exists.

after Brown (1976)

rotating or is variable and discontinuous. In both situations an overprinting effect of strains is seen on the grains. Jamison (1974) states that the NDA tensor can be viewed as the sum of the NDA-C tensor and the NDA-T tensor, these tensors being derived from the compressional and tensional axes respectively. Irrotational singular stress fields produce a bimodal distribution of compression axes, whereas an equatorial distribution may indicate superimposed stress fields.

Since both NDA and least squares strain gauge techniques are based on twinning, they represent intragranular strains only and do not provide an estimate of strain accounted for by other mechanisms (for example, faults, pressure solution, etc.) (Stockmal, 1979).

4.2 Error and External Biases

The value of information obtained by numeric dynamic analysis is subject to scrutiny due to errors associated with sample collecting, microscope measurement, external biases of mechanical and human origin, and theoretical assumptions. Samples obtained in the field were marked by horizontal lines and an arrow of know azimuth. During thin section preparation, the samples were re-oriented in the lab. Jamison (1974) very roughly estimates the maximum reasonable error that may be introduced during each step of this process as 5°, giving a maximum possible error due to orientation of 10°. Hopefully the error is substantially less than this due to careful measurement and the chance of cancellation of orientation errors.

During the course of measurements of twin lamellae and c-axes on the universal stage, the chance for numerous errors exists. A reasonable estimate of precision is approximately ±2° based on an intuitive feel for the process. As data were collected, they were also plotted on a stereonet to observe the angular relationship between the c and e poles. These two poles should ideally be 26° apart (see Figure A2, Appendix I). If the measured orientations deviated by more than ±4° from this value, the grain was re-measured. Grains with two or more twin sets were preferentially measured to provide a second internal method of measurement consistency. With two twin sets, <u>both</u> must be oriented 26°±4° to the c-axis. The relatively large range of accepted values is due to the problems inherent in determining the orientation of the c-axis through extinction. The computer program also gives the calculated angle between c and e to further screen out error measurements.

Measurement of twinned grains on the universal stage is limited to the extent of rotation about the horizontal axis (about 50°). This is an absolute maximum. Figure 4.21 indicates that twin lamellae could only be measured effectively if they are oriented at an angle greater than 65° to the plane of the thin section. Grains with horizontal (within 35°) c-axes were the only grains incorporated in this study. Calcite c-axes may also be deduced when they are in a vertical position, but

Figure 4.21 Lower hemisphere, equal area plots of poles to crystallographic c-axes and e-twin planes for calcite. Note angular zonation of observed measurements and random orientation of c-axes.

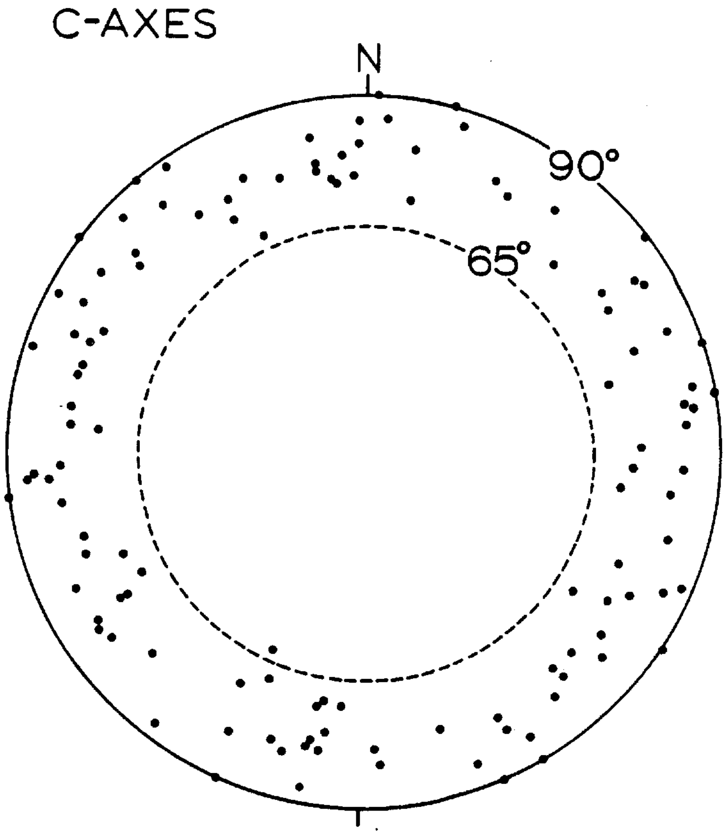
C-AXES
N
90°
65°

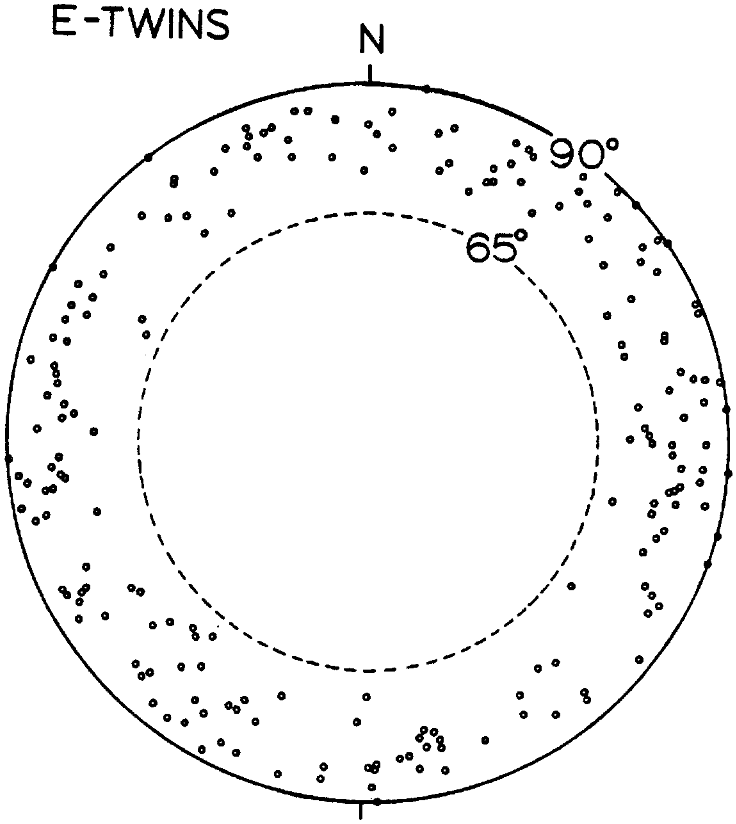
E-TWINS
N
90°
65°

due to the difficulty the author found in consistently identifying these, they were not used. Therefore out of a possible 180° orientation of c-axes, only those within a specific 70° arc were used. This bias of measuring only those grains inclined within a specific angular range to the plane of the thin section may be remedied by cutting two orthogonal thin sections. Jamison (1974) used three mutually perpendicular thin sections to provide complete statistical analyses of the biasing resulting from the limitations of universal stage rotation.

Calculation of strain magnitudes through this technique requires various initial assumptions (see Appendix I, Section A-4). Figure 4.21 illustrates that c-axes within the samples investigated are randomly oriented. It is assumed that each grain acts as an individual independent strain gauge. This may not be strictly correct; plate 3.32A suggests that twinning within one grain may induce twinning in the adjacent grain in some instances. Experimental evidence by Twombly (1980) and field work by Moffat (1980) also indicate this.

4.3 NDA Results

Twin measurements were obtained according to the procedure outlined in Section 3.1. For a more complete summary of this technique, see Groshong (1976). The data were then run through the computer program TWIN (see Appendix II). Data was edited by:

Figure 4.31 Poles to computer determined compression axes. Ideal distributions for non-rotational strain should be bimodal along a great circle.

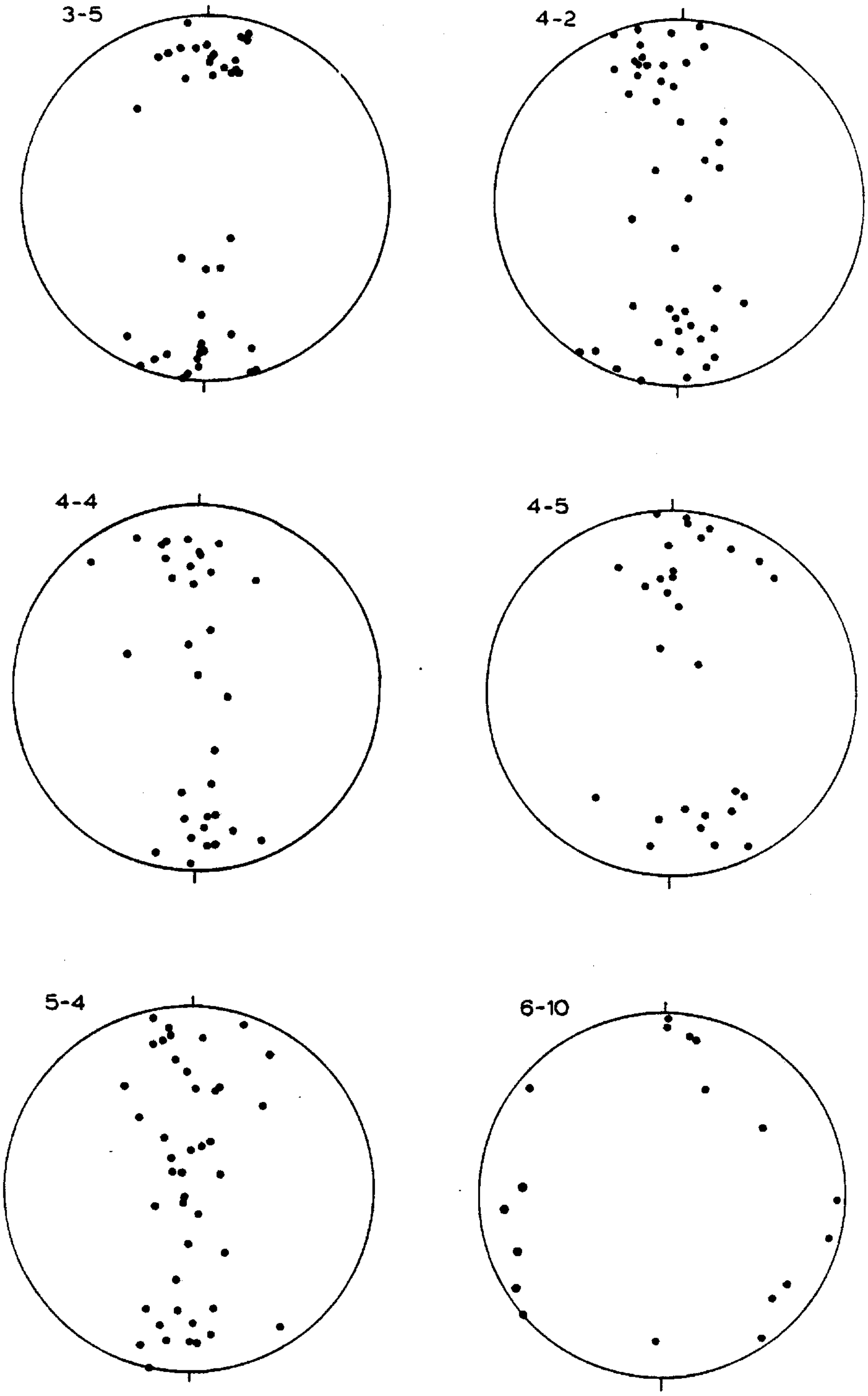
3-5
4-2
4-4
4-5
5-4
6-10

TABLE 4.3A

COMPRESSION AXES DISTRIBUTIONS

Sample	Formation	Results
5-4 *	Livingstone	- indefinite, tending toward equatorial
4-5 *	Livingstone	- bimodal
4-4 *	Livingstone	- bimodal
4-2 *	Livingstone	- slightly bimodal
3-5 #	Rocky Mountain	- strongly bimodal
6-10@	Mount Head	- random

Structural subdomains:

* Exshaw Thrust Plate

McConnell Thrust Plate

@ Heart Mountain Syncline

TABLE 4.3B

NDA RESULTS

Numeric Dynamic Analysis (Stress)

SAMP.	NDA_1		NDA_2		NDA_3	
	magn.	orient	magn.	orient	magn.	orient
5-4	.219	199/41	.025	351/45	-.243	096/15
4-5	.435	228/79	.003	007/08	-.437	098/07
4-4	.250	246/67	-.037	350/06	-.213	082/23
4-2	.277	208/80	.009	355/09	-.286	086/06
3-5	.579	244/81	.021	090/08	-.600	359/04
6-10	.108	204/54	.050	041/35	-.158	306/08

Least Squares Strain

SAMP.	E_1		E_2		E_3	
	magn.	orient	magn.	orient	magn.	orient
5-4	.911	177/02	-.433	018/88	-.478	267/01
4-5	.182	267/63	-.007	144/15	-.175	048/21
4-4	.116	163/08	.014	258/27	-.130	058/60
4-2	.078	035/46	-.037	151/23	-.041	258/35
3-5	.166	164/01	.027	048/87	-.193	254/03
6-10	.151	053/08	-.064	286/78	-.088	144/10

Average NDA_1, NDA_2, NDA_3 with beds rotated to horizontal:

NDA_1 = 246/03 NDA_2 = 340/02 NDA_3 = 159/84

STRUCTURAL INTERPRETATIONS

5.1 Mega- and Mesoscopic Fabrics

Regional strike of bedding, fold axes and faults within the Front Ranges indicates an orogenic transport direction of approximately 067°. Local variations in this trend suggest that in the Heart Mountain region, transport was approximately 055°.

Within the thesis area, the principal megascopic structures of note are:

(1) the lateral termination of the B thrust to the NW

(2) the development of a gently northward plunging conical fold adjacent, and parallel, to the Exshaw Thrust

(3) very steep (essentially vertical) C and D imbricates of the Exshaw Thrust

Evidence gathered suggests that (1) and (2) above may be related to displacement transfer between deformational features. Many accounts of thrust faults coring into anticlinal structures have been published, but few studies have incorporated field observations and modelling predictions. Gardner and Spang (1973) propose three modes of displacement transfer based on experimental evidence and provide geologic analogues from the Front Ranges. These are:

(1) simple thrust to fold transfers

(2) doubly terminated thrust transfers, and

(3) multiple thrust to fold transfers

The termination of the B thrust and the synclinal peak at Heart Mountain seem to fit into the first case given above with a few minor modifications. Figure C of plate 1 in Gardner and Spang (1973) seems to simulate the geological conditions at Heart Mountain quite well. The deformational model as it applies to Heart Mountain will be elaborated on in Section 5.4 during the discussion of structural development, but Table 5.1A summarizes the deformational characteristics of the experimental model and those observed at Heart Mountain.

Deformation at Heart Mountain differs significantly from that outlined in the Multiple Thrust transfer model in fault geometry. Whether this is a function of lithologic variations producing significant changes in the expression of deformation, or theoretical inadequacies of the model, cannot be ascertained from this study. For this reason, the simplest model is chose, and the effect of the previous faults (C and D) are added separately as complicating features.

The lack of arcuate trace of the thrust fault at the terminus is interpreted to result from a much smaller gradient of displacement transfer from the B thrust to the

TABLE 5.1A

EXPERIMENTAL MODEL-THESIS AREA COMPARISON

EXPERIMENTAL MODEL (Gardner and Spang, 1973)	HEART MOUNTAIN (this study)
- syncline develops on strike with thrust undergoing displacement transfer, anticline offset but en echelon	- syncline on strike with thrust traces, anticline faulted and/or eroded off
- folding has conical geometry (atypical for thrust zones), becoming broader away from the thrust termination	- syncline is conical and broadens away from the termination of the thrust
- local transport direction diverges from regional direction in the displacement transfer region	- transport direction at Heart Mountain is locally divergent from regional trend
- fanning effect of thrust plate produces σ_1 normal to the advancing edge, and σ_3 parallel to the advancing edge	- twin data indicates that σ_1 is normal to the fault strike, and σ_3 parallel to the fault strike (see Figures 5.25 and 5.26)
- tension gashes at fault terminus	- tension gashes(?) (plate 2.3IV) at fault terminus
- folding begins at termination tip	- folding begins before fault termination
- fault block is a homogeneous single layer	- stratigraphy is non-homogeneous, the structure is probably determined by the thick, competent Palliser and Livingstone Formations
- fold axes and thrust traces are arcuate in termination region	- thrust traces show no deviation, fold axis is slightly arcuate

syncline since some displacement transfer also occurs to the C and D thrusts, over a distance of a least 1 kilometer. Thus the simple shear generated at the terminus is spread over a distance therefore decreasing the gradient of displacement transfer, and the fault is not as arcuate. The "overlap" of the B thrust and the syncline can also be accounted for in this manner.

Gardner and Spang (1973) observe all these features within their experimental model at strains of about 10 per cent. This is comparable to the 8.5 per cent strain that Groshong estimates for the limit of valid NDA results.

Part of the uncertainty involved in producing a model for the deformation is that the wedge of Mount Head and Livingstone Formations comprising the syncline are totally fault bounded and observable along strike only for a distance of about 2 km. No correlation across the Bow River Valley is seen.

Folding within the Front Ranges generally is cylindrical and of a flexural slip nature (Brown, 1976). These conditions indicate that the kinematic b-axis corresponds to the fold hinge (145°), the a-axis is normal to the b-axis and in the plane of bedding, and the c-axis is vertical. These correspond to σ_2, σ_1, and σ_3 respectively (see Section 2.2).

Fracture patterns within the thesis area are plotted in Figure 2.41. This illustrates that the strong joints are oriented approximately perpendicular to bedding and parallel to the transport direction suggested by fold axes (i.e. the ac structural plane). Moffat (1980) finds very similar results in the Rundle Thrust sheet. Figure 4.21 also demonstrates that these fractures are normal to the regional strike not the local strike, suggesting that their orientation is determined early due to a regional stress field. The "strong joints" observed in this study correspond to the S_I joints of Babcock (1973) which trend 065° and are found in all stratigraphic units throughout virtually all of Alberta. Babcock did not document these joint sets in the Front Ranges, but later studies (as well as this one) substantiate that such a regional set exists throughout the Front Ranges. Regional joint patterns seem to dictate the orientation of transverse faults, etc. and apparently their orientations are determined well before the visible deformation of the Front Ranges took place. Shear fractures with σ_1 bisecting the planes were generally not observed in the thesis area. Fractures are assumed to be extensional in nature and normal to the plane of compression.

Thrust planes within the thesis area steepen toward the west, suggesting that successive (more easterly) thrusts rotated the previous thrust to a steeper angle.

5.2 NDA Interpretations

Numerical results obtained and presented in Table 4.3B are graphically depicted in stereographic plots in Figures 5.21 to 5.23. These graphical representations are much more relevant for interpretive purposes.

Stockmal (1979) describes the typical cases of deformation expected within the Foreland Fold and Thrust Belt and the associated twinning response, this is briefly summarized in Table 5.2A. Figure 5.24 illustrates the geometry of these cases.

Analysis of the data shown in Figure 5.22 suggests that in all cases, except samples 3-5 and 6-10, deformation is of Stockmal type 1 with compression parallel to bedding in the transport plane and extension normal to bedding. Twinning of calcite grains is therefore interpreted to have occurred early in the deformation history (while the beds were still horizontal) and subsequently carried along with the thrust to their present location. These results are consistent with the results of Jamison (1974) for other areas within the Exshaw plate. Figure 5.25 illustrates the NDA determined stress axes with bedding rotated to horizontal.

Results from stylolite orientations seem to substantiate the belief that twinning occurred early. Stylolites form normal to compression as a pressure solution feature. Most stylolites within the thesis area are in the

LEAST SQUARES AND NDA AXES

LEAST SQUARES STRAIN AXES

E1 (max· compression) ● +1·0

E2 (intermediate) ●○ ±0·2

E3 (max· tensile) ○ -1·2

NDA STRESS AXES

NDA1 (max· compression) □

NDA2 (intermediate) □△

NDA3 (max· tension) △

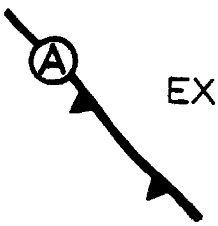

EXSHAW THRUST

SCALE

0 0.5 km

CONTOUR INTERVAL
250 FEET

Figure 5.22 Lower hemisphere, equal area plots of computer generated NDA and Least Squares strain axes. Bedding is indicated by a great circle. Numbers represent strain values, assuming an original (pre-strain) unit sphere; tension is negative.

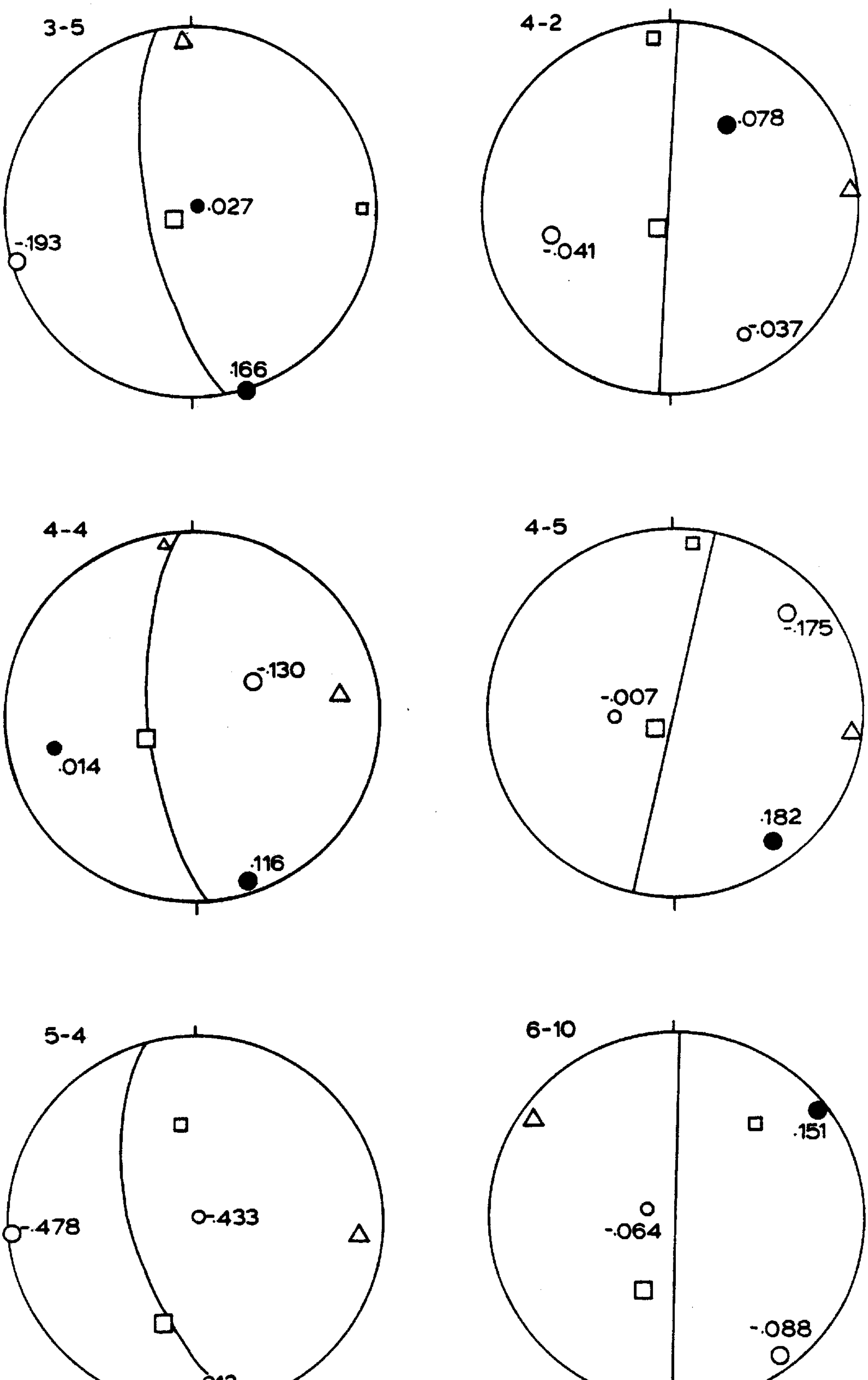
3-5
-.193
.027
.166
4-2
.078
-.041
-.037
4-4
-.130
.014
.116
4-5
-.175
-.007
.182
5-4
-.478
-.433
.912
6-10
.151
-.064
-.088

Figure 5.23 Geological distribution of NDA results from Figure 5.22.

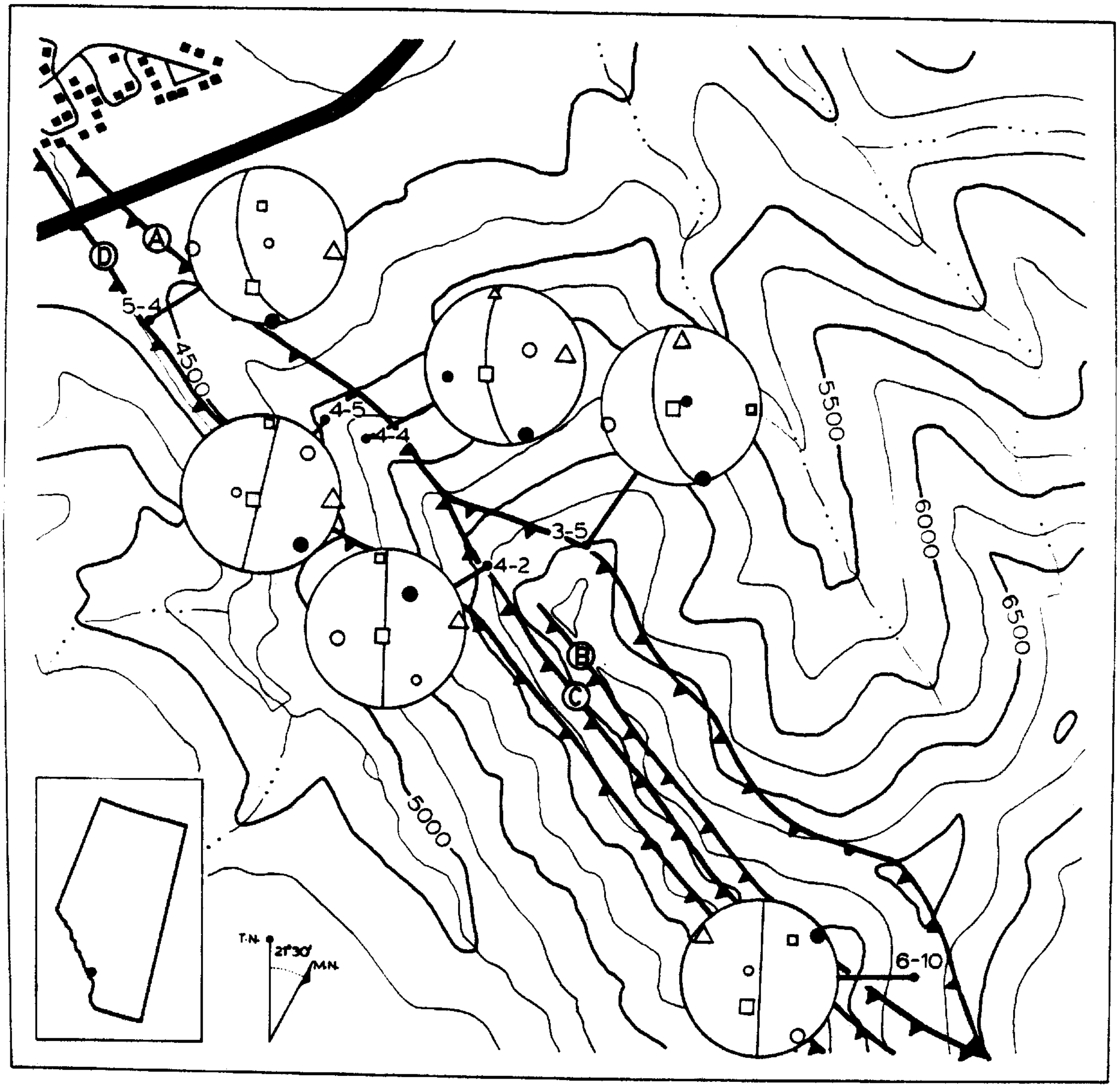
A
D
B
C
5-4
4500
4-5
4-4
3-5
4-2
5500
6000
6500
5000
6-10
T.N.
21°30'
M.N.

Figure 5.24 Stress fields associated with folded and thrust faulted terrain.

after Stockmal (1979)

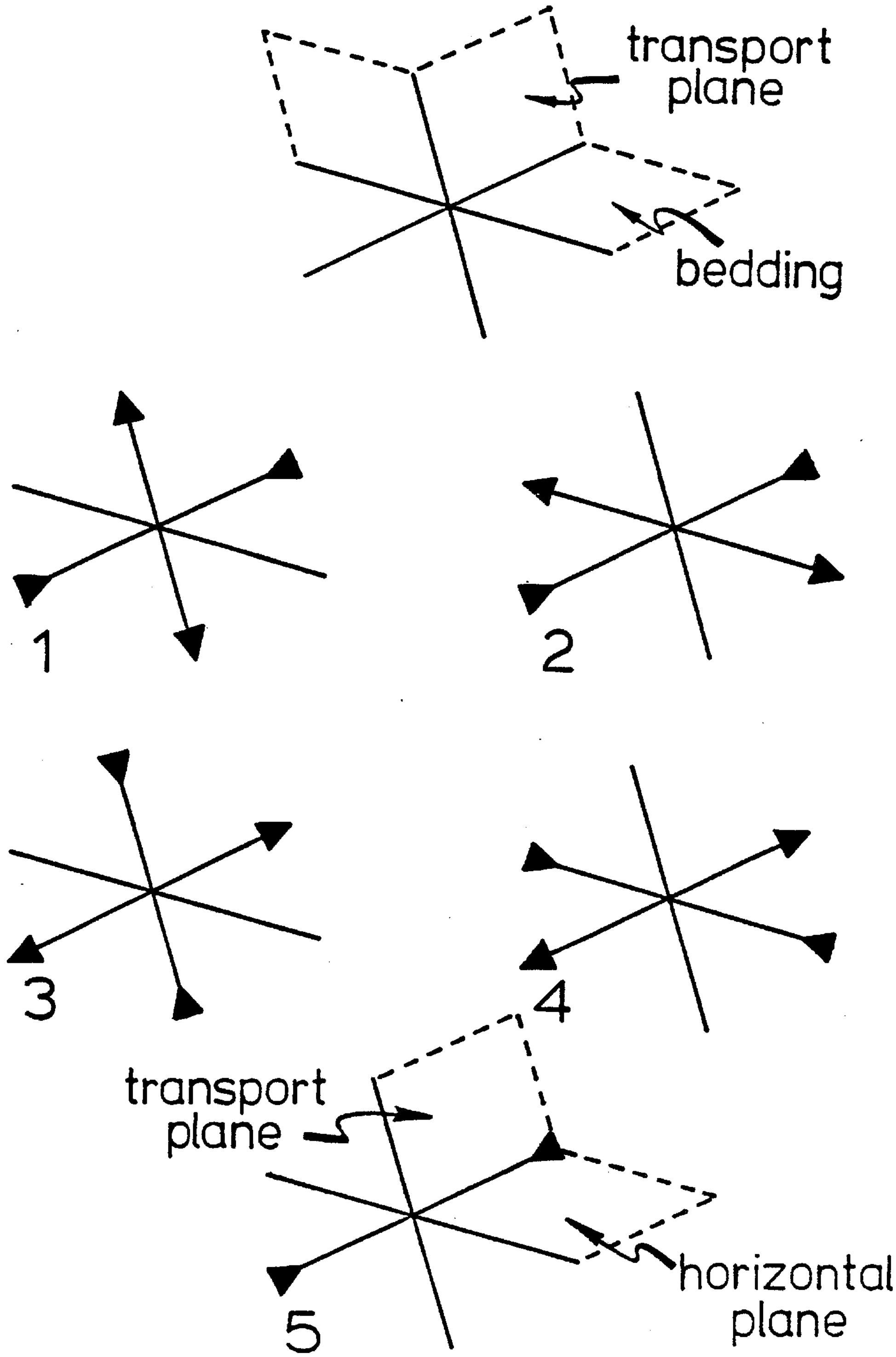
transport
plane
bedding
1
2
3
4
transport
plane
horizontal
plane
5

TABLE 5.2A

STRESS DISTRIBUTIONS ASSOCIATED WITH

FOLD AND THRUST BELTS

Case	Stress Distribution	Comments
1	- σ_1 parallel to bedding in the transport plane - σ_3 normal to bedding	- early stage deformation - plane strain in the transport plane
2	- σ_1 parallel to bedding in the transport plane - σ_3 parallel to bedding and normal to transport plane	- twinning occurs after the initiation of thrusts - thrust sheets fan out
3	- σ_1 normal to bedding - σ_3 parallel to bedding in the transport plane	- twins form on the extensional side of a neutral surface in a buckled layer
4	- σ_1 normal to the transport plane and parallel to bedding - σ_3 parallel to transport plane, within the plane of bedding	- similar to case 3 - typical of the core of a fold or adjacent to a step thrust ramp
5	- σ_1 horizontal and parallel to the transport plane	- late strain overprint after the structure is set

Figure 5.25 NDA results, bedding rotated to horizontal.

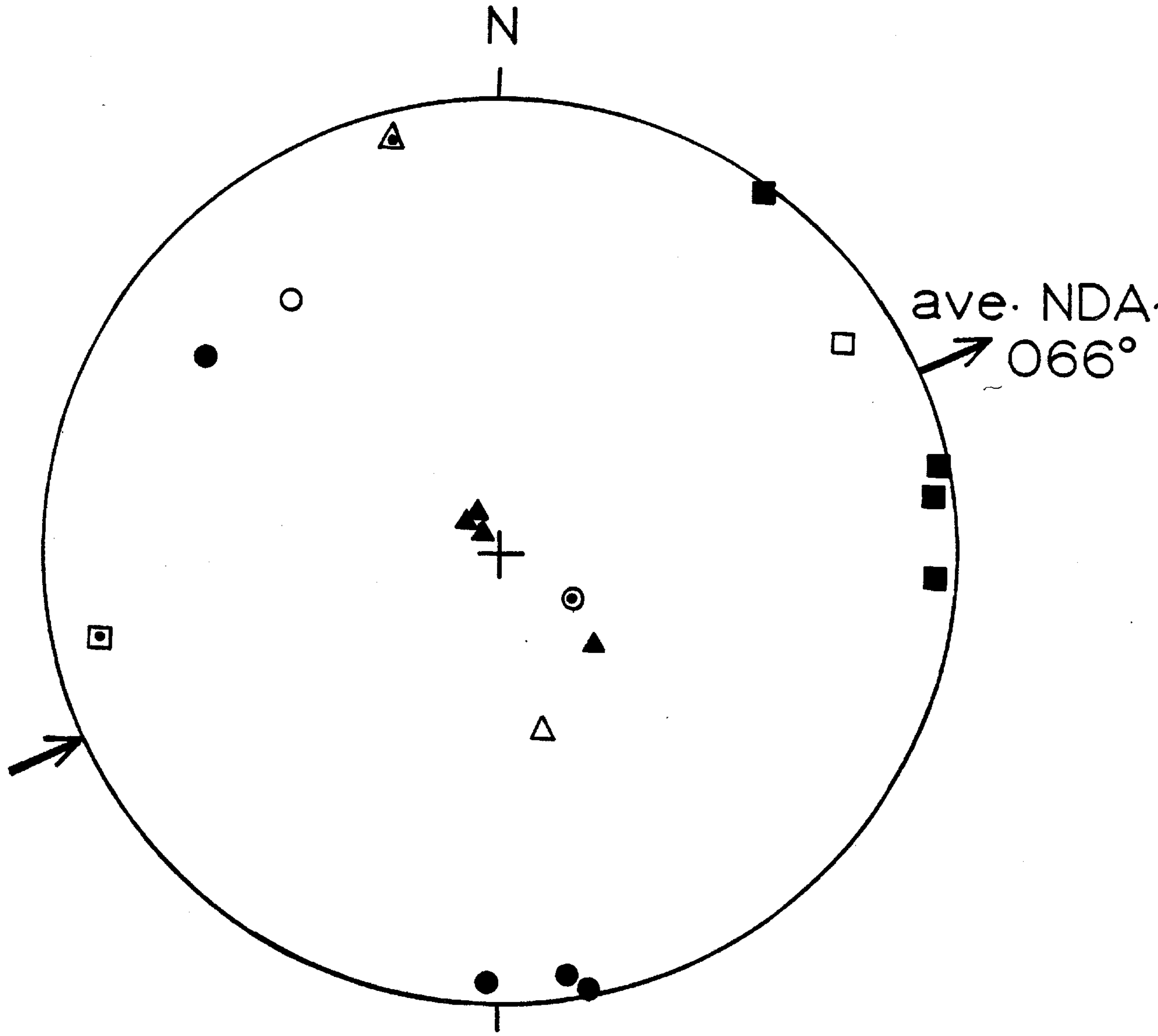

■ NDA_1 max· compression

● NDA_2 intermediate

▲ NDA_3 max· tension

sample

3-5 ⊙

6-10 ○

plane of bedding; a few are oriented normal to bedding. Neither twin results nor megascopic structures suggest vertical compression, so the stylolites might not be of tectonic origin (Brown, 1976). Since they are bedding plane parallel, they could form in response to the lithostatic load. They are also seen to cut twinned calcite grains in many instances, suggesting that they formed after the twinning event. Twinning appears to have taken place with bedding horizontal therefore, before the overburden was sufficiently thick to cause stylolitization.

Alternately, stylolitization may result from a local, temporary vertical σ_1 in response to tectonic loading. P.M. Clifford (pers. comm., 1982) suggests that the transformation of σ_1 from horizontal to vertical (so as to induce bedding plane parallel stylolites) may take place in the footwall of the thrust. Loading due to the overthrust material in a "piggy back" fashion may locally, temporarily be greater than that which previously formed the twins. In this case, stylolitization advances eastward, synchronously with thrusting, and the timing of carbonate twinning may be later in the deformational history than that described previously.

Sample 6-10 gives poor results; compression still appears in the plane of transport and parallel with bedding, but the orientation of NDA_3 does not fit well into any specified case. Some variability in the orientation of NDA axes and Least Squares strain axes, for sample 6-10, and, to some degree, sample 5-4, suggest that deformation was not irrotational. Figure 4.31 and Table 4.3A substantiate this. Sample 6-10 was the only sample of Mount Head Formation obtained that was coarse enough for NDA techniques. These anomalous results are accounted for in folding mechanisms described in Section 6.2.

Stockmal (1979) in work on the Lewis Thrust at Mount Kidd determines a type 2 stress field in unfolded samples. Sample 3-5 from the McConnell Thrust plate also indicates a type 2 stress field. Jamison (1974) found similar results from a more intensive study of the McConnell Thrust plate. Prevailing theories of Front Range structure suggest that the McConnell and Rundle Thrusts are major "basement" thrusts and that the Lac des Arcs and Exshaw Thrusts join the McConnell at depth above the Precambrian basement (Price, 1970). Microstructural evidence suggests that these "basement thrusts" have an inherently different stress regime (one producing a fanning of the thrust and a tensional axis in the plane of bedding normal to the transport direction) from "minor" thrusts such as the Exshaw.

Based upon the observations from Figure 5.22 and the work of Jamison (1974), the thesis area has been divided into three primary fault bounded structural domains. These are:

(1) the McConnell Thrust Plate

(2) the Heart Mountain Syncline Wedge

(3) the Exshaw Thrust Plate

Figure 5.26 illustrates these regions, with the determined stress distribution for each given. Results for the Exshaw and McConnell Thrust plates compare favourably with those of previous workers. The orientation of the NDA_1 axis from sample 6-10 in the Heart Mountain syncline, is in general agreement with that of Jamison (1974); in both studies NDA_2 and NDA_3 orientations did not fit any pattern of Stockmal's cases (see Table 5.2A). Figure 5.27 is a comparison of the results from the Heart Mountain syncline obtained in this study to those of Jamison (1974). Data are very limited and ambiguous and may be indicative of a more complex deformation history of the syncline (see Section 6.2).

Sample 4-2 is somewhat anomalous in that it falls into the structural regime of the Exshaw Thrust plate quite well, but it was mapped in the field just inside the Heart Mountain syncline wedge. This most likely can be attributed to an error in the placement of the trace of the thrust.

Work along the Moine Thrust in Scotland by Weathers et al (1979) prompted the plotting of Figure 5.28. A rough indication of a logarithmic increase in maximum principal compressive stress (NDA_1) with distance to the A thrust is seen, which might be expected intuitively. Similar attempts at relating NDA_1 to distance from the other thrusts did not prove useful. This reaffirms the assumption (see Section 2.3) that the A thrust is the major thrust of the four incorporated in this study. The A thrust is therefore considered

Figure 5.26 Stress field (as determined from micro-structural evidence) variations amongst structural domains within the thesis area.

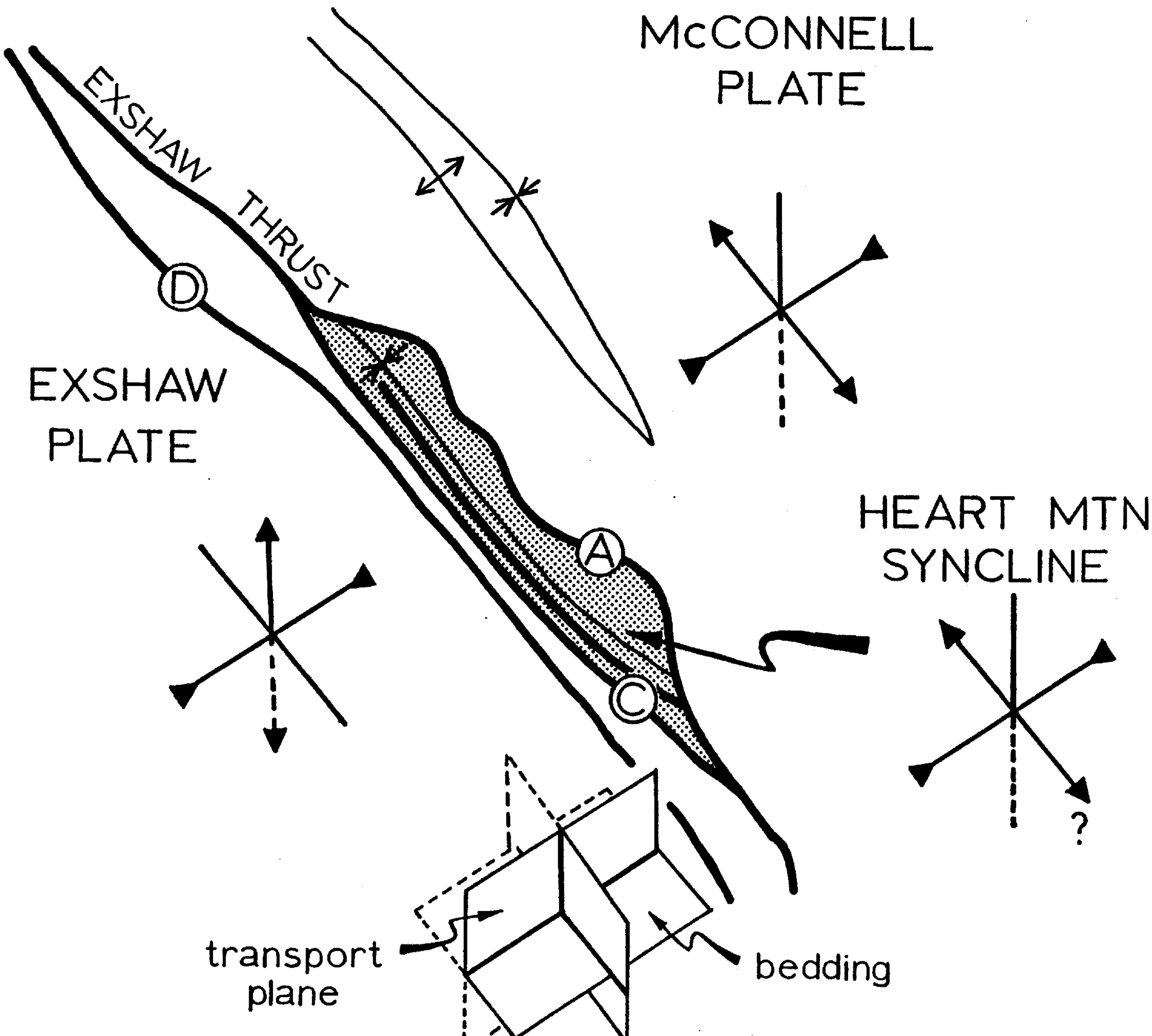

McCONNELL
PLATE
EXSHAW THRUST
EXSHAW
PLATE
HEART MTN.
SYNCLINE
D
A
C
?
transport
plane
bedding

Figure 5.27 Comparison of NDA results for the Heart Mountain syncline from this study and from that of Jamison (1974).

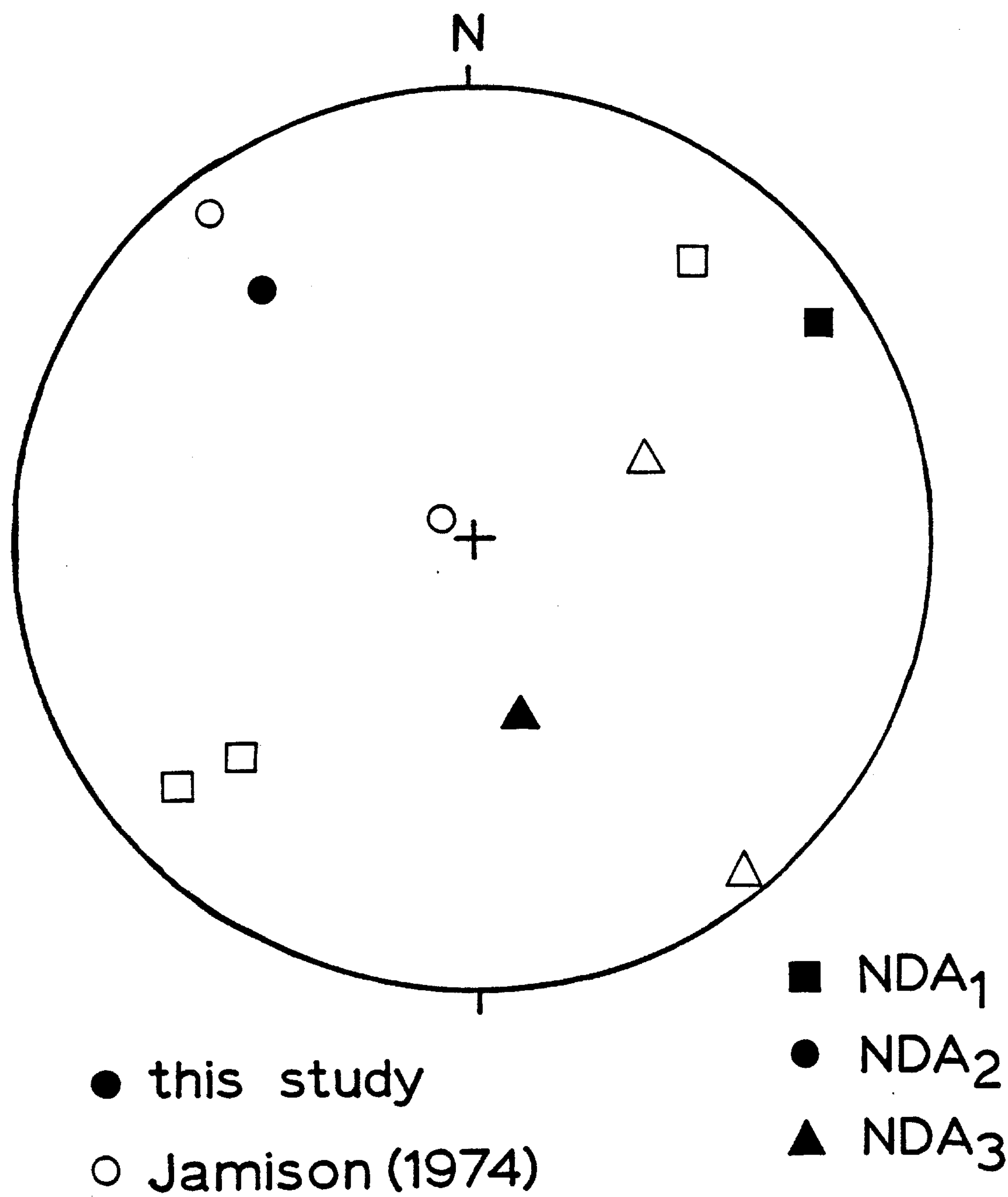
N
NDA1
NDA2
NDA3
this study
Jamison (1974)

Figure 5.28 Principal compressive stress (NDA_1) versus stratigraphic distance to A thrust. Stress scale is logarithmic.

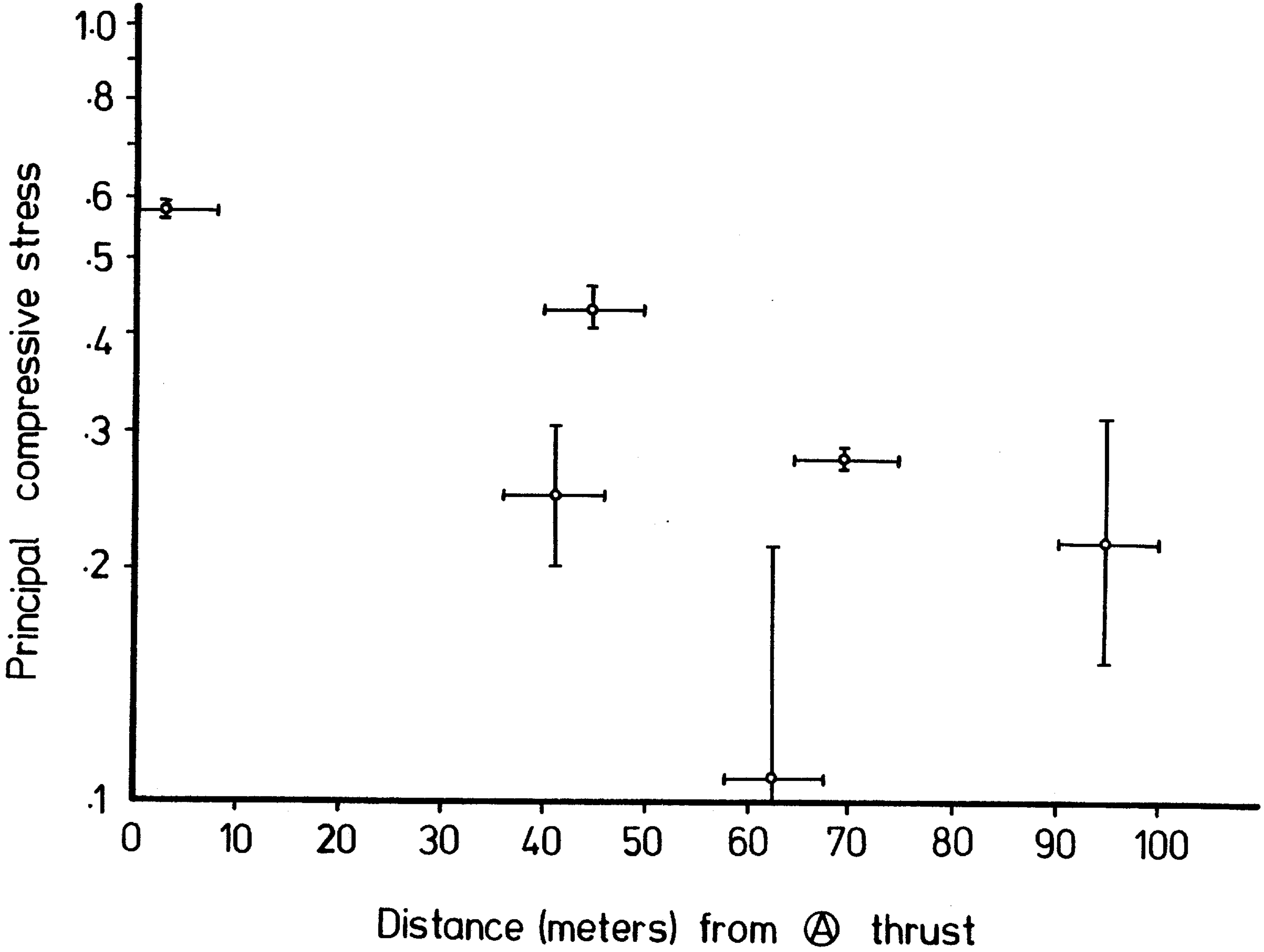
1.0
.8
.6
.5
.4
.3
.2
.1
Principal compressive stress
0
10
20
30
40
50
60
70
80
90
100
Distance (meters) from Ⓐ thrust

to be the boundary between the McConnell and Exshaw plates.

Following the format outlined by Jamison and Spang (1976), the stress magnitude along the Exshaw thrust has been calculated. This method is outlined in Appendix I, The Mechanics of Carbonate Twinning. Ghent and Miller (1974) in a study of authigenic mineral formation in the Cretaceous beneath the McConnell Thrust, and structural reconstructions suggest that the overburden pressure was approximately 1500 bars (based primarily on the lack of authigenic lawsonite). Authigenic minerals also suggest a temperature between 150° and 280°C. Experimental values for the critical shear stress for e twinning in calcite are quite rare in the literature. Higgs and Handin (1959) experimentally determine the critical shear stress of dolomite as approximately 1160 bars. Critical shear values for dolomite are typically about 5 times those for calcite, therefore suggesting a critical shear stress of about 250 bars.

From equation (1) in Appendix I, the conditions for twinning occur when:

$$\tau_o \geqq \tau_c = (\Delta\sigma)\ S_o$$

For a complete description the reader should see Appendix I. S_o can be calculated from the point count data presented in Table 3.3A (average percentage of grains containing one or more twin sets is 32.81); this gives S_o value of 0.356 (utilizing Figure A4). Therefore the differential stress is simply:

$$\Delta\sigma = \tau_c/S_o = \frac{250 \text{ bars}}{0.356} = 702 \text{ bars}$$

More realistically, this should be stated as $(0.356)^{-1}\ \tau_c$ or $2.809\ \tau_c$ owing to the uncertainty of the value of critical shear stress.

Jamison (1974) calculates a value of 2500 bars for the differential stress on the McConnell Thrust approximately 4 km east of the present thesis area. This value he considered to be somewhat high. Our much lower value of approximately 700 bars seems in accordance with the notion put forward that the Exshaw Thrust is minor in comparison to the McConnell Thrust.

NDA results do not show a consistent pattern of variation in principal compressive stress throughout the area. Values of NDA_1 appear relatively constant along the length of the fault even though the deformation expression changes (folding to the northwest and termination along strike of the B thrust). This would seem to indicate that either:

(1) Variations in stress magnitude take place at a level greater than the resolution of the technique

(2) Stress maintains relative consistency and a transfer of displacement mechanism occurs between the various fault splays and/or between the fault and the fold

5.3 Comparison of Results

Analyses on micro-, meso- and megascopic scales all confirm that both the regional and local compressive stresses were to the southwest and in the plane of bedding, and extension is normal to bedding and in the plane of transport.

Regionally, fold axes and strikes indicate that the flexural slip folding and thrust faulting occurred with σ_1 oriented 067/00. Locally, the trend is 055/00. Fracture orientations correspond with those of type S_I of Babcock (1973) and trend parallel to the inferred compression 065/00, corresponding to the regional not the local stress distribution. Numeric dynamic analyses of calcite twin lamellae produce a mean σ_1 at 066/03 and σ_3 at 159/84 (nearly vertical) for the Exshaw Thrust plate. Results for the Heart Mountain syncline and the McConnell Thrust plate suggest that σ_2 and σ_3 have exchanged positions; σ_3 now lies in the regional strike.

Both microscopic deformational features (computed NDA_1) and mesoscopic features (fracture intensity) indicate that deformation increases toward the fault plane. The logarithmic increase seen agrees with that of previous workers on the Moine Thrust.

5.4 Inferred Structural Development

Inferred chronological structural development of the thesis area is based on deformational features at all scales. Relative timings of the bulk effect of particular deformation mechanisms are emphasized, keeping in mind that local variations, complications, and overlapping of events certainly occurred.

Twinning of calcite is inferred to have developed very early in the history in response to a regional Laramide stress field with σ_1 horizontal and normal to the present structural trend; σ_2 horizontal and paralel to the present structural trend, and σ_3 essentially vertical. Brown (1976) contends that twinning may have occurred after the initiation of thrusting in his thesis area, but still in response to this same regional stress field.

Synchronously with twin formation is the development of microfractures. Coalescence of these microfractures into joints and the opening of these joints, was inhibited by the lithostatic load. Fracture orientations (Figure 2.41) are dependent upon these early formed microfractures.

Stylolites are seen to cut twinned calcite grains, and are parallel to bedding. Brown (1976) observed similar relationships, but determined that the stylolites were not of tectonic origin. As postulated in Section 5.2, these may be a thrust loading phenomenon, thus indicating synchronous development of thrusts and stylolites. The alternate interpretation is that twinning may have been initiated during the period of sediment accumulation well before thrusting occurred. A few stylolites are seen normal to bedding. These are most likely of tectonic origin, and related to the previously described stress field.

Megascopic deformation is initiated when the differential stress becomes such that the D thrust begins to propagate in a listric, concave up fashion from the underlying McConnell "basement" thrust. In a similar fashion, the C and B thrusts develop when the increased loading resulting from the previous thrust plate triggers a new thrust, rotating previous thrusts to a steeper angle. Each imbrication of the thrust occurs at a relatively high stratigraphic level and propagates primarily along the base of the thick, competent Livingstone or Palliser Formations before stepping through the Livingstone Formation as it cuts upwards.

Within the thesis area, displacement along the B thrust gradually dies out laterally. Transfer of displacement to re-activate the D and C thrusts and to a set of conical folds takes place. Folding is of a "buckle" nature containing a neutral surface and more complex, variable stress fields. Flexural slip folding, typical of cylindrical folds within the Front Ranges does not take place.

With continued increase in differential stress, the A thrust migrates upwards from the McConnell Thrust with an arcuate strike. Folding and the B thrust are truncated leaving an exposure of the Heart Mountain syncline for a distance of about 2 km. Locally late stage twinning may also occur during this period.

Much later erosion and release of tectonic stresses allows for the opening of the regional fracture set.

Megascopic deformational sequences are summarized in the form of block diagrams in Figure 5.41. A structural section, complete with lithologies is given in Figure 5.42.

Figure 5.41 Cartoon block sketches of inferred megascopic structural development of the Exshaw Thrust in the vicinity of Heart Mountain. Thrusts advance from the southwest, with the additional lithostatic pressure caused by loading triggering a new thrust (a). Subsequent thrusts rotate previous thrusts to steeper angles (b). Lateral termination (c) of the B thrust involves a transfer of displacement to a conical syncline (d) and eventual separation of this syncline from adjacent rocks by later thrusting (e). Fracture orientations are developed well before stage 1, and are rotated with the megascopic deformation and opened at a late stage (after stage 4) after removal of a substantial amount of overburden. Stylolitization is thought to occur in each footwall as the result of tectonically implaced overburden.

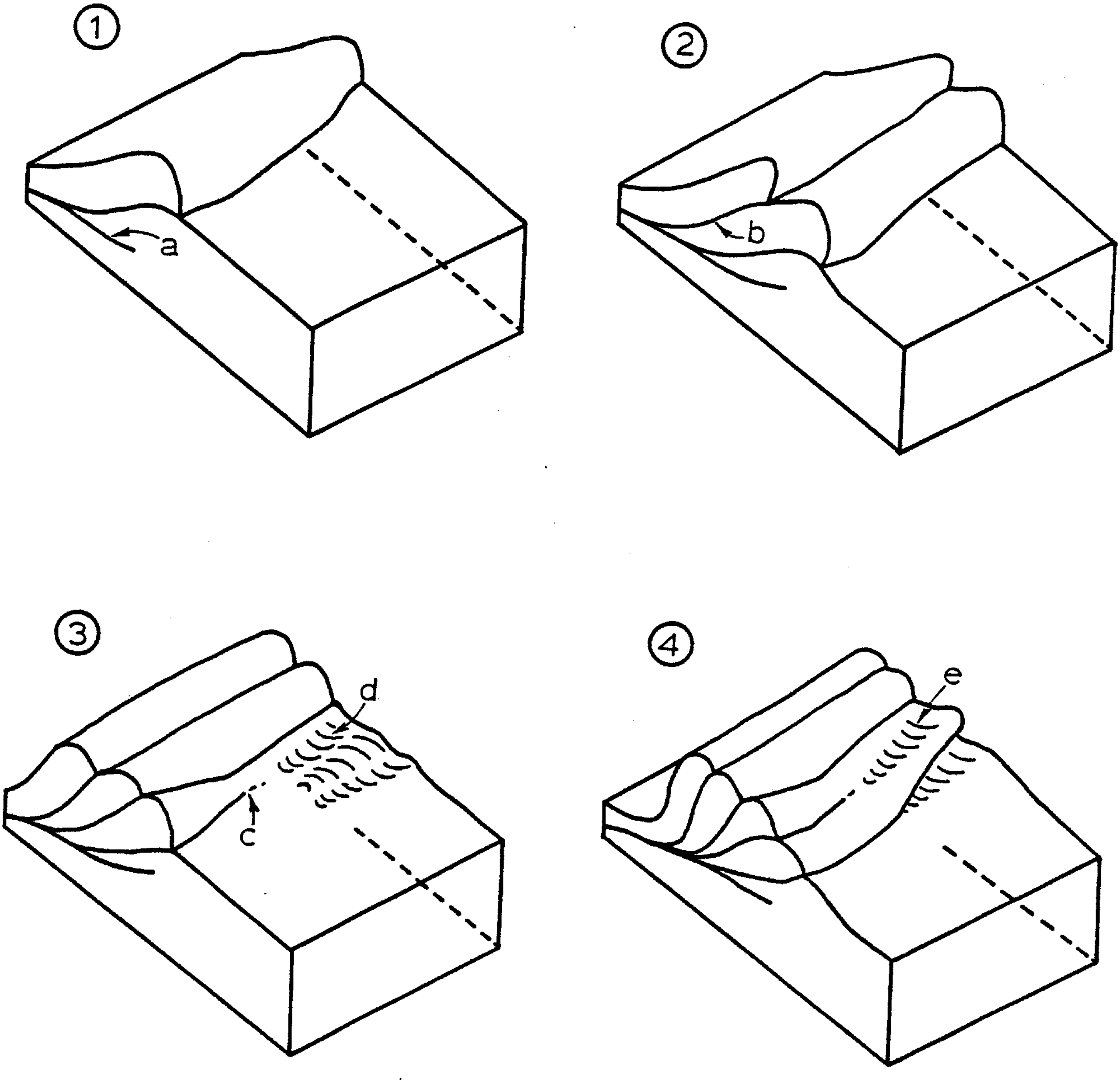
1
a
2
b
3
d
c
4
e

Figure 5.42 Structural section perpendicular to strike of the eastern margin of the Front Ranges, including the thesis area. Note imbrications at high structural levels and coring of thrusts into anticlines to solve room problems.

STRUCTURAL SECTION

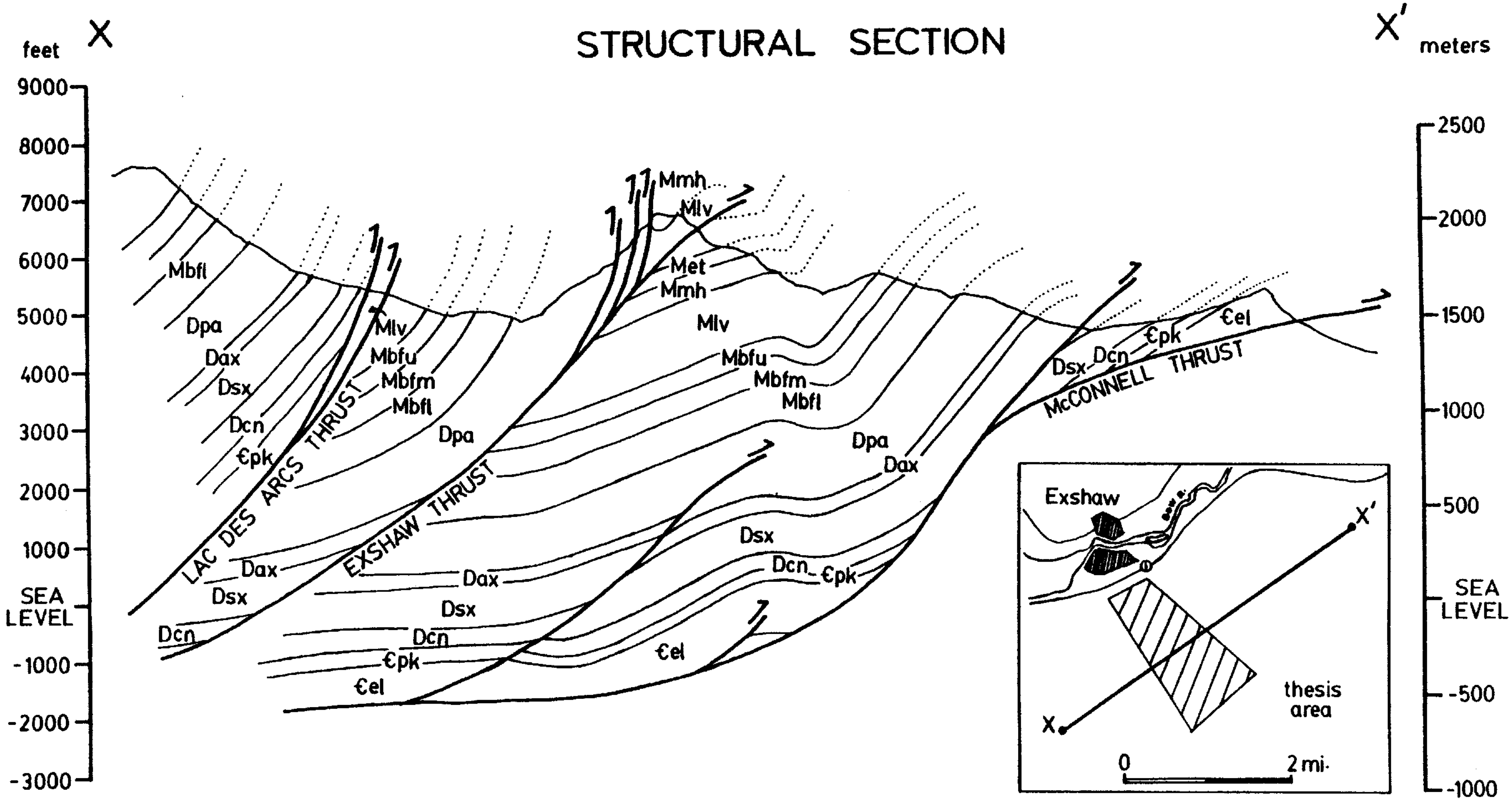

COMPARISON TO PREVIOUS CONCEPTS OF FRONT RANGE STRUCTURE

6.1 Previous Geologic Mapping

The government survey map (1265A, Canmore, east half) containing the present thesis area was compiled by Price (1970) and generally represents an assimilation of graduate work by Price and Bielenstein as well as the extensive work of Clark (1949). Of these, only Clark (1949) appears to have made actual ground traverses within the thesis area. The present geologic map (Figure 2.12) differs from the survey map in several respects:

(1) A thin slice of Spray River Formation that Price has concluded to exist in the footwall of the A thrust was not found on ground traverse.

(2) A few minor changes in the placement of the location of stratigraphic contacts were made.

(3) The B thrust is proposed (albeit somewhat questionably) not to terminate laterally to the southeast before the A thrust. Evidence suggests that it may merge with the A thrust just southeast and outside of the present thesis area.

(4) Following (3), the thin slice of Livingstone

Formation paralleling the steep slope of the arrete to the immediate southwest of Heart Mountain, is proposed not to exist. The synclinal wedge of Mount Head Formation is therefore extended approximately 50 more meters to the southeast and is assumed to be truncated by the A thrust.

(5) The A thrust in reality is comprised of three closely spaced bedding plane parallel thrusts exploiting more argillaceous units within the carbonate sequence. Of these three, the lowermost one has the greatest apparent displacement, and is the one mapped on the survey map (1265A).

The geologic map of the thesis area is illustrated in Figure 2.12.

6.2 Folding

Folding within the thesis area is conical in nature, not concentric as Dahlstrom (1970) has suggested as norm. In light of this, and the repeated confirmation of the mechanical relationship between concentric folds and thrust faults (Price and Mountjoy, 1970), the mechanism of formation of the Heart Mountain syncline appears inherently different from the majority of folds within the Front Ranges and Foothills.

Concentric folding does not completely dominate Front Range structure though; Norris (1971) and Brown (1976) document the existence of chevron folds. Brown continues to contend that chevron folding is dominant over concentric folding, with concentric folding existing only at high structural levels above a coring thrust. Mechanically these also differ from the Heart Mountain syncline.

The Heart Mountain syncline approximates a parallel fold, with a minor amount of thickening in the nose (especially in the thinly bedded Mount Head Formation). Evidence of flexural slip (as proposed by Brown, 1976) was not observed consistently. Only one slickenstriation has been observed, and that on a piece of float. Gardner and Spang (1973) desdribe the formation of folding resulting from displacement transfer (the interpretation presented here) as "buckling" of the material. Folding theories incorporating tangential and longitudinal strain, and the formation of a neutral surface are those generally used to explain "buckling" (Hobbs et al, 1976). Neutral surface theories require a transfer of the extension direction from normal to the fold hinge at the base of the syncline, to parallel to the fold hinge at the top of the syncline, as illustrated in Figure 6.21. Discrepancies seen in the orientation of NDA_3 (extension axes) of Jamison (1974), and those between his and the results obtained in this study may be accounted for in this manner. Samples may have been chosen at different structural levels within the

Figure 6.21 Strain distributions within a neutral surface fold. The folded medium is homogeneous. Within the layer, σ_1 remains at a constant orientation normal to the fold axis, and σ_2 and σ_3 change orientation depending on the location (above or below the neutral surface).

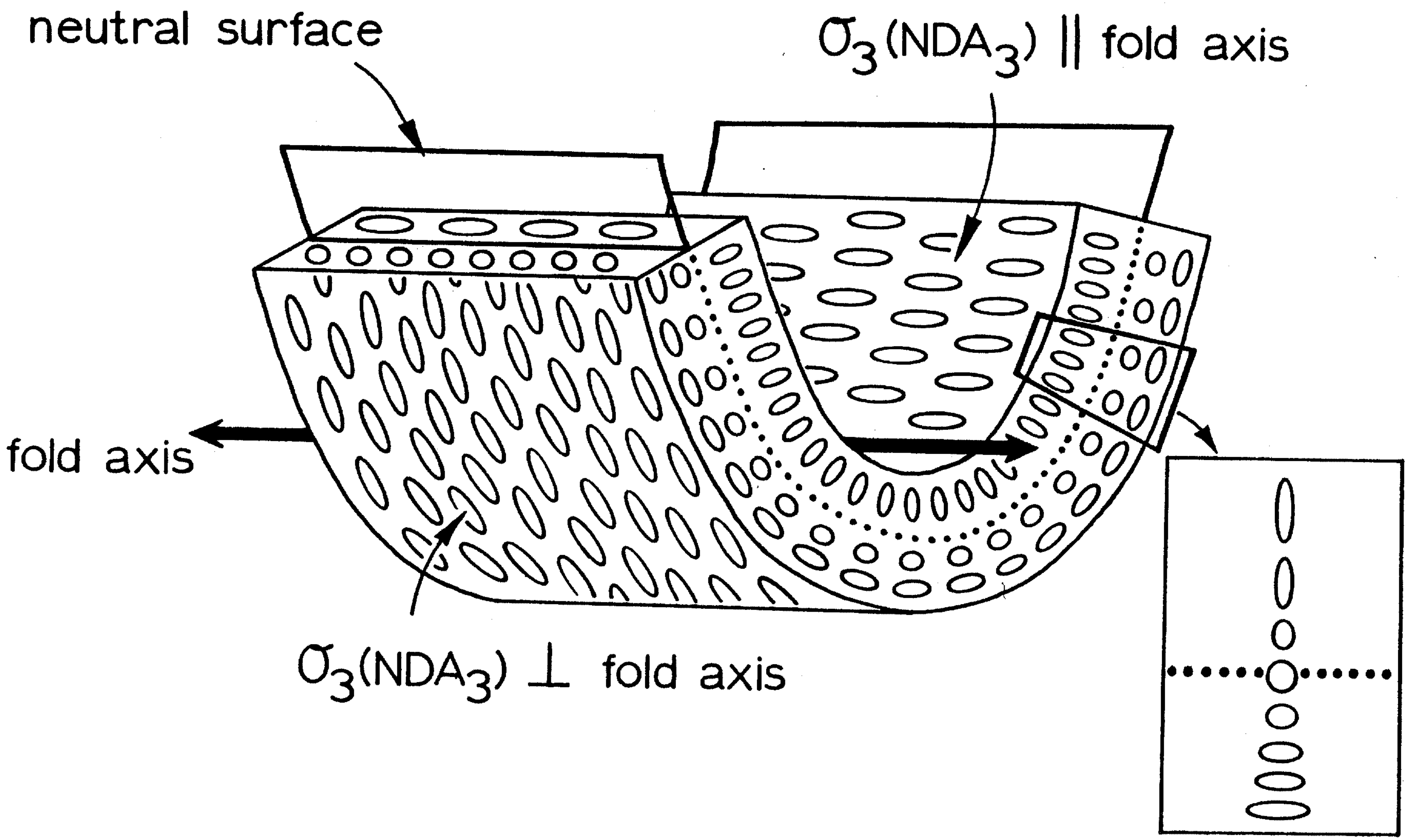
neutral surface
$\sigma_3(NDA_3) \parallel$ fold axis
fold axis
$\sigma_3(NDA_3) \perp$ fold axis

syncline. This is consistent with the random orientation of compression axes seen for sample 6-10 from within the Heart Mountain syncline (see Table 4.3A).

6.3 Thrusting

Thrusting within the thesis area appears relatively simple and correlates well with the style of thrusting described in Section 1.4. For all cases except the B thrust, the thrusts are interpreted to be simple imbricates, at a relatively high stratigraphic level. Thrusting generally occurs along the bottom of the very competent Livingstone Formation and migrates eastward, with each successive thrust rotating previous thrusts to a steeper angle. Evidence (Figure 5.28) suggests that the last thrust, the A thrust, has the greatest amount of displacement. This is consistent with Dahlstrom (1970). Folded thrusts, although common in the Front Ranges, are not seen in the thesis area. Spang et al (1981) interpret what is here called the C thrust as a steeply dipping axial surface of an isoclinal fold above the decollement surface of the A thrust.

Brown contends that faulting occurred after the formation of the isoclinal fold (S. Brown, pers. comm., 1981). Evidence gathered suggests that this is not a reasonable interpretation for the following reasons:

(1) Lithological thicknesses of the Livingstone Formation would be required to vary substantially across this isoclinal fold-cum-fault. Compare stratigraphic thicknesses of the Livingstone Formation to the east and west of the C thrust as shown in plate 2.3I.

(2) NDA results indicate that the Exshaw plate (which contains the C thrust) has a distinctly different stress field from the Heart Mountain syncline. Spang et al (1981) suggest that this isoclinal fold/fault and the Heart Mountain syncline are formed by the same deformational event. An enigma in stress distribution would therefore be present.

(3) This mechanism of folding and later faulting provides no explanation for the termination of the B thrust.

(4) Evidence gathered suggests that the A thrust (rather than the D thrust as Spang et al (1981) would propose) is the major thrust.

Termination of the B thrust within the thesis area appears consistent with the model proposed by Gardner & Spang (1973). In this manner, the existence of both the thrust termination and the syncline can be accounted for in a single model.

6.4 Fracturing

Fracturing on the mesoscopic scale within the thesis area consisted of two sets mutually orthogonal with bedding, and a random set. Numerous other workers have noted similar orthogonal fracture distributions. The determination of the dominant set oriented 065/00 agrees with that of Brown (1976) and Norris (1956).

Numerous theories for the origin of these joints have been postulated, including:

(1) basement movements
(2) extensional stresses associated with arcing b fabric axes
(3) residual elastic strain, and
(4) convex sides of cumulative neutral surfaces.

(Brown, 1976)

All are plausible and could yield the observed orientation, parallel and perpendicular to the Rocky Mountains. The interpretation here is that they formed as a result of the release of residual elastic strain, with their orientation being defined well before thrusting and folding associated with the Laramide Orogeny, but by this same stress field. The initiation of the microscopic fracture orientations is assumed to be carried passively during the faulting and folding phase, generally insensitive to local stress field changes, only to be opened up after erosional unloading.

Brown (1976) comes to a similar conclusion, based primarily on the close correlation of Front Range joint sets to regional sets extending through all of Alberta and into Saskatchewan noted by Babcock (1973).

CONCLUSIONS

Detailed field mapping and laboratory analysis of rocks adjacent to the Exshaw Thrust and contained within the Heart Mountain syncline has indicated that:

(1) Heart Mountain straddles the boundary between the Exshaw and McConnell plates. Each plate contains a characteristic stress field distribution.

(2) Megascopic deformation consists of four steep, concave up, subparallel imbricate thrusts (believed to join in the subsurface) and a conical syncline, totally allochthonous, wedged between two of these thrusts.

(3) Folding/faulting mechanisms proposed by Spang et al (1981) for Heart Mountain do not appear consistent with data obtained and a new deformation model is developed for Heart Mountain.

(4) Folding is inferred to have developed synchronously with the B thrust, and deviates in deformational style from cylindrical folds typically associated with the Front Ranges. Displacement transfer from the laterally terminating B thrust to the syncline and other

faults, is the proposed mechanism for the formation of the syncline.

(5) Folding is of a "buckle" nature (no evidence for flexural slip is seen) involving tangential and longitudinal strain which requires the existence of a neutral deformational surface. Anomalous results in the orientation of principal stresses obtained from the Heart Mountain syncline are accounted for by sample collecting both above and below this neutral surface.

(6) Megascopic deformation proceeded from west to east, with the last thrust, the A thrust, being the most shallowly dipping and containing the greatest amount of displacement.

(7) Fracture analysis suggests that an orthogonal fracture set exists, parallel and perpendicular to the regional structural trend of the Rocky Mountains; both are normal to bedding. The set perpendicular to the structural trend (therefore in the plane of transport) is the strongest set. Orientations are believed to have formed early (before macroscopic deformation) in the Laramide Orogeny, and are consistent with a regional set observed throughout all of Alberta. Late, local fracture sets are

imposed over these sets in response to faulting and folding. All fracture sets open late, after a substantial amount of overburden has been removed.

(8) Numeric dynamic analyses indicate that twinning occurred early in the deformation history, with beds still horizontal. Stylolite/twin relationships suggest that twinning occurred at least pre-thrusting, and perhaps even during sediment accumulation.

(9) Deformation within the Exshaw plate is primarily non-rotational, while that within the Heart Mountain syncline appears to contain a substantial rotational component.

(10) The regional stress field was singular and in most locations non-rotational. Overprinting of strains are not observed.

(11) The differential stress responsible for the development of calcite twinning reached a magnitude of approximately 700 bars. This value is taken to be a minimum since the technique does not take into account intergranular expressions of stress.

REFERENCES

BABCOCK, E.A., 1973, Regional Jointing in Southern Alberta: Can. Journ. Earth Sci., v. 10, pp. 1769-1781.

BALLY, A.W., GORDY, P.L. and G.A. STEWART, 1966, Structure, seismic data and orogenic evolution of the Southern Canadian Rocky Mountains: Bull. Can. Petrol. Geol., v. 14, pp. 3370381.

BEACH, H.H., 1943, Moose Mountain and Morley map areas, Alberta: Geol. Surv. Canada memoir 236.

BEALES, F.W., 1950, The late Paleozoic formations of south-western Alberta: Geol. Surv. Canada paper 50-27, 72p.

BROWN, S.P., 1976, Geometry and mechanical relationship of Folds to a Thrust Fault using a minor thrust in the Front Ranges of the Canadian Rocky Mountains: unpub. M.Sc. thesis, Univ. of Calgary, 161pp.

BROWN, S.P. and J.H. SPANG, 1978, Geometry and mechanical relationship of Folds to Thrust Fault propagation using a minor thrust in the Front Ranges of the Canadian Rocky Mountains: Bull. Can.Petrol. Geol., V. 26, 4, pp. 551-571.

CARTER, N.L. and B.C. RALEIGH, 1969, Principal stress directions from plastic flow in crystals: Bull. Geol. Soc. Amer., v. 80, pp. 1231-1264.

CHINN, A.A., and R.H. KONIG, 1973, Stress Inferred from Calcite twin lamellae in relation to regional structure of northwest Arkansas: Bull. Geol. Soc. Amer., v. 84, pp. 3731-3736.

CHRISTIE, J.H., 1958, Dynamic interpretation of the fabric of a dolomite from the Moine Thrust-zone in northwest Scotland: Amer. Journ. Sci., v. 256, pp. 159-170.

CLARK, L.M., 1949, Geology of the Rocky Mountain Front Ranges near the Bow River, Alberta: A.A.P.G. Bull., v. 33, 4, pp. 614-633.

CONEL, J.E., 1962, Studies of the development of fabrics in some naturally deformed limestones: unpub. Ph.D. thesis, Calif. Inst. of Tech., 257p.

DAHLSTROM, C.D.A., 1970, Structural geology in the eastern margin of the Canadian Rocky Mountains: Bull. Can. Petrol. Geol., v. 18, pp. 332-406.

DAWSON, G.M., 1886, Report on the region in the vicinity of the Bow and Belly Rivers, Northwest Territories: Geol. Nat. Hist. Surv. Can., Annual Report, v. 1, pt. B.

deWIT, R. and D.J. McCLAREN, 1950, Devonian sections in the Rocky Mountains between Crowsnest Pass and Jasper, Alberta: Geol. Surv. Canada paper 50-23.

DOUGLAS, R.J.W., 1956, Nordegg, Alberta: Geol. Surv. of Canada paper 55-34.

DOUGLAS, R.J.W., and P. HARKER, 1958, Mississippian Succession in Mount Head area, Alberta: in Goodman, A.J. (ed), Jurassic and Carboniferous of Western Canada, Amer. Assoc. Petrol. Geol., John Andrew Allen Memorial Volume, pp. 177-189.

ELLIOT, D., 1976 (a), The energy balance and deformation mechanisms of thrust sheets: Phil. Trans. R. Soc. Lond., v. 283, pp. 289-312.

FRIEDMAN, M., 1963, Petrofabric Analysis of Experimentally Deformed Calcite-Cemented Sandstones: Journ. Geol., v. 71, pp. 12-37.

FRIEDMAN, M. and G.M. SOWERS, 1970, Petrofabrics: A critical review, Can. Journ. Earth Sci., v. 7, pp. 447-497.

GALLUP, W.B., 1956, Bow Valley Sketches: 6'th Annual Field Conference guide book, Bow Valley, A.S.P.G., p. 1-6.

GARDNER, D.A.C., and J.H. SPANG, 1973, Model Studies of the Displacement Transfer Associated with Overthrust Faulting: Bull. Can. Petrol. Geol., v. 21, 4, pp. 534-552.

GHENT, E.D. and B.E. MILLER, 1974, Zeolite and Clay Carbonate assemblages in the Blairmore Group (Cretaceous) Southern Alberta Foothills: Contr. Mineral. and Petrol., v. 44, pp. 313-329.

GRETENER, P.E., 1972, Thoughts on overthrust faulting in a layered sequence: Bull. Can. Petrol. Geol, v. 20, 3, pp. 583-607.

GROSHONG, R.H., 1972, Strain calculated from twinning in calcite: Bull. Geol. Soc. Amer., v. 83, pp. 2025-2038.

_______________, 1974, Experimental Test of Least-Squares Strain gauge calculation using twinned calcite: Bull. Geol. Soc. Amer., v. 85, pp. 1855-1864.

_______________, 1976, Use of the Four Axis Universal Stage in Rock Deformation Analysis: Cities Service Oil Company Tech. Report #53, Tulsa, Oklahoma.

GROSS, K.A., 1965, X-ray Line Broadening and Stored Energy in Deformed and Annealed Calcite: Phil. Mag., V. 12, 118, pp. 801-813.

GROSS, K.A. and M.S. PATERSON, 1965, Natural X-ray line broadening in limestones and marbles: Amer. Journ. Sci., v. 263, pp. 238-244.

HAFNER, W., 1951, Stress distributions and faulting, Bull. Geol. Soc. of Amer., v. 62, pp. 373-398.

HOBBS, B.E., MEANS, W.D., and P.F. WILLIAMS, 1976, An Outline of Structural Geology, New York, John Wiley and Sons, 571 p.

JAMISON, W.R., 1974, NDA of the McConnell Thrust Plate: unpub. M.Sc. thesis, Univ. of Calgary, 98 p.

JAMISON, W.R. and J.H. SPANG, 1976, Use of calcite twin lamellae to infer differential stress: Bull. Geol. Soc. Amer. v. 87, pp. 868-872.

KERR, P.F., 1977, Optical Mineralogy - chpt. 7, New York, McGraw-Hill Book Co., pp.

KINDLE, E.M., 1924, Standard Paleozoic Section of Rocky Mountains near Banff, Alberta: Pan. Am. Geologist, v. 42, 2, pp. 113-124.

McCONNELL, R.G., 1887, Report on the Geological Structure of the Rocky Mountains: Geol. Nat. Hist. Surv. Canada, Ann. Report, 188b, pt. D.

McGUGAN, A., and J.E. RAPSON, 1963, Permian Stratigraphy and nomenclature, western Alberta and adjacent regions: Guide book, Edmonton Geological Society, 5'th annual field trip, pp. 52-64.

MOFFAT, I.W., 1980, Geometry and Mechanisms of Transverse Faulting, Rocky Mountain Front Ranges, Canmore, Alberta: unpub. M.Sc. thesis, Univ. of Calgary, 193p.

MOORE, P.F., 1958, Late Paleozoic Stratigraphy in the Rocky Mountains and Foothills of Alberta - A critical historical review: in Goodman, A. (ed), A.A.P.G. symposium on Jurassic and Carboniferous of Western Canada, pp. 145-176.

NIDD, E. and J.W. AMBROSE, 1971, Computerized Solutions for some problems of fold geometry: Can. Journ. Earth Sci., v. 8, pp. 688-693.

NORRIS, D.K., 1956, Structural Conditions in coal mines of the Canmore area, Alberta: A.S.P.G., 6'th Annual Field Conference Guide Book, pp. 59-65.

____________, 1971, Comparative Study of the Castle River and other folds in the eastern Cordillera of Canada: Geol. Surv. Can. Bull. 205, 58 p.

PENNER, D.G., 1958, Mississippian stratigraphy of the southern Alberta plains: in Goodman, A.J. (ed), Jurassic and Carboniferous of western Canada, Amer. Assoc. Petrol. Geol., John Andrew Allen Memorial Volume, pp. 260-288.

PRICE, R.A., 1970, Canmore, Alberta; Maps 1265A and 1266A, Geol. Surv. Can., 1:50,000.

PRICE R.A. and E.W. MOUNTJOY, 1970, Geologic Structure of the Canadian Rocky Mountains between Bow and Athabasca Rivers - a progress report: in Wheeler (ed) Structure of the Southern Canadian Cordillera, Geol. Assoc. Can., spec. paper 6, pp. 7-25.

PRICE, R.A., 1980, The southeastern Canadian Cordillera: superimposed divergent, convergent and strike-slip displacements at the western margin of the North American plate: Prog. with Abs., v. 5, G.A.C/M.A.C. Annual Mtg.

RAASCH, G.O. 1956, The Permian Rocky Mountain Group in Alberta: Alberta Soc. Petrol. Geol; Guidebook, 6'th Ann. Field Conf., pp. 114-119.

RIEK, G.A. and J.B. CURRIE, 1974, A study of relations between rock fabric and joints in sandstone: Can. Journ. Earth Sci., v. 11, 9, pp. 1253-1268.

SHIMER, H.W., 1926, Upper Paleozoic faunas of the Lake Minnewanka section, near Banff, Alberta: Geol. Surv. Can. Bull. v. 42, pp. 1-84.

SPANG, J.H., 1972, Numerical dynamic analysis of calcite twin lamellae: Bull. Geol. Soc. Amer., v. 83, pp. 467-472.

SPANG, J.H. and W.M. CHAPPLE, 1969, Twinning Strain Measurements from a naturally folded limestone: Geol. Sco. Amer. Abs. with Programs, pt. 7 (Ann. Mtg.), pp. 210-211.

SPANG, J.H. and J. van der LEE, 1975, Numerical dynamic analysis of quartz deformation lamellae and calcite and dolomite twin lamellae, Bull. Geol. Soc. Amer., v. 86, pp. 1266-1272.

SPANG, J.H., BROWN, S.P., STOCKMAL, G.S. and I. MOFFAT, 1981, Structural Geology of the Foothills and Front Ranges West of Calgary, Alberta: G.A.C./M.A.C. Ann. Mtg.

STOCKMAL, G.S., 1979, Structural Geology of the northern termination of the Lewis Thrust, Front Ranges, southern Canadian Rocky Mountains: unpub. M.Sc. thesis, Univ. of Calgary, 174 p.

TURNER, F.J. and L.E. WEISS, 1963, Structural analysis of metamorphic tectonites: New York, McGraw-Hill Book Co., pp. 134-147, 545 p.

UNDERHILL, D.H., 1972, The Nature of Deformation in Experimentally deformed Calcite-cemented Sandstones: unpub. Ph.D. thesis, McMaster University, 198 p.

WARREN, P.S., 1947, Age and subdivisions of the Rocky Mountain Formation at Banff, Alberta [abs]: Geol. Soc. Amer. Bull., v. 58, no. 12, pt. 2, p. 1238.

WEATHERS, M.S., COOPER, R.F., KOHLSTEDF, O.L. and J.M. BIRD, 1979, Differential stress determined from deformation induced microstructures of the Moine Thrust Zone: Journ. Geophy. Res., v. 84, pp. 7495-7509.

WHEELER, J.O. and H. GABRIELSE, 1972, The Cordilleran structural province: in Price, R.A. and Douglas, R.J.W. (eds) Variations in Tectonic Styles in Canada, G.A.C. spec. paper II, pp. 1-81.

APPENDIX I

MICROSTRUCTURAL STRAIN ANALYSIS OF CALCITE AND DOLOMITE TWIN LAMELLAE

A-1 Mechanics of Carbonate Twinning

Petrofabric studies (Turner et. al, 1954) have indicated that twinning in calcite and dolomite crystals occurs preferentially along specific crystallographic planes in response to a differential applied stress. Both translation and twin gliding occur, but at the temperatures involved in the deformation of the thesis area, the dominant mechanism for twinning is glide along the e$\{01\bar{1}2\}$ and f$\{02\bar{2}1\}$ planes for calcite and dolomite respectively.

Twin gliding in calcite is initiated when a critical resolved shear stress, τ_c, along the glide line in the e-plane is exceeded. Gliding along the appropriate crystallographic plane takes place when:

$$\tau_o = (\sigma_1 - \sigma_3) S_o \geqq \tau_c \qquad (1)$$

where τ_o = resolved shear stress

$\sigma_1 - \sigma_3$ = differential stress

τ_c = critical shear stress

S_o = resolved shear stress coefficient

Figure A1 Calcite crystallography.

after Turner & Weiss (1963)

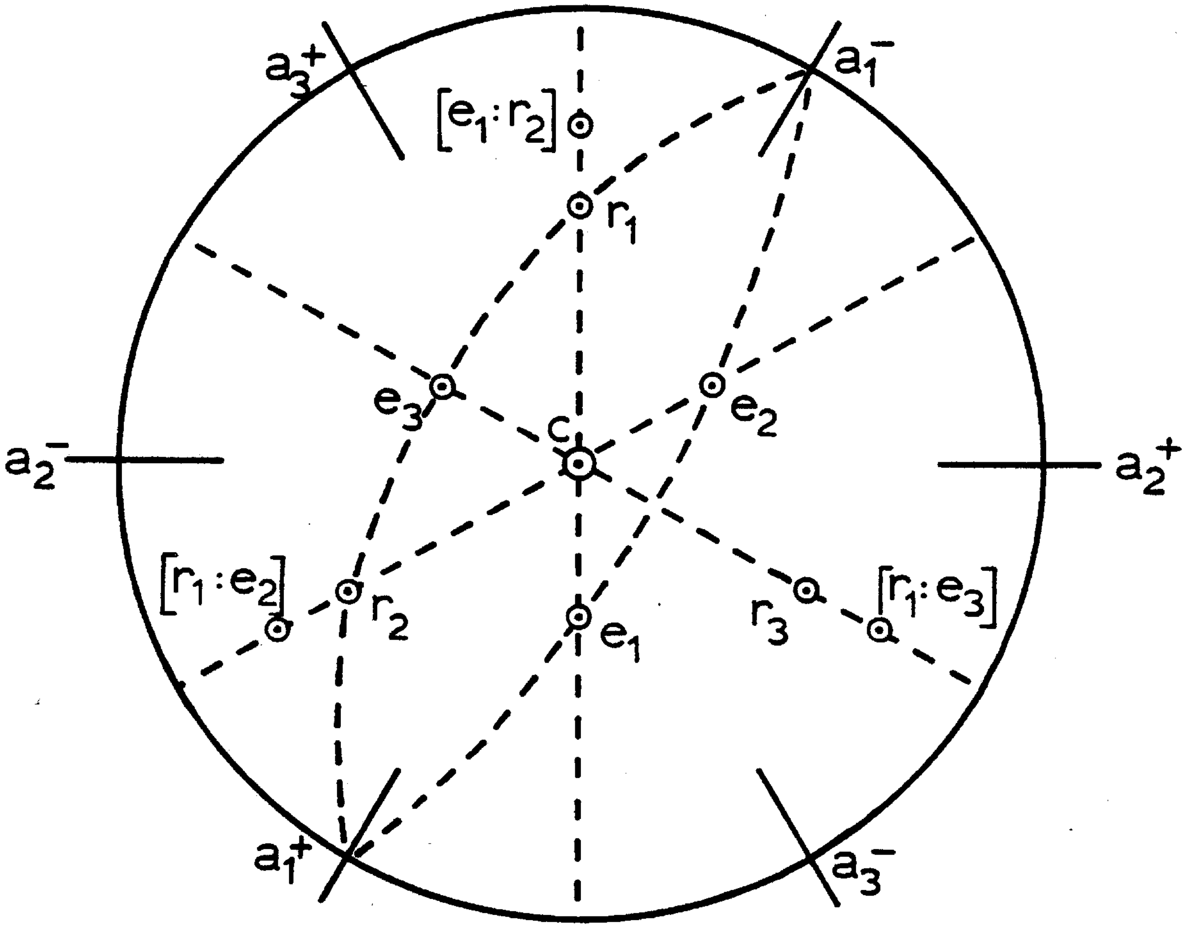

a_3^+
a_1^-
$[e_1 : r_2]$
r_1
e_3
e_2
c
a_2^-
a_2^+
$[r_1 : e_2]$
r_2
e_1
r_3
$[r_1 : e_3]$
a_1^+
a_3^-

S_o can be calculated:

$$S_o = (\cos X)(\cos L) \qquad (2)$$

where X = angle between σ_1 and twin plane

L = angle between σ_1 and glide line

The glide line in calcite is the intersection of the $e_1\{01\bar{1}2\}$ and $r_2\{10\bar{1}1\}$ planes. Gliding is most easily achieved when the maximum compressive and extensive stresses are oriented at 45° to the twin plane or 26° and 63° to the c-axis in calcite and dolomite respectively.

For every point on an equal area projection 3 possible values for S_o exist, one for each twin plane. Figure A3 shows the distribution of the largest value of S_o. By using the other values of S_o, the number of grains containing 2 or 3 twin sets for a particular value of $\Delta\sigma$ can be predicted. Figure A4 shows such a plot. Similarly, the logic works in reverse: if the per cent of grains with a particular number of twin sets is noted, then S_o can be read from Figure A4; if τ_c is known, then $\Delta\sigma$ can be determined utilizing equation (1).

A-2 Dynamic Analysis

Irrotational stress fields responsible for twinning in randomly oriented calcite grains may be determined by the method of dynamic analysis. The technique involves:

Figure A2 Angular relationships between principal stress axes and geometry of calcite and dolomite twins. Shear along the glide plane is a maximum when σ_1 is oriented 45° away.

after Spang (1972)

CALCITE

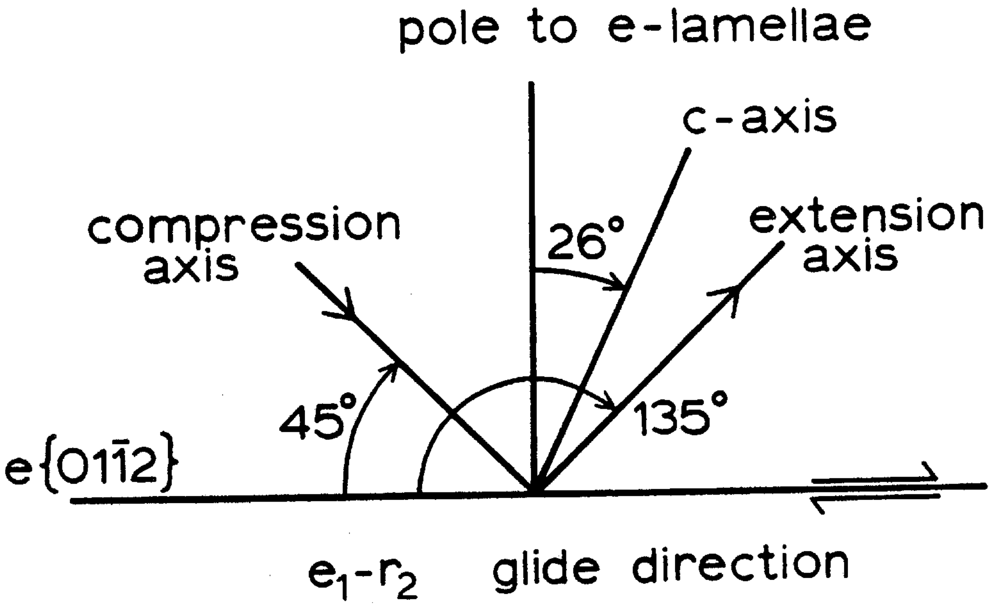

DOLOMITE

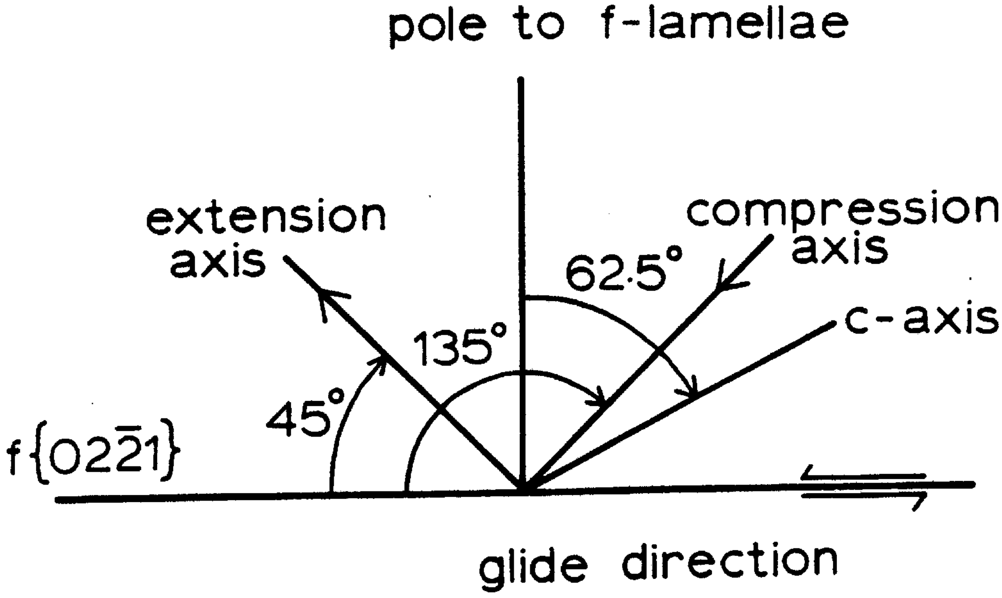

Figure A3 Contoured maximum values of S_o ($\tau_c/\Delta\sigma$) for calcite and dolomite.

after Spang (1972)

CALCITE

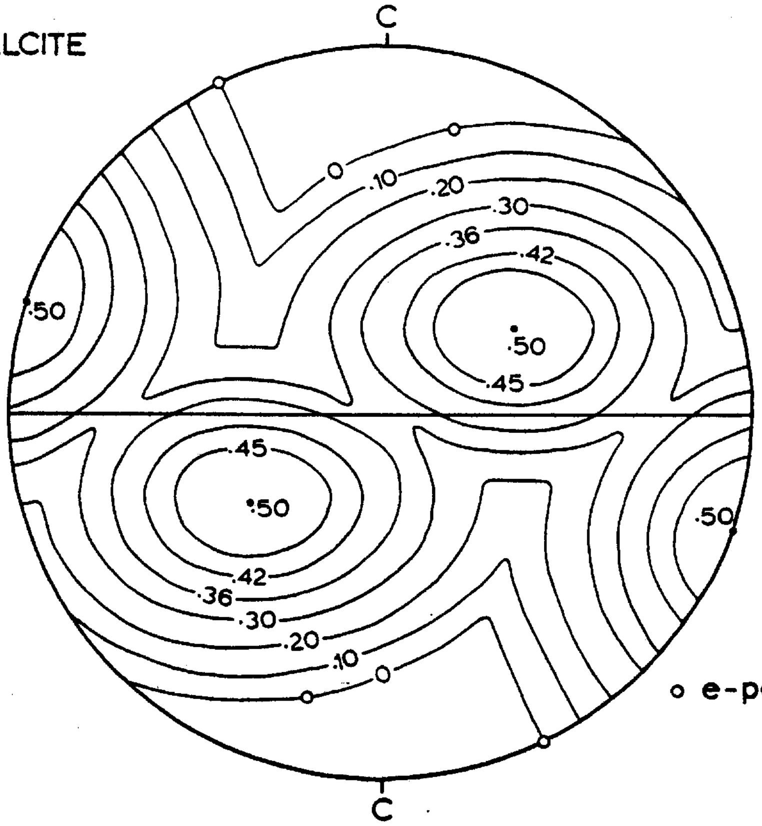

o e-pole

DOLOMITE

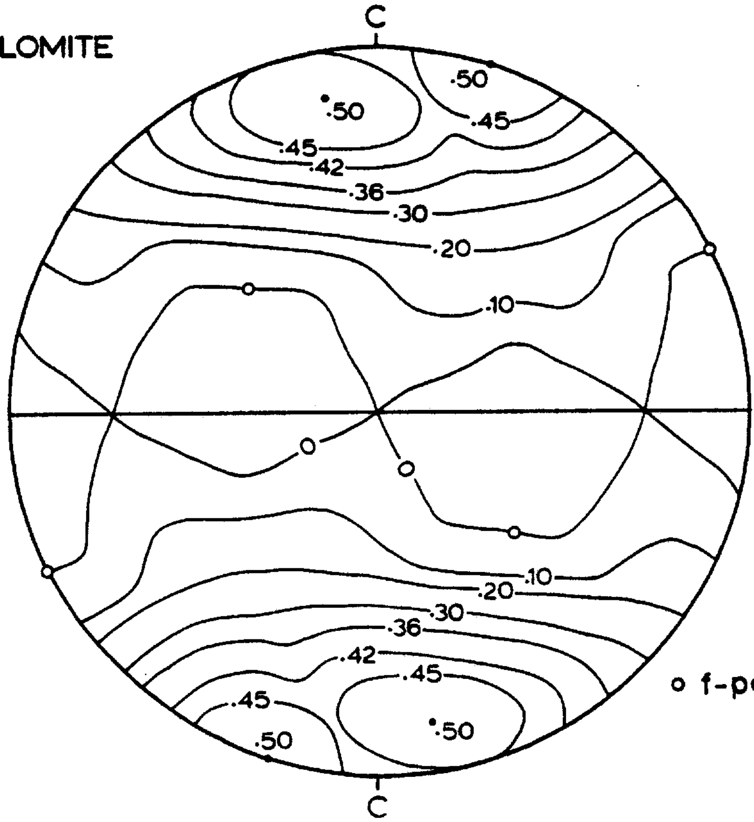

o f-pole

Figure A4 Twin set development versus S_o (stress magnitude determination curves) for calcite and dolomite.

after Spang (1972)

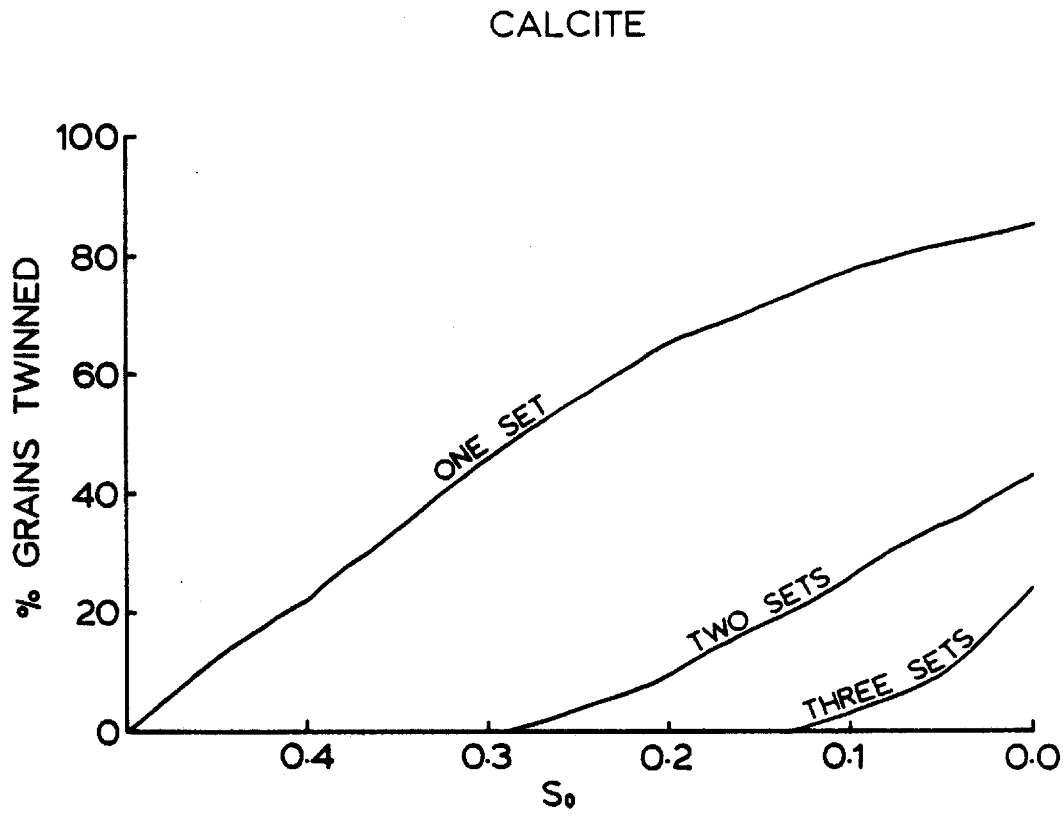
CALCITE
100
80
60
40
20
0
% GRAINS TWINNED
ONE SET
TWO SETS
THREE SETS
0·4
0·3
0·2
0·1
0·0
S_0

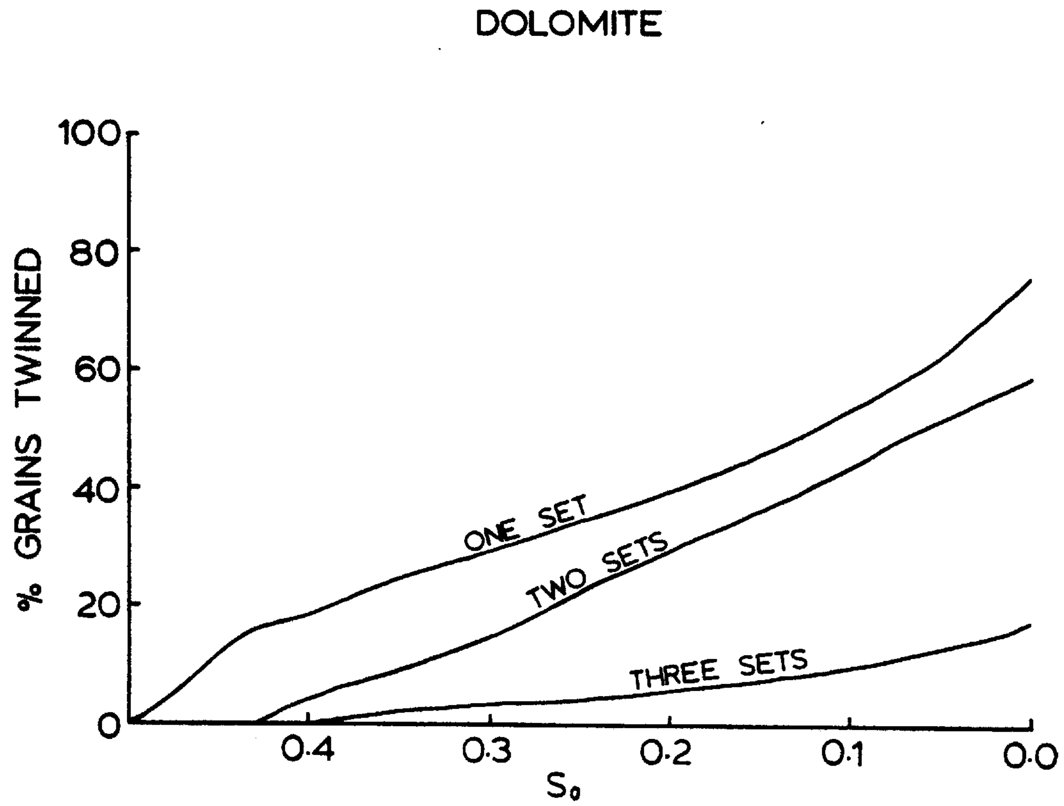
DOLOMITE
100
80
60
40
20
0
% GRAINS TWINNED
ONE SET
TWO SETS
THREE SETS
0·4
0·3
0·2
0·1
0·0
S_0

(1) determination of e_1 and c-axes orientations by means of a universal stage (Turner and Weiss, 1963; Groshong, 1976)

(2) plotting compression (σ_1) and tension (σ_3) axes in their most favourable position (45° to the twin plane) on an equal area stereonet

(3) contouring the data at 1 per cent unit area increments and determining estimates of σ_1 and σ_3

(4) graphically adjusting these axes to mutual orthogonality (Turner and Weiss, 1963). Published accounts of dynamic analyses techniques and results include those of Carter and Raleigh (1969), Friedman (1963) and Friedman and Sowers (1970)

A-3 Numeric Dynamic Analysis

The process of numeric dynamic analysis (NDA) allows for substantial decrease in errors inherent in contouring and rotating of axes to an orthogonal position by manipulating the data mathematically on a computer. Not only are the results more reliable, but the analysis of data is achieved much more quickly. In dynamic analysis it is assumed that the observed twin sets are the result of shear strains of equal magnitude, thus Spang (1972) arbitrarily assigns a tensor shear strain of 1.0. The strain can therefore be represented by a two-dimensional Mohr circle of infinitesimal strain with radius equal to 1.0, hence σ_1 equals σ_3 which equals 1.0 and twinning occurs with no volume change.

The strain in any twin set $\varepsilon_{\alpha\beta}$ can therefore be represented by the second order tensor:

$$\varepsilon_{\alpha\beta} = \begin{vmatrix} 1.0 & 0 & 0 \\ 0 & -1.0 & 0 \\ 0 & 0 & 0 \end{vmatrix} \qquad (3)$$

where 1.0 is the principal compressive axis
-1.0 is the principal tension axis

(Spang, 1972)

Due to the random orientation of crystals and the crystallographic control on twin orientation, shear tensors must be rotated to a common plane of reference using the second order tensor transformation equation:

$$\varepsilon'_{ij} = \varepsilon_{\alpha\beta} l_{\alpha i} l_{\beta j} \qquad (4)$$

where $l_{\alpha i}$ and $l_{\beta j}$ are direction cosines

The direction cosines rotate the tensor into the thin section coordinate system. A bulk strain tensor is obtained by finding the average rotated strain tensor for the twin sets. The strain ellipsoid is represented by this bulk strain tensor. The orientation and magnitude of the principal axes of the strain ellipsoid are obtained by solving the eigenvectors and eigenvalues respectively. In this fashion, principal strain axes are required to be orthogonal due to the mathematics of eigen-analysis. These strain fields are then used to infer the strain field in nature at the time of twinning.

A-4 Absolute Strain Calculation

Conel (1962) made the first attempt to quantify the relationship between amount of twinning and magnitude of intragranular strain. For a partially twinned carbonate grain, Conel deduced that the engineering shear strain is:

$$\gamma = \frac{2}{t} * \sum_{i=1}^{N} [t_i * \tan(\alpha/2)] \qquad (5)$$

where N = number of twins

t = width of the host grain perpendicular to twin plane

t_i = thickness of twins

α = change in angle of the {1011} face in response to twinning

See Figure A5

By substituting the value of α for calcite, the tensor shear strain perpendicular to the twin plane (e) and the glide direction (g) is given by:

$$\Gamma_{eg} = \frac{0.347}{t} * \sum_{i=1}^{N} t_i \qquad (6)$$

For comparison with other twin set strains they are ro-

Figure A5 Shear strain in a partially twinned calcite grain. The values t_1 and t_2 are the widths of the twins; t is the width of the host grain perpendicular to the twin plane; α is the angle of rotation of the grain edge from the untwinned to the twinned position and is equal to 38°17'; ψ is the change of an original right angle. The engineering shear strain, γ, is $\tan\psi$ or $\gamma = q/t$. The length p_i is equal to $2t_i \tan(\alpha/2)$. The length of q is the sum of p_i for each twin. The shear strain in a partially twinned grain is thus:

$$\gamma = \Sigma p_i / t$$

after Conel (1962); Moffat (1980)

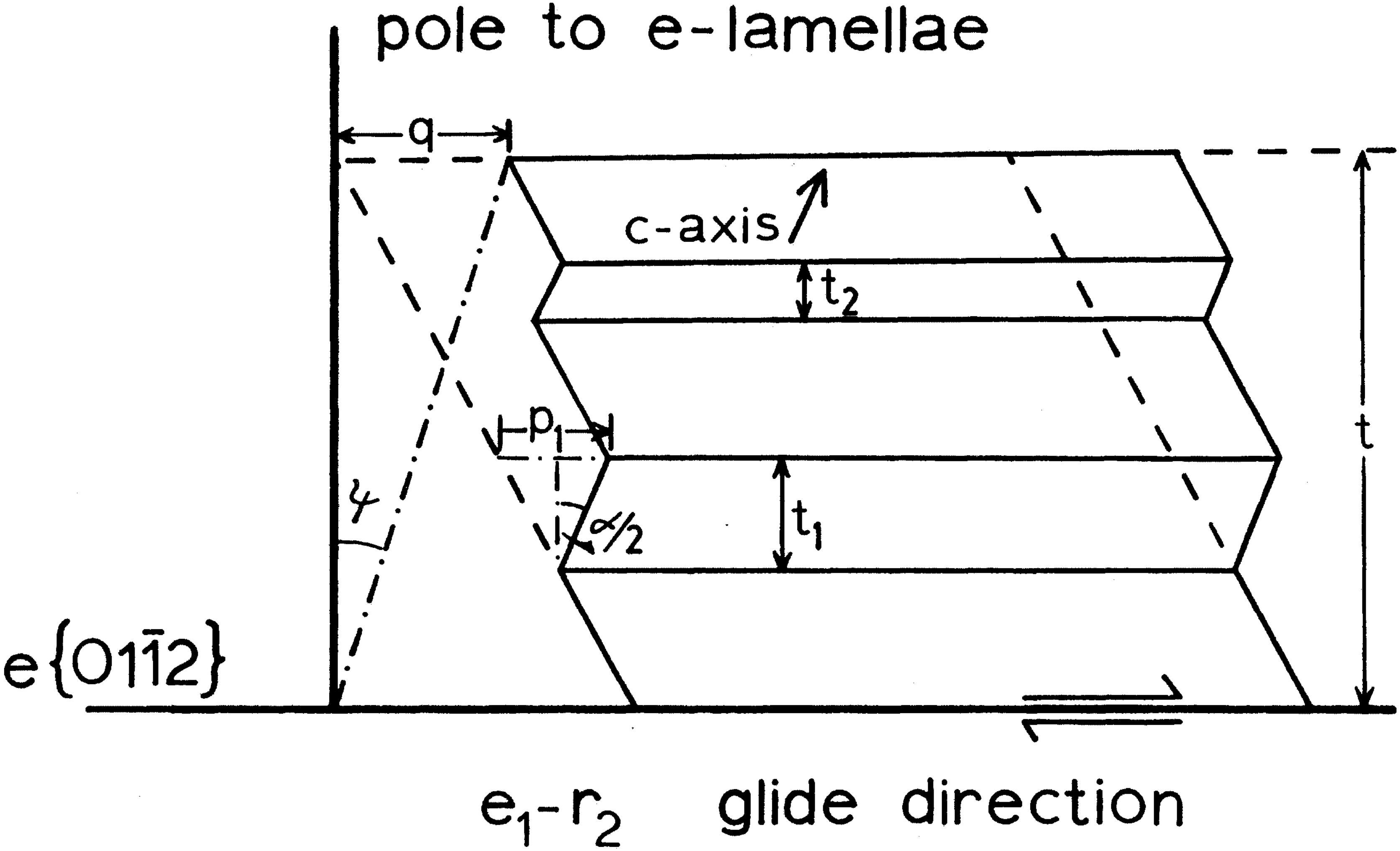
pole to e-lamellae
q
c-axis
t_2
p_1
ψ
$\alpha/2$
t_1
t
$e\{01\bar{1}2\}$
$e_1 - r_2$ glide direction

tated into a common plane using the tensor transformation equationtion (2) given above. The matrix defining the principal axes of infinitesimal strain for each twin set becomes:

$$\varepsilon'_{ij} = \begin{vmatrix} 1/2\ \tan\psi & 0 & 0 \\ 0 & -1/2\ \tan\psi & 0 \\ 0 & 0 & 0 \end{vmatrix} \qquad (7)$$

Conel (1962) redefines the strain tensor in terms of a Cartesian coordinate system used in thin section orientation as:

$$\begin{aligned} \varepsilon_{xx} &= \tfrac{1}{2}\ (l_T^{\ 2} - l_c^{\ 2}) * \tan\psi \\ \varepsilon_{yy} &= \tfrac{1}{2}\ (m_T^{\ 2} - m_c^{\ 2}) * \tan\psi \\ \varepsilon_{zz} &= \tfrac{1}{2}\ (n_T^{\ 2} - n_c^{\ 2}) * \tan\psi \\ \varepsilon_{xy} &= \tfrac{1}{2}\ (l_T m_T - l_c m_c) * \tan\psi \\ \varepsilon_{xz} &= \tfrac{1}{2}\ (l_T n_T - l_c m_c) * \tan\psi \\ \varepsilon_{yz} &= \tfrac{1}{2}\ (m_T n_T - m_c n_c) * \tan\psi \end{aligned} \qquad (8)$$

where l, m, n are the direction cosines

The direction cosines apply to the compression and extension axes represented by the subscripts c and T respectively. By multiplying the ratio of the area of the grain to the area of all grains measured and by summing all of these area weighted components, Conel arrived at a new measure of "bulk strain". Spang and Chapple (1972) modified this "bulk strain" by taking the unweighted average; results proved to be superior and microscopic observation time was decreased.

Inadequacies in Conel's technique were reviewed by Groshong (1972), these being:

(1) A complete set of strain components are attainable from a single twin set, this being more information than should be obtained from a single measurement

(2) Bulk strain tensor components were functions of the twin set measured, therefore results could be inconsistent

(3) Statistical treatment of the variability in determined strains from a sample was not attempted

Groshong (1972) contends that each calcite twin set is an internal strain gauge measuring positive shear only. Assuming that e twinning occurs at the lowest resolved shear stress, then the rigidity of the e plane is lower than, or equal to the rigidity of the total aggregate of grains. At higher strain levels though, grain boundary effects increase the "effective" twin rigidity; an underestimate of bulk strain results. Groshong (1972) makes the assumptions that:

(1) Least squares solution to the strain gauge equation produces an unbiased estimate of total strain

(2) Strain is considered homogeneous over a small region larger than the grain in question

(3) Twinning is in response to externally applied stress and not as a result of crystal growth

(4) Less than half of the grain may be twinned otherwise determination of which portions are host and which

are twin cannot be made conclusively

(5) Each twin set within a single crystal can be treated independently

Using the tensor transformation equation as previously described, Groshong (1972) determines the measured strain in a twin set:

$$\begin{aligned}\Gamma_{eg} &= (l_e l_g - n_e n_g)\varepsilon_x + (m_e m_g - n_e n_g)\varepsilon_y \\ &+ (l_c m_g + m_e l_g)\Gamma_{xy} + (m_e n_g + m_e l_g)\Gamma_{yz} \\ &+ (n_e l_g + l_e n_g)\Gamma_{zx}\end{aligned} \tag{9}$$

where l, m, n are the direction cosines rotating the tensor into Cartesian coordinates for the e- and g-axes;

where ε_x and ε_y are the appropriate normal strains;

and Γ_{xy}, Γ_{yz} and Γ_{zx} are shear strains associated with the appropriate planes

Assuming zero volume change, the ε_z term was eliminated from equation (9) by noting:

$$\varepsilon_z = -(\varepsilon_x + \varepsilon_y) \tag{10}$$

As opposed to Conel's technique, Groshong's determination of twin strain requires measurements from at least five grains in order to simultaneously solve equation (9) for its five unknowns. Statistical measures of the precision of the determined deviatoric strains can be made if a suitable population exists, which is usually 50 grains.

The least squares estimate of strain within the aggregate is determined by Groshong (1972) as

$$\hat{\beta}_j = (X'X)^{-1} X'Y \qquad (11)$$

where X is the date matrix with components X_{ij}

Y is the column vector with components Γ_j

X' is X transpose

-1 indicates the inverse operator

The errors associated with five of the six strain components of the aggregate $\hat{\beta}_j$ are:

$$\hat{\beta}_j = [c_{jj}(Y'Y) - \beta_j X''Y)/n - 5]^{1/2} \qquad (12)$$

where c_{jj} is the diagonal component of the $(X'X)^{-1}$ matrix

n is the number of measurements

The error associated with the sixth strain component is:

$$\varepsilon_z \pm (\text{error}^2 \text{ of } \varepsilon_x + \text{error}^2 \text{ of } \varepsilon_y)^{1/2} \qquad (13)$$

These calculated standard errors reflect how well the least squares analysis fits the data. Deviations of the measured shear strain values from the calculated values can be determined using the calculated principal strains. A negative expected value in calcite implies a negative sense of shear for that twin set, which is an impossibility according to our previous assumptions. Obviously then we have either substantial measurement errors, inhomogeneous strain, or a series of superimposed homogeneous strains. If substantial numbers of grains produce negative expected values, then the possibility of multiple deformations and overprinted strains exists. By removing these values and running them separately, it is possible to see if a new orientation and magnitude of strain axes can be determined with low statistical variation.

Statistically, the quality of results can be greatly improved by removing those grains which exhibit the largest negative and positive expected values; generally the largest 20 per cent (Groshong, 1974).

APPENDIX II

FORTRAN77 TWIN PROGRAM

(after Groshong, pers.
comm., 1982)

```
      PROGRAM TWIN(INPUT,OUTPUT,TWIN,TAPE1=TWIN,TAPE3=OUTPUT)
C
C     PURPOSE: CALCULATE BEST FIT STRAIN TENSOR FROM REAL SIMPLE SHEAR
C              STRAIN DATA
C
C     FIRST CARD CONTAINS PROGRAM OPTIONS
C   EXPLANATION OF PROGRAM OPTIONS:
C     IDATA = 1 PRINT UNCHANGED INPUT DATA, = 0 OMIT
C     IEGPSI = 1 PRINT BEARING AND PLUNGE OF E,C AND G AXES, THE ANGLE
C              BETWEEN C AND E, AND TANPSI/2, = 0 OMIT
C     ICT = 1 COMPUTE AND PRINT COMPRESSION AND TENSION AXES,
C           LAMELLAE SPACING INDEX, = 0 OMIT
C     ICON = 1 DO SPANG NUMERICAL DYNAMIC ANALYSIS, = 0 OMIT
C           IMPORTANT: ICT MUST = 1 IF ICON = 1
C     IDEV = 1 PRINT DEVIATIONS OF TWIN SET STRAINS FROM COMPUTED STRAIN
C            TENSOR, = 0 OMIT.
C     ICOMPR = 1 FOR EACH DATA SET READ IN A TEST VALUE OF THE STRAIN
C              TENSOR, USE TO FIND EXPECTED VALUES FOR MEASURED TWIN
C              SETS AND COMPUTE DEVIATIONS FROM MEASURED VALUES.
C            = 0 OMIT.
C
C     SECOND CARD CONTAINS SPECIAL INFORMATION
C   EXPLANATION OF SPECIAL INFORMATION
C     RATIO = FRACTION OF ACTUAL TWIN PER MEASURED MICROTWIN THICKNESS
C     IFUDGE = EFFECTIVE THICKNESS OF THICK TWINS: = 1 USE OUTER
C              THICKNESS, = 2 USE INNER THICKNESS, = 3 USE AVERAGE
C              THICKNESS, = 4 NOT DEFINED PROPERLY
C
C   EXPLANATION OF INPUT DATA VARIABLES:
C
C    INITIALIZATION CARDS, IN ORDER
C     SLIDEA AND SLIDEB = THIN SECTION I.D. NUMBER:
C            IROTAT = 0 DON'T ROTATE, = 1 ROTATE TO COORDINATE SYSTEM
C            SPECIFIED BY THE FOLLOWING DIRECTION COSINES:
C            ALPHA1,BETA1,GAMMA1 (COSINE FROM NEW +XYZ AXES TO T.S. +X)
C            ALPHA2,BETA2,GAMMA2 (COSINE FROM NEW +XYZ AXES TO T.S. +Y)
C            ALPHA3,BETA3,GAMMA3 (COSINE FROM NEW +XYZ AXES TO T.S. +Z)
C     CMBINE= IS DECK TO BE COMBINED WITH FOLLOWING DECK?
C           IF CMBINE = 0 DON'T COMBINE, = 1 COMBINE WITH NEXT DATA SET
C     TESTX,TESTY,TESTXY,TESTYZ,TESTXZ,TESTZ,THETA = OPTIONAL: SEE ABOVE
C            TEST VALUES ARE THE STRAIN COMPONENTS (AS FRACTIONS)
C            INDICATED BY THE LAST LETTER(S).  THETA IS 2-D ROTATION
C            REQUIRED TO PUT TEST VALUES INTO THIN SECTION COORDINATE
C            SYSTEM.  NO ROTATION, THETA = 0.0
C
C    DATA CARD VARIABLES
C     GRAIN = GRAIN I.D. NUMBER.  GRAIN = 999. TERMINATES INPUT FOR ONE
C             SLIDE.  IF NEXT CARD IS 1., ANOTHER DATA SET IS READ,
C             IF 999. PROGRAM TERMINATES.
C     CVIV = OPTIC AXIS, U-STAGE INNER VERTICAL
C     CVP = OPTIC AXIS, U-STAGE N-S
C     KODEC = OPTIC AXIS, U-STAGE N-S DIRECTION CODE: DIP E = 2, W = 4
C     TWINIV = TWIN POLE, U-STAGE INNER VERTICAL
C     TWINP = TWIN POLE, U-STAGE E-W
C     KODEE = TWIN POLE, U-STAGE E-W DIRECTION CODE: DIP N =1, S = 3
C     TOTALM = NUMBER OF MICROTWINS
C     THICKM = MEASURED THICKNESS OF MICROTWINS IN MICRONS
C     TOTALT = NUMBER OF THICK TWINS
C     THICKO = MEASURED OUTER THICKNESS OF THICK TWINS IN MICRONS
C     THICKI = MEASURED INNER THICKNESS OF THICK TWINS IN MICRONS
C     WIDTHN = WIDTH OF GRAIN NORMAL TO TWIN SET IN MICRONS
C     WIDTHP = WIDTH OF GRAIN PARALLEL TO TWIN SET IN MICRONS
C
C   EXPLANATION OF COORDINATE SYSTEM
C
C     +X = LONG AXIS (LENGTH) OF THIN SECTION = U-STAGE NORTH
C     +Y = SHORT AXIS (WIDTH) OF THIN SECTION = U-STAGE EAST
C     +Z = NORMAL TO XY PLANE (THICKNESS) OF THIN SECTION = U-STAGE DOWN
C
C   ADDITIONAL NOTE
C     THE ORDER OF STRAIN COMPONENTS IN THE SUBSCRIPTED VARIABLES ESLIDE
C     AND ERROR IS: 1=X,2=Y,3=XY,4=YZ,5=XZ,6=Z.  BUT IN SLISTR AND CONEL
C     IS: X,XY,Y,XZ,YZ,Z (FOR INPUT INTO SUBROUTINE EIGEN)
C
      DIMENSION CVIV(150),CVP(150),KODEC(150),TWINIV(150),
     1TWINP(150),KODEE(150),TOTALM(150),THICKM(150),TOTALT(150),
     2THICKO(150),PC(150),QC(150),RC(150),ANGLE(150),
     3ANGCVE(150),THICKI(150)
      DIMENSION DIRCG(150,3),DIRCE(150,3),TENSHR(150),COEFMX(150,6),
     1ESLIDE(6),ERROR(6),GRAIN(150),CAXIS(150,3),TAXIS(150,3),
     2WIDTHN(150),WIDTHP(150)
      COMMON DIRCG,DIRCE,TENSHR,COEFMX,ESLIDE,ERROR,RATIO,IFUDGE,
     1GRAIN,SLIDEA,SLIDEB,CAXIS,TAXIS,WIDTHN,WIDTHP
C
      READ (1,106) IDATA,IEGPSI,ICT,ICON,IDEV,ICOMPR
  106 FORMAT(I2,7X,5(I1,9X))
C
      READ(1,110)RATIO,IFUDGE
  110 FORMAT(F5.0,4X,I1)
C
   26 NPREV = 1
C      NPREV = COMBINED NUMBER OF TWIN SETS IN PREVIOUS DATA SET(S)
      NUM = 0
C      NUM = CUMULATIVE NUMBER OF TWIN SETS
   27 READ(1,10) SLIDEA,SLIDEB,IROTAT,ALPHA1,BETA1,GAMMA1,
     1ALPHA2,BETA2,GAMMA2,ALPHA3,BETA3,GAMMA3
   10 FORMAT(2A3,1X,I1,9(1X,F6.5))
```

```
C
   28 READ (1,11) CMBINE
   11 FORMAT (I1)
C
      IF (ICOMPR) 132,132,130
  130 READ (1,131) TESTX,TESTY,TESTXY,TESTYZ,TESTXZ,TESTZ,THETA
  131 FORMAT(F6.1,3X,F6.1,4X,F6.1,4X,F6.1,4X,F6.1,4X,F6.1,4X,F6.1)
  132 CONTINUE
C
      N = NUM+1
    3 READ(1,1)GRAIN(N),CVIV(N),CVP(N),KODEC(N),TWINIV(N),TWINP(N),
     1KODEE(N),TOTALM(N),THICKM(N),TOTALT(N),THICKO(N),THICKI(N),
     2WIDTHN(N),WIDTHP(N)
    1 FORMAT(F5.1,2X,F4.1,1X,F3.1,1X,I1,2X,F4.1,1X,F3.1,1X,I1,2X,
     1F4.1,1X,F4.1,2X,F4.1,1X,F4.1,1X,F4.1,2X,F5.1,1X,F5.1)
      IF(GRAIN(N)-999.)2,4,2
    2 N=N+1
      GO TO 3
    4 NUM=N-1
C
      NUMB=NUM-NPREV+1
      IF(IDATA) 100,100,101
  101 WRITE(3,102) SLIDEA,SLIDEB,NUMB
  102 FORMAT(1H1,'THIN SECTION  ',2A3,5X,'NUMBER OF TWIN SETS IS ',I5)
      WRITE(3,103)
  103 FORMAT(1H0,'GRAIN',3X,'OPTIC AXIS ORIENTATION',2X,'TWIN SET ORIENT
     1ATION',5X,'MICROTWINS',12X,'THICK TWINS',22X,'GRAIN WIDTHS'/
     21H ,10X,'INNER VERT',2X,'PLUNGE',5X,'INNER VERT',2X,'PLUNGE',3X,
     3'NUMBER THICKNESS',2X,'NUMBER OUTER-INNER THICKNESS',4X,'NORMAL TO
     4, PARALLEL TO TWIN'/)
      DO 104 I = NPREV,NUM
  104 WRITE(3,105) GRAIN(I),CVIV(I),CVP(I),KODEC(I),TWINIV(I),TWINP(I),

     1KODEE(I),TOTALM(I),THICKM(I),TOTALT(I),THICKO(I),THICKI(I),
     2WIDTHN(I),WIDTHP(I)
  105 FORMAT(1H ,F5.1,8X,F4.0,5X,F3.0,2X,I1,8X,F4.0,5X,F3.0,2X,I1,5X,
     1F4.0,3X,F4.2,6X,F4.0,3X,F4.2,3X,F4.2,15X,F6.0,6X,F6.0)
      IF(IROTAT.EQ.0) GO TO 100
      WRITE(3,107)ALPHA1,BETA1,GAMMA1,ALPHA2,BETA2,GAMMA2,
     1ALPHA3,BETA3,GAMMA3
  107 FORMAT(1H0,'DATA WILL BE ROTATED ACCORDING TO THE FOLLOWING DIRECT
     1ION COSINES'/1H0,
     2'L1 = ',F8.5,3X,'M1 = ',F8.5,3X,'N1 = ',F8.5/1H ,
     3'L2 = ',F8.5,3X,'M2 = ',F8.5,3X,'N2 = ',F8.5/1H ,
     4'L3 = ',F8.5,3X,'M3 = ',F8.5,3X,'N3 = ',F8.5)
C
C     CALCULATE BEARING AND PLUNGE
C    DANGER  FOR SYSTEMATIC ORIENTATION ERROR SEE FN. BEARIN
  100 DO 5 I = NPREV,NUM
      CVIV(I)=BEARIN(CVIV(I),KODEC(I))
    5 TWINIV(I)=BEARIN(TWINIV(I),KODEE(I))
C     CVIV AND TWINIV ARE NOW BEARINGS, IN DEGREES
C     VARIABLES KODEC AND KODEE ARE NOT USED PAST THIS POINT
C
      DO 6 I = NPREV,NUM
      CALL DIRCOS(CVIV(I),CVP(I),PC(I),QC(I),RC(I))
    6 CALL DIRCOS(TWINIV(I),TWINP(I),DIRCE(I,1),DIRCE(I,2),DIRCE(I,3))
C
C     ROTATE TO DIFFERENT COORDINATE SYSTEM IF REQUIRED
      IF(IROTAT) 33,33,31
   31 DO 32 I=NPREV,NUM
      CALL ROTATE(PC(I),QC(I),RC(I),ALPHA1,ALPHA2,ALPHA3,
     1BETA1,BETA2,BETA3,GAMMA1,GAMMA2,GAMMA3)
   32 CALL ROTATE(DIRCE(I,1),DIRCE(I,2),DIRCE(I,3),
     1ALPHA1,ALPHA2,ALPHA3,BETA1,BETA2,BETA3,GAMMA1,GAMMA2,GAMMA3)
C     ALL DIRECTIONS ARE IN THE DIFFERENT COORDINATE SYSTEM PAST HERE
   33 CONTINUE
C
C     FIND THE ACUTE ANGLE BETWEEN CV AND E IN RADIANS (ANGCVE)
      DO 7 I = NPREV,NUM
      A=PC(I)*DIRCE(I,1)+QC(I)*DIRCE(I,2)+RC(I)*DIRCE(I,3)
      ANGLE(I)=57.2957795*ACOS(A)
C
C     CHECK TO SEE THAT ANGLE BETWEEN OPTIC AXIS AND E IS ACUTE
      IF(ANGLE(I)-90.) 136,136,135
  135 PC(I)=-PC(I)
      QC(I)=-QC(I)
      RC(I)=-RC(I)
  136 CONTINUE
C
    7 ANGCVE(I)=ACOS(ABS(A))
      DO 40 I = NPREV,NUM
      CALL STRAIN(THICKM(I),TOTALM(I),THICKO(I),THICKI(I),TOTALT(I),I)
   40 CALL GAXIS(PC(I),QC(I),RC(I),DIRCE(I,1),DIRCE(I,2),DIRCE(I,3),
     1ANGCVE(I),DIRCG(I,1),DIRCG(I,2),DIRCG(I,3))
C
      IF (IEGPSI) 112,111,112
  112 WRITE(3,8) SLIDEA,SLIDEB,NUMB,RATIO,IFUDGE
    8 FORMAT(1H1,'SLIDE ',2A3,'   NUMBER OF TWIN SETS IS',I5,'    THICKTWI
     1N/MICROTWIN RATIO = ',F5.3,'    THICK TWIN OPTION IS  ',I1)
      IF(IROTAT.EQ.0) GO TO 35
      WRITE(3,34)
   34 FORMAT(1H0,'ANGLES ARE WITH RESPECT TO ROTATED COORDINATE SYSTEM'/
     1)
   35 WRITE(3,30)
   30 FORMAT(1H0,'GRAIN',3X,'BEARING C     PLUNGE C',4X,'BEARING E     PLU
     1NGE E',4X,'ANGLE(C,E)',4X,'BEARING G     PLUNGE G',7X,
     2'TANPSI/2'/)
```

```
      DO 41 I = NPREV,NUM
      CALL BEARPL(PC(I),QC(I),RC(I),BEARC,PLUNC,KC)
      CALL BEARPL(DIRCE(I,1),DIRCE(I,2),DIRCE(I,3),BEARE,PLUNE,KE)
      CALL BEARPL(DIRCG(I,1),DIRCG(I,2),DIRCG(I,3),BEARG,PLUNG,KG)
      ANGCE=ANGCVE(I)*57.2957795
   41 WRITE(3,42) GRAIN(I),BEARC,PLUNC,BEARE,PLUNE,ANGCE,BEARG,PLUNG,
     1TINSHR(I)
   42 FORMAT(1H ,F5.1,5X,F5.1,7X,F5.1,8X,F5.1,7X,F5.1,7X,F5.1,10X,F5.1,
     17X,F5.1,9X,F9.7)
  111 CONTINUE
C
C     FIND COMPRESSION AND TENSION AXES, SPACING INDEX
      IF(ICT) 125,125,120
  120 WRITE(3,121) SLIDEA,SLIDEB
  121 FORMAT(1H1,13X,'DYNAMIC ANALYSIS OF THIN SECTION  ',2A3/)
      IF (IROTAT.EQ.0) GO TO 126
      WRITE(3,34)
  126 WRITE(3,122)
  122 FORMAT(1H0,'GRAIN',6X,'COMPRESSION AXES',9X,'TENSION AXES',9X,
     1'NO. OF LAMELLAE'/
     21H ,11X,'BEARING    PLUNGE',7X,'BEARING    PLUNGE',7X,'PER MILLIMETE
     3R'//)
      DO 123 I=1,NUM
      CALL CTAXIS(PC(I),QC(I),RC(I),DIRCE(I,1),DIRCE(I,2),DIRCE(I,3),
     1ANGCVE(I),I)
      CALL BEARPL(TAXIS(I,1),TAXIS(I,2),TAXIS(I,3),BTENS,PTENS,K)
      CALL BEARPL(CAXIS(I,1),CAXIS(I,2),CAXIS(I,3),BCOMP,PCOMP,K)
      SINDEX=(TOTALM(I)+TOTALT(I))/(WIDTHN(I)*0.001)
  123 WRITE(3,124) GRAIN(I),BCOMP,PCOMP,BTENS,PTENS,SINDEX
  124 FORMAT(1H ,F5.1,7X,F5.1,4X,F5.1,9X,F5.1,4X,F5.1,13X,F5.1)
C
      IF (CMBINE) 114,114,113
  113 NPREV = NUM+1
      GO TO 27
  114 CONTINUE
C
      IF (ICON.EQ.0) GO TO 125
      CALL SPANG(NUM)
C
  125 CALL DATA(NUM)
      CALL REGRES(NUM,5)
      CALL TIDYUP
      CALL PRIN
C
      IF (IDEV) 141,141,140
  140 CALL DEVIAT(NUM)
  141 CONTINUE
C
      IF(ICOMPR) 134,134,133
  133 CALL CMPARE(TESTX,TESTY,TESTXY,TESTYZ,TESTXZ,TESTZ,THETA,NUM)
  134 CONTINUE
C
C     FINAL CARD IS 999. TO END RUN; 1. TO BEGIN AGAIN
      READ(1,50) FINIS
   50 FORMAT(F5.1)
      IF (FINIS-999.) 26,51,26
   51 CONTINUE
      STOP
      END
      FUNCTION BEARIN(SIV,KODE)
C
C     THIS FN. ONLY APPLIES IF IV READS  0 WHEN THE LONG AXIS OF THE
C     THIN SECTION IS N-S IN THE MICROSCOPE
C
      GO TO(1,2,3,4),KODE
    1 BEARIN=180.-SIV
      IF(BEARIN) 5,6,6
    2 BEARIN=270.-SIV
      IF(BEARIN) 5,6,6
    3 BEARIN=360.-SIV
      IF(BEARIN) 5,6,6
    4 BEARIN= 90.-SIV
      IF(BEARIN) 5,6,6
    5 BEARIN=360.+BEARIN
C     SIV IS STAGE INNER VERTICAL
C     KODE IS DIRECTION CODE,1=N.,2=E.,3=S.,4=W.
    6 RETURN
      END
      SUBROUTINE DIRCOS(BARING,PLUNGE,P,Q,R)
      P=COS(PLUNGE*.01745)*COS(BARING*.01745)
      Q=COS(PLUNGE*.01745)*SIN(BARING*.01745)
      R=SIN(PLUNGE*.01745)
C     P=COS(VECTOR,N.), Q=COS(VECTOR,E.), R=COS(VECTOR,DOWN)
      RETURN
      END
      SUBROUTINE ROTATE(P,Q,R,AL1,AL2,AL3,BET1,BET2,BET3,GAM1,GAM2,GAM3)
      ROL= AL1*P+AL2*Q+AL3*R
      ROM = BET1*P+BET2*Q+BET3*R
      R = GAM1*P+GAM2*Q+GAM3*R
      P=ROL
      Q=ROM
      RETURN
      END
      SUBROUTINE CTAXIS(PC,QC,RC,PE,QE,RE,ANGCVE,N)
C
C     PURPOSE: TO CALCULATE DIRECTION COSINES OF COMPRESSION AND
C              TENSION AXES
C
```

```
C
      DIMENSION DIRCG(150,3),DIRCE(150,3),TENSHR(150),COEFMX(150,5),
     1ESLIDE(6),ERROR(6),GRAIN(150),CAXIS(150,3),TAXIS(150,3),
     2WIDTHN(150),WIDTHP(150)
      COMMON DIRCG,DIRCE,TENSHR,COEFMX,ESLIDE,ERROR,RATIO,IFUDGE,
     1GRAIN,SLIDEA,SLIDEB,CAXIS,TAXIS,WIDTHN,WIDTHP
C
C     FIND T AXIS
    2 A=QC*RE-QE*RC
      B=PE*RC-PC*RE
      C=PC*QE-PE*QC
      D=(A**2)+(B**2)+(C**2)
      IF(C) 6,5,6
    5 C=.0000001
    6 IF(D) 3,3,4
    3 D= .00001
    4 ANGT=COS(45.*.0174533-ANGCVE)
      YA=(QC*C-RC*B)*.70711
      YB=(RC*A-PC*C)*.70711
      ZA=(QE*C-RE*B)*ANGT
      ZB=(RE*A-PE*C)*ANGT
      TAXIS(N,1)=(YA-ZA)/D
      TAXIS(N,2)=(YB-ZB)/D
      TAXIS(N,3)=-(A*(YA-ZA)+B*(YB-ZB))/(C*D)
C
C     FIND C AXIS
      ANGT=COS(45.*.0174533+ANGCVE)
      ZA=(QE*C-RE*B)*ANGT
      ZB=(RE*A-PE*C)*ANGT
      CAXIS(N,1)=(YA-ZA)/D
      CAXIS(N,2)=(YB-ZB)/D
      CAXIS(N,3)=-(A*(YA-ZA)+B*(YB-ZB))/(C*D)
      RETURN
      END
      SUBROUTINE GAXIS(PC,QC,RC,PE,QE,RE,ANGCVE,PG,QG,RG)
C
C     PURPOSE: TO CALCULATE THE DIRECTION COSINES OF A VECTOR IN THE
C                G-GLIDE DIRECTION (PG,QG,RG)
C     REQUIRED INPUT: PC,QC,RC:PE,QE,RE; ANGCVE
C     OUTPUT: PG,QG,RG
C
C     FIND GAXIS
    2 COSCVG=COS(90.*.0174533-ANGCVE)
      A=QC*RE-QE*RC
      B=PE*RC-PC*RE
      C=PC*QE-PE*QC
      D=A**2+B**2+C**2
      IF (D) 3,3,4
    3 D=.000001
    4 RG=((PE*B-QE*A)*COSCVG)/D
      QG=((RE*A-PE*C)*COSCVG)/D
      PG=((QE*C-RE*B)*COSCVG)/D
      RETURN
      END
      SUBROUTINE BEARPL(P,Q,R,BEARIN,PLUNGE,K)
      PP=P
      QQ=Q+.00001
      RR=R
      THETA=57.29578*ATAN(PP/QQ)
      K=0
      IF(RR) 10,9,9
   10 PP=-P
      QQ=-Q
      RR=-R
      K=1
    9 IF(PP) 4,1,1
    1 IF(QQ) 3,2,2
    2 BEARIN=90.-THETA
      GO TO 7
    3 BEARIN=270.-THETA
      GO TO 7
    4 IF(QQ) 3,2,2
    7 D=57.29578*ACOS(RR)
      PLUNGE=90.-D
C     PLUNGE ON LOWER HEMISPHERE,K=0; UPPER HEMISPHERE,K=1
      RETURN
      END
      SUBROUTINE STRAIN(THICKM,TOTALM,THICKO,THICKI,TOTALT,I)
C
C     PURPOSE: GENERATE STRAIN DUE TO TWINNING
C     TENSHR IS TENSOR SHEAR STRAIN
C
      DIMENSION DIRCG(150,3),DIRCE(150,3),TENSHR(150),COEFMX(150,5),
     1ESLIDE(6),ERROR(6),GRAIN(150),CAXIS(150,3),TAXIS(150,3),
     2WIDTHN(150),WIDTHP(150)
      COMMON DIRCG,DIRCE,TENSHR,COEFMX,ESLIDE,ERROR,RATIO,IFUDGE,
     1GRAIN,SLIDEA,SLIDEB,CAXIS,TAXIS,WIDTHN,WIDTHP
C
      THICKM=RATIO*THICKM
      IF(TOTALT) 6,5,6
    6 GO TO (1,2,3,4),IFUDGE
    1 THICKT = THICKO
      GO TO 5
    2 THICKT=THICKI
      GO TO 5
    3 THICKT=(THICKO+THICKI)/2.
      GO TO 5
    4 THICKT=5000.
```

```
    5 TENSHR(I)=.347*((THICKM*TOTALM+THICKT*TOTALT)/WIDTHN(I))
      RETURN
      END
      SUBROUTINE DATA(N)
C
C     PURPOSE: TO CALCULATE STRAIN COEFFICIENT MATRIX IN SPECIFIED
C              COORDINATES FOR SIMPLE SHEAR MEASUREMENTS, ZERO
C              VOLUME CHANGE
C
      DIMENSION DIRCG(150,3),DIRCE(150,3),TENSHR(150),COEFMX(150,5),
     1ESLIDE(6),ERROR(6),GRAIN(150),CAXIS(150,3),TAXIS(150,3),
     2WIDTHN(150),WIDTHP(150)
      COMMON DIRCG,DIRCE,TENSHR,COEFMX,ESLIDE,ERROR,RATIO,IFUDGE,
     1GRAIN,SLIDEA,SLIDEB,CAXIS,TAXIS,WIDTHN,WIDTHP
C
C     DIRCE = DIRECTION COSINES OF E POLE (L1,M1,N1)
C     DIRCG = DIRECTION COSINES OF G GLIDE DIRECTION (L2,M2,N2)
C
      DO 4 I=1,N
      COEFMX(I,1)=DIRCE(I,1)*DIRCG(I,1)-DIRCE(I,3)*DIRCG(I,3)
      COEFMX(I,2)=DIRCE(I,2)*DIRCG(I,2)-DIRCE(I,3)*DIRCG(I,3)
      COEFMX(I,3)=DIRCE(I,1)*DIRCG(I,2)+DIRCE(I,2)*DIRCG(I,1)
      COEFMX(I,4)=DIRCE(I,2)*DIRCG(I,3)+DIRCE(I,3)*DIRCG(I,2)
    4 COEFMX(I,5)=DIRCE(I,3)*DIRCG(I,1)+DIRCE(I,1)*DIRCG(I,3)
C
C     THE COEF ARE IN ORDER OF EX,EY,EXY,EYZ,EXZ
      RETURN
      END
      SUBROUTINE REGRES(NUM,NCOL)
C
C     PURPOSE: LEAST SQUARES FIT, GIVEN DATA MATRIX (COEFMX) AND
C              MEASURED VARIABLE VECTOR (TENSHR)
C
      DIMENSION COEFTR(5,150),L(5),M(5),COVECT(25),XY(5)
      DIMENSION DIRCG(150,3),DIRCE(150,3),TENSHR(150),COEFMX(150,5),
     1ESLIDE(6),ERROR(6),GRAIN(150),CAXIS(150,3),TAXIS(150,3),
     2WIDTHN(150),WIDTHP(150)
      COMMON DIRCG,DIRCE,TENSHR,COEFMX,ESLIDE,ERROR,RATIO,IFUDGE,
     1GRAIN,SLIDEA,SLIDEB,CAXIS,TAXIS,WIDTHN,WIDTHP
C
C     CALCULATE COVARIANCE MATRIX: (X'X) INVERSE
      DO 10 J=1,NCOL
      DO 10 I=1,NUM
   10 COEFTR(J,I)=COEFMX(I,J)
      DO 11 J=1,NCOL
      JI=(J-1)*NCOL
      DO 11 I=1,NCOL
      ZIJ=0.0
      DO 12 K=1,NUM
   12 ZIJ=COEFTR(J,K)*COEFMX(K,I)+ZIJ
   11 COVECT(I+JI)=ZIJ
      CALL MINV(COVECT,NCOL,D,L,M)
C
C     ESTIMATE MODEL PARAMETERS: ESLIDE
      DO 30 I=1,NCOL
      XY(I)=0.0
      DO 30 J=1,NUM
   30 XY(I)=COEFTR(I,J)*TENSHR(J)+XY(I)
      DO 31 I=1,NCOL
      II=(I-1)*NCOL
      ESLIDE(I)=0.0
      DO 31 J=1,NCOL
   31 ESLIDE(I)=ESLIDE(I)+COVECT(J+II)*XY(J)
      ESLIDE(6)=-ESLIDE(1)-ESLIDE(2)
C
C     CALCULATE SSE
      YY=0.0
      DO 40 I=1,NUM
   40 YY=YY+TENSHR(I)**2
      BXY=0.0
      DO 41 I=1,NCOL
   41 BXY=BXY+ESLIDE(I)*XY(I)
      SSE=YY-BXY
C
C     CALCULATE STANDARD ERROR FOR MODEL PARAMETERS
C     ORDER OF ERROR SAME AS ESLIDE
      IF(NUM-NCOL) 45,44,45
   44 VARNCE=0.0
      GO TO 46
   45 VARNCE=SSE/FLOAT(NUM-NCOL)
      IF(VARNCE) 58,46,46
   46 JDIAG=1
      DO 47 I=1,NCOL
      IF(COVECT(JDIAG)) 58,49,49
   49 ERROR(I)=SQRT(VARNCE)*SQRT(COVECT(JDIAG))
   47 JDIAG=JDIAG+1+NCOL
      ERROR(6)=SQRT(ERROR(1)**2+ERROR(2)**2)
C
C     PRINT OUT RESULTS
   58 WRITE(3,50) NUM
   50 FORMAT(1H1,30X,'LEAST SQUARES STRAIN CALCULATION',5X,
     1'NO. OF TWIN SETS = ',I3//)
      WRITE(3,52) D
   52 FORMAT(1H0,15X,'VARIANCE-COVARIANCE MATRIX',10X,'DETERMINANT =',
     1E15.7/)
      DO 57 I=1,5
   57 WRITE(3,53) COVECT(I),COVECT(I+5),COVECT(I+10),COVECT(I+15),
```

```
      1COVECT(I+20)
   53 FORMAT(1H ,9X,5(E15.7,3X))
      WRITE(3,51) SSE,VARNCE
   51 FORMAT(1H0,11X,'SUM OF SQUARES OF ERROR = ',F15.6,10X,
     1'SAMPLE VARIANCE = ',F15.6/)
      WRITE(3,54)
   54 FORMAT(1H0//1H ,20X,'ESTIMATED TENSOR IN SLIDE COORDINATES: EXTENS
     1ION IS +'/)
      WRITE(3,55) ESLIDE
   55 FORMAT(1H0,'EX=',E14.7,3X,'EY=',E14.7,3X,'EXY=',E14.7,3X,
     1'EYZ=',E14.7,3X,'EXZ=',E14.7,3X,'EZ=',E14.7)
      WRITE(3,56)
   56 FORMAT(1H0//1H ,25X,'STANDARD ERROR OF STRAIN COMPONENTS'/)
      WRITE(3,55) ERROR
      RETURN
      END
      SUBROUTINE TIDYUP
C
C     PURPOSE: FIND PRINCIPAL STRAINS IN 3 DIMENSIONS
C
      DIMENSION SLISTR(6),PRINAX(9)
      DIMENSION DIRCG(150,3),DIRCE(150,3),TENSHR(150),COEFMX(150,5),
     1ESLIDE(6),ERROR(6),GRAIN(150),CAXIS(150,3),TAXIS(150,3),
     2WIDTHN(150),WIDTHP(150)
      COMMON DIRCG,DIRCE,TENSHR,COEFMX,ESLIDE,ERROR,RATIO,IFUDGE,
     1GRAIN,SLIDEA,SLIDEB,CAXIS,TAXIS,WIDTHN,WIDTHP
C
      SLISTR(1)=ESLIDE(1)
      SLISTR(2)=ESLIDE(3)
      SLISTR(3)=ESLIDE(2)
      SLISTR(4)=ESLIDE(5)
      SLISTR(5)=ESLIDE(4)
      SLISTR(6)=ESLIDE(6)
      CALL EIGEN(SLISTR,PRINAX,3,0)
      CALL BEARPL(PRINAX(1),PRINAX(2),PRINAX(3),BEAR1,PLUNG1,K1)
      CALL BEARPL(PRINAX(4),PRINAX(5),PRINAX(6),BEAR2,PLUNG2,K2)
      CALL BEARPL(PRINAX(7),PRINAX(8),PRINAX(9),BEAR3,PLUNG3,K3)
      WRITE(3,1)
    1 FORMAT(1H0,//1H0,5X,'PRINCIPAL STRAINS',9X,'BEARING',5X,'PLUNGE'/)
      WRITE(3,2) SLISTR(1),BEAR1,PLUNG1
      WRITE(3,2) SLISTR(3),BEAR2,PLUNG2
      WRITE(3,2) SLISTR(6),BEAR3,PLUNG3
    2 FORMAT(1H ,6X,E14.7,12X,F5.1,6X,F5.1)
      RETURN
      END
      SUBROUTINE PRIN
C     PURPOSE: FIND PRINCIPAL STRAINS AND AXES IN PLANE OF THIN SECTION
C
C     ANGLES ARE POSITIVE CLOCKWISE BECAUSE OF COORDINATE SYSTEM
C
      DIMENSION DIRCG(150,3),DIRCE(150,3),TENSHR(150),COEFMX(150,5),
     1ESLIDE(6),ERROR(6),GRAIN(150),CAXIS(150,3),TAXIS(150,3),
     2WIDTHN(150),WIDTHP(150)
      COMMON DIRCG,DIRCE,TENSHR,COEFMX,ESLIDE,ERROR,RATIO,IFUDGE,
     1GRAIN,SLIDEA,SLIDEB,CAXIS,TAXIS,WIDTHN,WIDTHP
C
    1 EXY=ESLIDE(3)
    3 EX=ESLIDE(1)
      EY=ESLIDE(2)
      ANGRDN=(2.*EXY)/(EX-EY)
      TWOANG = ATAN(ANGRDN)
      IF(ABS(ANGRDN)-1.5707963) 17,16,16
   16 TWOANG=TWOANG+SIGN(.7853982,ANGRDN)
   17 ANG= TWOANG*57.29578/2.
    6 FA=(EX-EY)/2.
      RADIUS=SQRT((FA**2)+EXY**2)
      CENTER=(EX+EY)/2.
      EMIN=CENTER+RADIUS
      EMAX=CENTER-RADIUS
C
C     PRINT RESULTS
      WRITE(3,7) SLIDEA,SLIDEB
    7 FORMAT(//1H0,'STRAIN IN PLANE OF THIN SECTION ',2A3,'  TENSION IS
     1+'/)
      WRITE(3,8) EMAX
    8 FORMAT(1H ,'MAXIMUM COMPRESSIVE STRAIN = ',E14.7)
      WRITE(3,9) EMIN
    9 FORMAT(1H ,'MINIMUM COMPRESSIVE STRAIN = ',E14.7)
      IF(EX-EY) 10,10,18
   18 WRITE(3,19) ANG
   19 FORMAT(1H0,'ANGLE FROM Y AXIS TO MAXIMUM COMPRESSIVE STRAIN AXIS,
     1POSITIVE CLOCKWISE = ',E14.7,' DEGREES')
      GO TO 14
   10 WRITE(3,11) ANG
   11 FORMAT(1H0,'ANGLE FROM X AXIS TO MAXIMUM COMPPESSIVE STRAIN AXIS,
     1POSITIVE CLOCKWISE = ',E14.7,' DEGREES')
   14 RETURN
      END
      SUBROUTINE DEVIAT(I)
C
C     PURPOSE: FIND EXPECTED VALUE OF STRAIN IN SLIDE COORDINATES AND
C              DEVIATION FROM MEASURED VALUE
C
      DIMENSION DIRCG(150,3),DIRCE(150,3),TENSHR(150),COEFMX(150,5),
     1ESLIDE(6),ERROR(6),GRAIN(150),CAXIS(150,3),TAXIS(150,3),
     2WIDTHN(150),WIDTHP(150)
      COMMON DIRCG,DIRCE,TENSHR,COEFMX,ESLIDE,ERROR,RATIO,IFUDGE,
     1GRAIN,SLIDEA,SLIDEB,CAXIS,TAXIS,WIDTHN,WIDTHP
```

```
C
      WRITE(3,2) SLIDEA,SLIDEB
    2 FORMAT(1H1,10X,'DEVIATIONS OF MEASURED STRAINS FROM CALCULATED STR
     1AINS FOR THIN SECTION ',2A3/
     21H ,'GRAIN',8X,'TANPSI/2',8X,'EXPECTED VALUE',6X,'TANPSI/2 - E.V.
     3'/)
      DO 3 N=1,I
      EXPECT=DIRCE(N,1)*DIRCG(N,1)*ESLIDE(1)+
     1DIRCE(N,2)*DIRCG(N,2)*ESLIDE(2)+
     2DIRCE(N,3)*DIRCG(N,3)*ESLIDE(6)+
     3(DIRCE(N,2)*DIRCG(N,3)+DIRCG(N,2)*DIRCE(N,3))*ESLIDE(4)+
     4(DIRCE(N,3)*DIRCG(N,1)+DIRCG(N,3)*DIRCE(N,1))*ESLIDE(5)+
     5(DIRCE(N,1)*DIRCG(N,2)+DIRCG(N,1)*DIRCE(N,2))*ESLIDE(3)
      DEV=TENSHR(N)-EXPECT
    3 WRITE(3,1) GRAIN(N),TENSHR(N),EXPECT,DEV
    1 FORMAT(1H ,F5.1,5X,F14.9,5X,F14.9,6X,F14.9)
      RETURN
      END
      SUBROUTINE CMPARE(TESTX,TESTY,TESTXY,TESTYZ,TESTXZ,TESTZ,THETA,N)
C
C     PURPOSE: FIND THE EXPECTED VALUES OF TWIN-SET STRAINS FROM A TEST
C              VALUE OF A STRAIN TENSOR AND THEIR DEVIATIONS FROM
C              MEASURED VALUES.
C
      DIMENSION DIRCG(150,3),DIRCE(150,3),TENSHR(150),COEFMX(150,5),
     1ESLIDE(6),ERROR(6),GRAIN(150),CAXIS(150,3),TAXIS(150,3),
     2WIDTHN(150),WIDTHP(150)
      COMMON DIRCG,DIRCE,TENSHR,COEFMX,ESLIDE,ERROR,RATIO,IFUDGE,
     1GRAIN,SLIDEA,SLIDEB,CAXIS,TAXIS,WIDTHN,WIDTHP
C
      WRITE (3,1) SLIDEA,SLIDEB
    1 FORMAT(1H1,10X,'DEVIATIONS OF MEASURED STRAINS FROM TEST-VALUE STR
     1AINS FOR THIN SECTION ',2A3//
     21H ,20X,'THE TEST-VALUE STRAIN TENSOR IS:'/)
      WRITE(3,2) TESTX,TESTY,TESTXY,TESTYZ,TESTXZ,TESTZ,THETA
    2 FORMAT(1H ,'EX# = ',F7.4,'  EY# = ',F7.4,'  EXY# = ',F7.4,
     1'  EYZ# = ',F7.4,'  EXZ# = ',F7.4,'  EZ# = ',F7.4//
     21H ,10X,'THE ANGLE, POSITIVE COUNTERCLOCKWISE IN DEGREES, FROM THE
     3 UNPRIMED (THIN SECTION)'/1H ,21X,'TO THE PRIMED COORDINATE SYSTEM
     4 = ',F6.2///)
      IF (THETA) 3,4,3
    3 THETA=THETA*.01745329
      EX=TESTX*COS(THETA)**2+TESTY*SIN(THETA)**2+TESTXY*SIN(2.*THETA)
      EY=TESTX*SIN(THETA)**2+TESTY*COS(THETA)**2-TESTXY*SIN(2.*THETA)
      EXY=.5*SIN(2.*THETA)*(TESTY-TESTX)+TESTXY*COS(2.*THETA)
      GO TO 5
    4 EX=TESTX
      EY=TESTY
      EXY=TESTXY
    5 EYZ=TESTYZ
      EXZ=TESTXZ
      EZ=TESTZ
      WRITE(3,6)
    6 FORMAT(1H ,20X,'THE TEST-VALUE STRAIN TENSOR IN THIN SECTION COORD
     1INATES IS:'/)
      WRITE(3,7) EX,EY,EXY,EYZ,EXZ,EZ
    7 FORMAT(1H ,' EX = ',F7.4,'  EY = ',F7.4,'  EXY = ',F7.4,'  EYZ = '
     1,F7.4,'  EXZ = ',F7.4,'  EZ = ',F7.4///)
      WRITE(3,8)
    8 FORMAT(1H ,'GRAIN',8X,'TANPSI/2',8X,'EXPECTED VALUE',6X,'TANPSI/2
     1- E.V.'/)
      SSE=0.0
      DO 9 I=1,N
      EXPECT=DIRCE(I,1)*DIRCG(I,1)*EX+DIRCE(I,2)*DIRCG(I,2)*EY+
     1DIRCE(I,3)*DIRCG(I,3)*EZ+
     2(DIRCE(I,2)*DIRCG(I,3)+DIRCG(I,2)*DIRCE(I,3))*EYZ+
     3(DIRCE(I,3)*DIRCG(I,1)+DIRCG(I,3)*DIRCE(I,1))*EXZ+
     4(DIRCE(I,1)*DIRCG(I,2)+DIRCG(I,1)*DIRCE(I,2))*EXY
      DEV=TENSHR(I)-EXPECT
      SSE=SSE+DEV**2
    9 WRITE(3,10) GRAIN(I),TENSHR(I),EXPECT,DEV
   10 FORMAT(1H ,F5.1,5X,F14.9,5X,F14.9,6X,F14.9)
      WRITE(3,11)SSE
   11 FORMAT(///1H ,'SUM OF SQUARES OF ERROR = ',F15.6)
      RETURN
      END
      SUBROUTINE SPANG(NUM)
C
C     PURPOSE: CALCULATE SPANG NUMERICAL DYNAMIC ANALYSIS.
C
      DIMENSION CONELS(6),STRAIN(150),PRINAX(9)
      DIMENSION DIRCG(150,3),DIRCE(150,3),TENSHR(150),COEFMX(150,5),
     1ESLIDE(6),ERROR(6),GRAIN(150),CAXIS(150,3),TAXIS(150,3),
     2WIDTHN(150),WIDTHP(150)
      COMMON DIRCG,DIRCE,TENSHR,COEFMX,ESLIDE,ERROR,RATIO,IFUDGE,
     1GRAIN,SLIDEA,SLIDEB,CAXIS,TAXIS,WIDTHN,WIDTHP
C
    9 DO 10 N=1,NUM
   10 STRAIN(N)=1.0/FLOAT(NUM)
      WRITE(3,11) SLIDEA,SLIDEB,NUM
   11 FORMAT(1H1,29X,'SPANG NUMERICAL DYNAMIC ANALYSIS'/
     11H0,22X,'THIN SECTION  ',2A3,5X,'NUMBER OF TWIN SETS = ',I3/)
      WRITE(3,12)
   12 FORMAT(1H0,10X,'NDA X',11X,'NDA XY',10X,'NDA Y',11X,'NDA XZ',10X,
     1'NDA YZ',10X,'NDA Z'/)
   13 DO 14 N=1,6
   14 CONELS(N)=0.0
```

```
      DO 15 N=1,NUM
      CONELS(1)=CONELS(1)+(TAXIS(N,1)**2-CAXIS(N,1)**2)*STRAIN(N)
      CONELS(3)=CONELS(3)+(TAXIS(N,2)**2-CAXIS(N,2)**2)*STRAIN(N)
      CONELS(6)=CONELS(6)+(TAXIS(N,3)**2-CAXIS(N,3)**2)*STRAIN(N)
      CONELS(2)=CONELS(2)+(TAXIS(N,1)*TAXIS(N,2)-CAXIS(N,1)*CAXIS(N,2))*
     1STRAIN(N)
      CONELS(4)=CONELS(4)+(TAXIS(N,1)*TAXIS(N,3)-CAXIS(N,1)*CAXIS(N,3))*
     1STRAIN(N)
   15 CONELS(5)=CONELS(5)+(TAXIS(N,2)*TAXIS(N,3)-CAXIS(N,2)*CAXIS(N,3))*
     1STRAIN(N)
      WRITE(3,16) CONELS
   16 FORMAT(1H0,7X,6(F11.7,5X))
      CALL EIGEN(CONELS,PRINAX,3,0)
      CALL BEARPL(PRINAX(1),PRINAX(2),PRINAX(3),BEAR1,PLUNG1,K)
      CALL BEARPL(PRINAX(4),PRINAX(5),PRINAX(6),BEAR2,PLUNG2,K)
      CALL BEARPL(PRINAX(7),PRINAX(8),PRINAX(9),BEAR3,PLUNG3,K)
      WRITE(3,17)
   17 FORMAT(1H0,10X,'EIGENVALUES AND EIGENVECTORS'/
     11H0,12X,'MAGNITUDE   BEARING PLUNGE')
      WRITE(3,18) CONELS(1),BEAR1,PLUNG1
      WRITE(3,18) CONELS(3),BEAR2,PLUNG2
      WRITE(3,18) CONELS(6),BEAR3,PLUNG3
   18 FORMAT(1H ,11X,F10.6,2X,F7.1,1X,F6.1)
   19 RETURN
      END
      SUBROUTINE EIGEN(A,R,N,MV)
C
C     ..................................................................
C
C        SUBROUTINE EIGEN
C
C        PURPOSE
C           COMPUTE EIGENVALUES AND EIGENVECTORS OF A REAL SYMMETRIC
C           MATRIX
C
C        USAGE
C           CALL EIGEN(A,R,N,MV)
C
C        DESCRIPTION OF PARAMETERS
C           A - ORIGINAL MATRIX (SYMMETRIC), DESTROYED IN COMPUTATION.
C               RESULTANT EIGENVALUES ARE DEVELOPED IN DIAGONAL OF
C               MATRIX A IN DESCENDING ORDER.
C           R - RESULTANT MATRIX OF EIGENVECTORS (STORED COLUMNWISE,
C               IN SAME SEQUENCE AS EIGENVALUES)
C           N - ORDER OF MATRICES A AND R
C           MV- INPUT CODE
C                   0   COMPUTE EIGENVALUES AND EIGENVECTORS
C                   1   COMPUTE EIGENVALUES ONLY (R NEED NOT BE
C                       DIMENSIONED BUT MUST STILL APPEAR IN CALLING
C                       SEQUENCE)
C
C        REMARKS
C           ORIGINAL MATRIX A MUST BE REAL SYMMETRIC (STORAGE MODE=1)
C           MATRIX A CANNOT BE IN THE SAME LOCATION AS MATRIX R
C
C        SUBROUTINES AND FUNCTION SUBPROGRAMS REQUIRED
C           NONE
C
C        METHOD
C           DIAGONALIZATION METHOD ORIGINATED BY JACOBI AND ADAPTED
C           BY VON NEUMANN FOR LARGE COMPUTERS AS FOUND IN 'MATHEMATICAL
C           METHODS FOR DIGITAL COMPUTERS', EDITED BY A. RALSTON AND
C           H.S. WILF, JOHN WILEY AND SONS, NEW YORK, 1962, CHAPTER 7
C
C     ..................................................................
C
      DIMENSION A(1),R(1)
C
C        ...............................................................
C
C        IF A DOUBLE PRECISION VERSION OF THIS ROUTINE IS DESIRED, THE
C        C IN COLUMN 1 SHOULD BE REMOVED FROM THE DOUBLE PRECISION
C        STATEMENT WHICH FOLLOWS.
C
C     DOUBLE PRECISION A,R,ANORM,ANRMX,THR,X,Y,SINX,SINX2,COSX,
C    1                 COSX2,SINCS,RANGE
C
C        THE C MUST ALSO BE REMOVED FROM DOUBLE PRECISION STATEMENTS
C        APPEARING IN OTHER ROUTINES USED IN CONJUNCTION WITH THIS
C        ROUTINE.
C
C        THE DOUBLE PRECISION VERSION OF THIS SUBROUTINE MUST ALSO
C        CONTAIN DOUBLE PRECISION FORTRAN FUNCTIONS.  SQRT IN STATEMENTS
C        40, 68, 75, AND 78 MUST BE CHANGED TO DSQRT.  ABS IN STATEMENT
C        62 MUST BE CHANGED TO DABS. THE CONSTANT IN STATEMENT 5 SHOULD
C        BE CHANGED TO 1.0D-12.
C
C        ...............................................................
C
C        GENERATE IDENTITY MATRIX
C
    5 RANGE=1.0E-6
      IF(MV-1) 10,25,10
   10 IQ=-N
      DO 20 J=1,N
      IQ=IQ+N
      DO 20 I=1,N
      IJ=IQ+I
```

```
      R(IJ)=0.0
      IF(I-J) 20,15,20
   15 R(IJ)=1.0
   20 CONTINUE
C
C        COMPUTE INITIAL AND FINAL NORMS (ANORM AND ANORMX)
C
   25 ANORM=0.0
      DO 35 I=1,N
      DO 35 J=I,N
      IF(I-J) 30,35,30
   30 IA=I+(J*J-J)/2
      ANORM=ANORM+A(IA)*A(IA)
   35 CONTINUE
      IF(ANORM) 165,165,40
   40 ANORM=1.414*SQRT(ANORM)
      ANRMX=ANORM*RANGE/FLOAT(N)
C
C        INITIALIZE INDICATORS AND COMPUTE THRESHOLD, THR
C
      IND=0
      THR=ANORM
   45 THR=THR/FLOAT(N)
   50 L=1
   55 M=L+1
C
C        COMPUTE SIN AND COS
C
   60 MQ=(M*M-M)/2
      LQ=(L*L-L)/2
      LM=L+MQ
   62 IF( ABS(A(LM))-THR) 130,65,65
   65 IND=1
      LL=L+LQ
      MM=M+MQ
      X=0.5*(A(LL)-A(MM))
   68 Y=-A(LM)/ SQRT(A(LM)*A(LM)+X*X)
      IF(X) 70,75,75
   70 Y=-Y
   75 SINX=Y/ SQRT(2.0*(1.0+( SQRT(1.0-Y*Y))))
      SINX2=SINX*SINX
   78 COSX= SQRT(1.0-SINX2)
      COSX2=COSX*COSX
      SINCS =SINX*COSX
C
C        ROTATE L AND M COLUMNS
C
      ILQ=N*(L-1)
      IMQ=N*(M-1)
      DO 125 I=1,N
      IQ=(I*I-I)/2
      IF(I-L) 80,115,80
   80 IF(I-M) 85,115,90
   85 IM=I+MQ
      GO TO 95
   90 IM=M+IQ
   95 IF(I-L) 100,105,105
  100 IL=I+LQ
      GO TO 110
  105 IL=L+IQ
  110 X=A(IL)*COSX-A(IM)*SINX
      A(IM)=A(IL)*SINX+A(IM)*COSX
      A(IL)=X
  115 IF(MV-1) 120,125,120
  120 ILR=ILQ+I
      IMR=IMQ+I
      X=R(ILR)*COSX-R(IMR)*SINX
      R(IMR)=R(ILR)*SINX+R(IMR)*COSX
      R(ILR)=X
  125 CONTINUE
      X=2.0*A(LM)*SINCS
      Y=A(LL)*COSX2+A(MM)*SINX2-X
      X=A(LL)*SINX2+A(MM)*COSX2+X
      A(LM)=(A(LL)-A(MM))*SINCS+A(LM)*(COSX2-SINX2)
      A(LL)=Y
      A(MM)=X
C
C        TESTS FOR COMPLETION
C
C        TEST FOR M = LAST COLUMN
C
  130 IF(M-N) 135,140,135
  135 M=M+1
      GO TO 60
C
C        TEST FOR L = SECOND FROM LAST COLUMN
C
  140 IF(L-(N-1)) 145,150,145
  145 L=L+1
      GO TO 55
  150 IF(IND-1) 160,155,160
  155 IND=0
      GO TO 50
C
C        COMPARE THRESHOLD WITH FINAL NORM
C
  160 IF(THR-ANRMX) 165,165,45
```

```
C        SORT EIGENVALUES AND EIGENVECTORS
C
  165 IQ=-N
      DO 185 I=1,N
      IQ=IQ+N
      LL=I+(I*I-I)/2
      JQ=N*(I-2)
      DO 185 J=I,N
      JQ=JQ+N
      MM=J+(J*J-J)/2
      IF(A(LL)-A(MM)) 170,185,185
  170 X=A(LL)
      A(LL)=A(MM)
      A(MM)=X
      IF(MV-1) 175,185,175
  175 DO 180 K=1,N
      ILR=IQ+K
      IMR=JQ+K
      X=R(ILR)
      R(ILR)=R(IMR)
  180 R(IMR)=X
  185 CONTINUE
      RETURN
      END

      SUBROUTINE MINV(A,N,D,L,M)
C
C     ..................................................................
C
C        SUBROUTINE MINV
C
C        PURPOSE
C           INVERT A MATRIX
C
C        USAGE
C           CALL MINV(A,N,D,L,M)
C
C        DESCRIPTION OF PARAMETERS
C           A - INPUT MATRIX, DESTROYED IN COMPUTATION AND REPLACED BY
C               RESULTANT INVERSE.
C           N - ORDER OF MATRIX A
C           D - RESULTANT DETERMINANT
C           L - WORK VECTOR OF LENGTH N
C           M - WORK VECTOR OF LENGTH N
C
C        REMARKS
C           MATRIX A MUST BE A GENERAL MATRIX
C
C        SUBROUTINES AND FUNCTION SUBPROGRAMS REQUIRED
C           NONE
C
C        METHOD
C           THE STANDARD GAUSS-JORDAN METHOD IS USED. THE DETERMINANT
C           IS ALSO CALCULATED. A DETERMINANT OF ZERO INDICATES THAT
C           THE MATRIX IS SINGULAR.
C
C     ..................................................................
C
      DIMENSION A(1),L(1),M(1)
C
C        ...............................................................
C
C        IF A DOUBLE PRECISION VERSION OF THIS ROUTINE IS DESIRED, THE
C        C IN COLUMN 1 SHOULD BE REMOVED FROM THE DOUBLE PRECISION
C        STATEMENT WHICH FOLLOWS.
C
C     DOUBLE PRECISION A,D,BIGA,HOLD
C
C        THE C MUST ALSO BE REMOVED FROM DOUBLE PRECISION STATEMENTS
C        APPEARING IN OTHER ROUTINES USED IN CONJUNCTION WITH THIS
C        ROUTINE.
C
C        THE DOUBLE PRECISION VERSION OF THIS SUBROUTINE MUST ALSO
C        CONTAIN DOUBLE PRECISION FORTRAN FUNCTIONS.  ABS IN STATEMENT
C        10 MUST BE CHANGED TO DABS.
C
C        ...............................................................
C
C        SEARCH FOR LARGEST ELEMENT
C
      D=1.0
      NK=-N
      DO 80 K=1,N
      NK=NK+N
      L(K)=K
      M(K)=K
      KK=NK+K
      BIGA=A(KK)
      DO 20 J=K,N
      IZ=N*(J-1)
      DO 20 I=K,N
      IJ=IZ+I
   10 IF( ABS(BIGA)- ABS(A(IJ))) 15,20,20
   15 BIGA=A(IJ)
      L(K)=I
      M(K)=J
   20 CONTINUE
```

```
C
C        INTERCHANGE ROWS
C
      J=L(K)
      IF(J-K) 35,35,25
   25 KI=K-N
      DO 30 I=1,N
      KI=KI+N
      HOLD=-A(KI)
      JI=KI-K+J
      A(KI)=A(JI)
   30 A(JI) =HOLD
C
C        INTERCHANGE COLUMNS
C
   35 I=M(K)
      IF(I-K) 45,45,38
   38 JP=N*(I-1)
      DO 40 J=1,N
      JK=NK+J
      JI=JP+J
      HOLD=-A(JK)
      A(JK)=A(JI)
   40 A(JI) =HOLD
C
C        DIVIDE COLUMN BY MINUS PIVOT (VALUE OF PIVOT ELEMENT IS
C        CONTAINED IN BIGA)
C
   45 IF(BIGA) 48,46,48
   46 D=0.0
      RETURN
   48 DO 55 I=1,N
      IF(I-K) 50,55,50
   50 IK=NK+I
      A(IK)=A(IK)/(-BIGA)
   55 CONTINUE
C
C        REDUCE MATRIX
C
      DO 65 I=1,N
      IK=NK+I
      HOLD=A(IK)
      IJ=I-N
      DO 65 J=1,N
      IJ=IJ+N
      IF(I-K) 60,65,60
   60 IF(J-K) 62,65,62
   62 KJ=IJ-I+K
      A(IJ)=HOLD*A(KJ)+A(IJ)
   65 CONTINUE
C
C        DIVIDE ROW BY PIVOT
C
      KJ=K-N
      DO 75 J=1,N
      KJ=KJ+N
      IF(J-K) 70,75,70
   70 A(KJ)=A(KJ)/BIGA
   75 CONTINUE
C
C        PRODUCT OF PIVOTS
C
      D=D*BIGA
C
C        REPLACE PIVOT BY RECIPROCAL
C
      A(KK)=1.0/BIGA
   80 CONTINUE
C
C        FINAL ROW AND COLUMN INTERCHANGE
C
      K=N
  100 K=(K-1)
      IF(K) 150,150,105
  105 I=L(K)
      IF(I-K) 120,120,108
  108 JQ=N*(K-1)
      JR=N*(I-1)
      DO 110 J=1,N
      JK=JQ+J
      HOLD=A(JK)
      JI=JR+J
      A(JK)=-A(JI)
  110 A(JI) =HOLD
  120 J=M(K)
      IF(J-K) 100,100,125
  125 KI=K-N
      DO 130 I=1,N
      KI=KI+N
      HOLD=A(KI)
      JI=KI-K+J
      A(KI)=-A(JI)
  130 A(JI) =HOLD
      GO TO 100
  150 RETURN
      END
```